REVIEW

Supercapacitor electrodes based on metal-organic compounds from the first transition metal series

Bulin Chen[1,2] | Linli Xu[1,2] | Zhiyuan Xie[3] | Wai-Yeung Wong[1,2]

[1]Department of Applied Biology and Chemical Technology and Research Institute for Smart Energy, The Hong Kong Polytechnic University, Hong Kong, China

[2]The Hong Kong Polytechnic University Shenzhen Research Institute, Shenzhen, China

[3]State Key Laboratory of Polymer Physics and Chemistry, Changchun Institute of Applied Chemistry, Chinese Academy of Sciences, Changchun, China

Correspondence
Wai-Yeung Wong, Department of Applied Biology and Chemical Technology and Research Institute for Smart Energy, The Hong Kong Polytechnic University, Hung Hom, Hong Kong, China.
Email: wai-yeung.wong@polyu.edu.hk

Abstract

Metal-organic compounds, including molecular complexes and coordination polymers, have attracted much attention as electrode materials in supercapacitors owing to their large surface area, high porosity, tailorable pore size, controllable structure, good electrochemical reversibility, and abundant active sites. Among the variety of metal-organic compounds exhibiting desired supercapacitor performances (high specific capacitance, long cycling life, high energy density, and power density), those with metals in the first transition metal series are the most studied due to their rich covalent states, light atom weight, environmental-friendliness, non-toxicity, and low cost. In this review, the recent reports on the metal-organic compounds of the first transition metal series as electrode materials in supercapacitors are summarized and their electrode and device performances are discussed in terms of different metal elements and typical multidentate ligands. Moreover, the current challenges, design strategies, future opportunities and further research directions are also highlighted for metal-organic compounds in the field of supercapacitors.

KEYWORDS

electrochemistry, first transition metal series, metal-organic compounds, metal-organic frameworks, supercapacitors

1 | INTRODUCTION

The tremendous increase of energy consumption in modern society leads to serious consequences, such as environmental pollution, global warming, and the depletion of fossil fuels. In order to overcome these issues, one way is to develop efficient, environmental-friendly and renewable energy resources, while another is to explore technologies associated with energy conversion and storage. Both the intermittent nature of renewable energy sources (such as

wind and solar power) and the transmission to the power grid require the energy storage systems (ESSs) such as batteries, fuel cells and supercapacitors (SCs).[1] SCs, with attractive properties of high power density, fast charge/discharge rate, long cycle life and good electrochemical reversibility, have bridged the power/energy gap (Figure 1) between traditional dielectric capacitors (with high power output) and batteries/fuel cells (with high energy storage) and have found the potential application in portable electronic products, electronic communication, electric vehicles, backup power storage, industrial energy/power management devices, aerospace, etc.[1,3-23]

A SC device comprises two electrodes, electrolyte (aqueous, organic, ionic liquid, solid, or redox active) and a separator preventing the electrical contact between electrodes. The electrodes can either be identical for the symmetric SCs (SSCs) or different for asymmetric SCs (ASCs). The performance of SC electrodes or SC devices is evaluated by a list of electrochemical parameters such as specific capacitance, cycling stability, energy density, and power density. In general, the electrode performance is adjusted in three-electrode system to optimize the working parameters before the actual assembly of the SC devices (two-electrode system). The specific capacitance (gravimetric capacitance, C_g in F g^{-1}, areal capacitance, C_a in F cm^{-2} and volumetric capacitance, C_v in F cm^{-3}) of the electrode in a three-electrode system can be either estimated by cyclic voltammetric (CV) method or galvanostatic charge-discharge (GCD, also noted as chronopotentiometry [CP]) method. The quantitative

calculation equations (Equations (1)-(3) for CV method and Equations (4)-(6) for GCD method) are shown below[24]:

$$C_g = \frac{1}{m \times s \times \Delta V} \int I(V)dV, \tag{1}$$

$$C_a = \frac{1}{a_e \times s \times \Delta V} \int I(V)dV, \tag{2}$$

$$C_v = \frac{1}{v_e \times s \times \Delta V} \int I(V)dV, \tag{3}$$

$$C_g = \frac{I \times \Delta t}{m \times \Delta V}, \tag{4}$$

$$C_a = \frac{I \times \Delta t}{a_e \times \Delta V}, \tag{5}$$

$$C_v = \frac{I \times \Delta t}{v_e \times \Delta V}, \tag{6}$$

where $\int I(V)dV$ is the integral area of CV curve (A V), s is the scan rate (V s^{-1}), ΔV is the total potential deviation of the voltage window (V), I is the discharge current (A), Δt is the discharge time (s), m is the mass of active material on the electrode (g), a_e is the electrode area (cm^2) and v_e is the electrode volume (cm^3). For the SC device in a two-electrode system, the specific capacitance can be expressed by the following equations (Equations (7)-(9) for CV method and Equations (10)-(12) for GCD method)[24]:

$$C_g = \frac{1}{(m^+ + m^-) \times s \times \Delta V} \int I(V)dV, \tag{7}$$

$$C_a = \frac{1}{2 \times a_d \times s \times \Delta V} \int I(V)dV, \tag{8}$$

$$C_v = \frac{1}{v_d \times s \times \Delta V} \int I(V)dV, \tag{9}$$

$$C_g = \frac{4 \times I \times \Delta t}{(m^+ + m^-) \times \Delta V}, \tag{10}$$

$$C_a = \frac{I \times \Delta t}{a_d \times \Delta V}, \tag{11}$$

$$C_v = \frac{I \times \Delta t}{v_d \times \Delta V}, \tag{12}$$

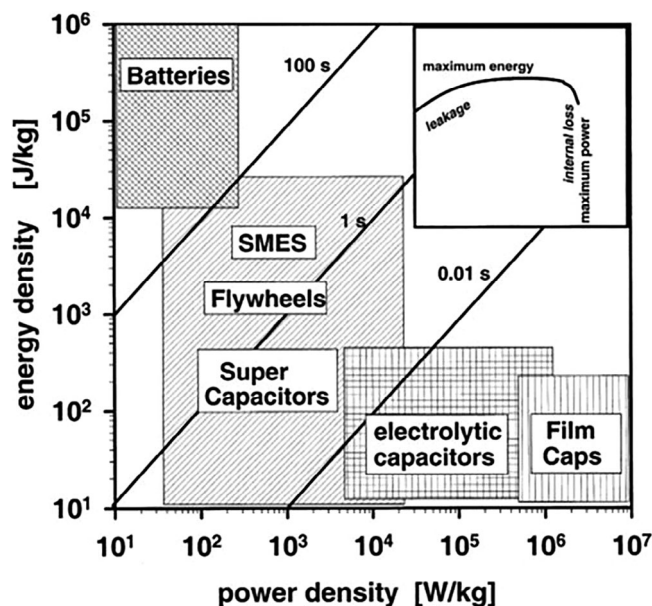**FIGURE 1** Ragone plot. Detail window shows energy drop due to internal dissipation and leakage losses for sufficiently high and low power. Reproduced with permission: Copyright 2000, Elsevier Science S.A.[2]

where $\int I(V)dV$ is the integral area of CV curve (A V), s is the scan rate (V s^{-1}), ΔV is the total potential deviation of the voltage window (V), I is the discharge current (A), Δt

is the discharge time (s), m^+ and m^- is respectively the mass of active material on the positive and negative electrode (g), a_d is the device area (cm^2) and v_d is the device volume (cm^3). The energy density (E, in Wh kg^{-1}, Wh cm^{-2}, or Wh cm^{-3}) and power density (P, in W kg^{-1}, W cm^{-2}, or W cm^{-3}) of the SC devices are obtained by GCD method and calculated by the following equations[24]:

$$E = \frac{C \times \Delta V^2}{4 \times 2 \times 3.6}, \tag{13}$$

$$P = \frac{E \times 3600}{\Delta t}, \tag{14}$$

where C is the specific capacitance (F g^{-1}, F cm^{-2}, or F cm^{-3}), ΔV is the total potential deviation of the voltage window (V) and Δt is the discharge time (s). The cycling stability in both three- and two-electrode system is estimated with the capacitance retention after a specific charge-discharge cycle number by either CV or GCD method. However, in a few cases, especially those for battery-SC hybrid applications, the authors only reported the specific capacity (in C g^{-1}/C cm^{-2}/C cm^{-3} or mAh g^{-1}/mAh cm^{-2}/mAh cm^{-3}) of the electrode materials based on metal-organic compounds.[25-39] Considering that the specific capacitance is the parameter reported in the most research papers of SC discipline, those literatures which only reported the specific capacity of transition metal-organic compounds of the first transition metal series as SC electrode materials are not included in this review. The stability (cycling stability, chemical stability, thermal stability, etc.) of the electrode material is also a critical parameter for the practical applications. The cycling stability is usually evaluated by the capacitance retention after a specific number of charge-discharge cycles. However, the chemical and thermal stabilities of SC electrode materials are rarely reported in the previous literature reports.

Depending on the storage mechanism or cell configuration, SCs can be classified into electrochemical double-layer capacitors (EDLCs), faradaic pseudocapacitors and hybrid supercapacitors (HSCs). The capacitance of EDLCs originates from the ion adsorption and desorption at the electrode-electrolyte interface without any electron transfer process and the electrode materials of EDLCs are mainly carbon-based materials with good conductivity and high specific surface area.[40,41] While Faradaic pseudocapacitors store charges via reversible redox reactions with electron transfer between the electrode and electrolyte, materials showing pseudocapacitance are usually metal oxides/nitrides/carbides/sulfides/phosphates/hydroxides, Prussian blue and its analogues, conductive polymers and sometimes functionalized porous carbon.[42-50] HSCs are the hybrid devices composed of an EDLC electrode and a pseudocapacitive or battery type electrode, combining the properties of both systems and leading to an intermediate performance in some cases.[1,14] In general, pseudocapacitors can hold 10 to 100 times higher specific capacitance values than EDLCs,[1,51-55] however, pseudocapacitors suffer from the poor mechanical stability due to the swelling and shrinking of electrodes caused by redox reactions and the low power performance as a result of the slower Faradaic processes involved.[56]

Metal-organic compounds refer to a class of chemical compounds that contain metal ions and organic ligands. Different from organometallic compounds, metal-organic compounds do not necessarily involve the metal-carbon bonds. As shown in Figure 2B, the metal-organic compounds can be divided into molecular complexes and metal coordination polymers, and typical structures of metal coordination polymers of different dimensions are demonstrated. It is worth noting that a previous paper has reviewed the MOFs of different spatial dimensions and their application in the SC field, and thus this paper would not focus on the dimension effect of the metal-organic compounds on the SC performance.[57] The metallation of the organic SC-electrode materials tends to bring about better performances due to the following factors: (a) The metallation helps generate extra redox activities by charge transport of both the metal atoms and the organic ligands. (b) Coordination compounds have wide structural diversity derived from various coordination number, geometry, and valence shell of the metal atoms. Recently, metal-organic compounds based on the first transition metal series have become one of the most popular candidates for high-performance active materials of SC electrodes, owing to their desired properties as presented below: (a) Metal-organic compounds of the first transition metal series possess advantages such as ease of synthesis, low cost, controllable structure and wide structural diversity. Besides, metals in the first transition metal series are non-toxic, less costly and abundant on the earth. (b) Rich valence states of transition metals allow the redox reaction activity and efficient electron transfer for pseudocapacitive mechanism. (c) Porous structures can be achieved by the tetrahedral or octahedral coordination nature of transition metals and the usage of multidentate ligands to form porous structures in metal coordination polymers (especially in metal-organic frameworks, MOFs). The EDLC mechanism benefits from this because more channels for the transmission of ions during the charge-discharge processes can be realized. (d) Compared to the subsequent transition metal series, the first transition metals have smaller molecular weights, which result in higher specific gravimetric capacitance values. Figure 2A illustrates the advantages of the first-transition metal-
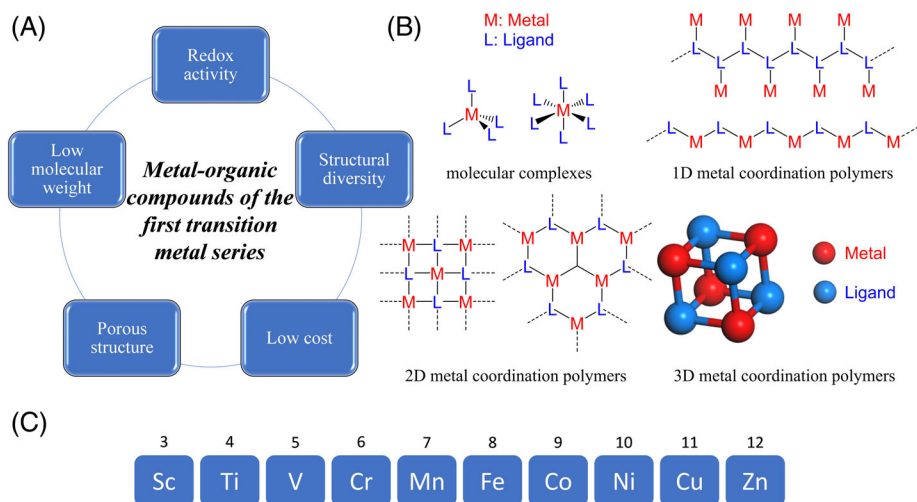
FIGURE 2 A, Advantages of the metal-organic compounds of the first transition metal series as the SC electrode materials. B, Schematic illustration of the classification of different metal-organic compounds. C, Elements in the first transition metal series

organic compounds as the SC electrode materials. Nevertheless, SC electrodes based on pristine metal-organic compounds sometimes are confronted with weak cycling stability and poor conductivity. To overcome these setbacks, three strategies are generally adopted[58]: (a) By preparing metal-organic compounds of particular topologies or architectures via various advanced synthetic technologies and solely applying them as SC electrodes to pursue high performances. (b) By compositing metal-organic compounds with conductive matrices (such as conductive polymers or carbon-based materials) to afford better conductivity and structural stability. (c) By utilizing metal-organic compounds (especially MOFs) as templates or precursors to yield various materials (such as metal oxides/nitrides/carbides/sulfides/hydroxides, porous carbon materials and multifold composites). The first two strategies focused on the metal-organic compounds themselves as SC electrode materials, while the last strategy converts them into inorganic materials. It is worth mentioning that there have been several reviews[59-65] on the SC materials that are derived from MOFs (such as carbon, metal oxides, metal sulfides, metal hydroxides, etc.) and those reports will not be covered generally in this paper.

To date, cobalt, nickel and copper have been the most reported metal elements for pristine or composite SC electrodes based on metal-organic compounds, not only in the first transition metal series (Figure 2C) but also among all metal elements in the whole periodic table. However, there are no papers yet on scandium- and titanium-organic compounds for SCs. Figure 3 depicts the development history of SC electrode materials (**I-XXI**) based on the metal-organic compounds of the first transition metal series, and some of the representative structures are given, with the years of their reports indicated. In 2012, Díaz and coworkers firstly performed SC tests on the known Zn/Co-MOF (**I** and **II**) materials, with a

dicarboxylate as the ligand.[66] Subsequently, more metal-organic compounds with various polycarboxylate ligands (Figure 4A) and nitrogen-based bridging ligands (Figure 4B) were applied in the SC field, and the metal elements were gradually expanded to nearly the whole first transition metal series. Gao's group firstly bridged the zeolitic imidazolate frameworks (ZIFs) with the SC electrode materials by preparing composites based on two representative ZIFs (**VI** and **VII**) in 2014.[68,69] In the following year, Zhang and coworkers designed a zinc-porphyrin monomer and prepared the SC electrodes by the electropolymerization method to afford a conducting metal-organic polymer (**IX**).[71] The metal-organic compounds exhibiting the SC properties were extended to those containing the Schiff-base ligands (**XV**),[75] ferrocene-based ligands (**XVI**)[76] and polyoxometalates (POMs, **XVII**)[77] in 2017. From 2018 onwards, research interests of the metal-organic compounds of the first transition metal series began to move to the two-dimensional MOFs (eg, **XVIII**, **XIX** and **XXI**) with planar polyamine and polyphenol ligands (Figure 9).[78,80] In 2019, there were three reports concerning ferrocene-modified materials and all of them showed great pseudocapacitive behaviors due to the redox activities of the ferrocene components.[79,81,82]

Previous reviews on SC electrodes related to metal-organic compounds mainly focused on the MOF-based electrode materials,[24,57,58,83-86] covering neither metal-organic molecular complexes nor non-framework metal coordination polymers. In this review, both SC electrodes and device performances of monometallic and bimetallic metal-organic compounds from the first transition metal series and their composites were comprehensively summarized for the first time. Metal-organic compounds used in SC electrodes sorted by different metal elements along with their representative organic ligands are presented in the respective sessions. Our discussion is further extended to various synthetic
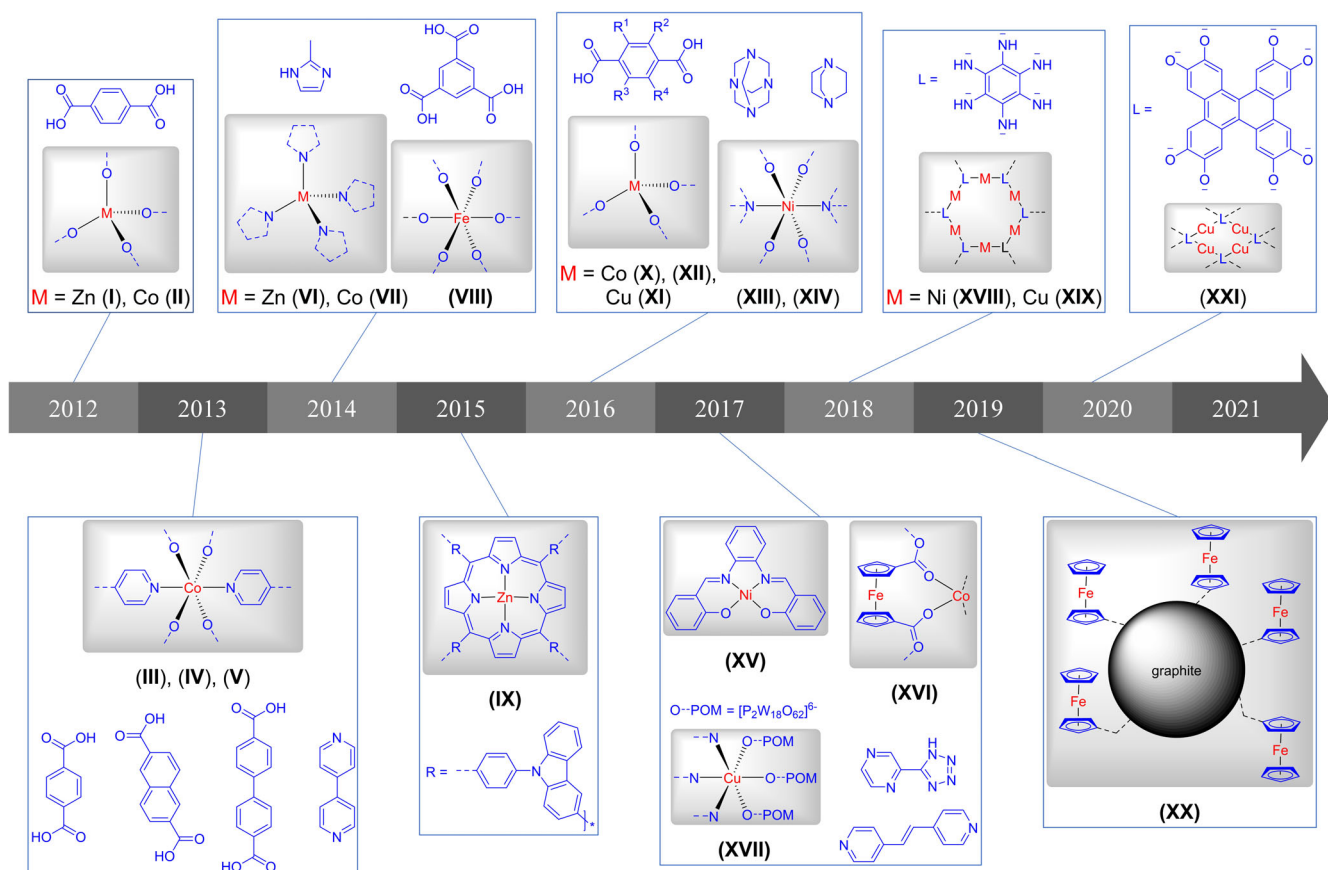
FIGURE 3 Development history of SC electrode materials based on the metal-organic compounds of the first transition metal series. MOF-5 (**I**) and Co8-MOF-5 (**II**).[66] CoBDC(DMF) (**III**), [Co$_3$(2,6-NDC)$_3$(bipy)$_{1.5}$] (**IV**) and [Co(BPDC)(H$_2$O)$_2$] (**V**).[67] ZIF-8 (**VI**).[68] ZIF-67 (**VII**).[69] MIL-100(Fe) (**VIII**).[70] (Zn-mTCPP)$_n$ (**IX**).[71] Co-LMOF (**X**).[72] [Cu(Br$_2$BDC)$_2$]H$_2$(triethylamine)$_2$ (**XI**) and [Co$_2$(Br$_2$BDC) (HCOO)$_2$(dimethylformamide)$_2$] (**XII**).[73] DMOF-ADC (**XIII**) and DMOF-NDC (**XIV**).[74] Ni(salphen) (**XV**).[75] [Co$_4$(FcDC)$_4$(bipy)$_4$(H$_2$O)$_6$] (**XVI**).[76] (H$_2$bpe)(Hbpe)$_2$[Cu(pzta)(H$_2$O)][P$_2$W$_{18}$O$_{62}$] (**XVII**).[77] Ni-HAB (**XVIII**) and Cu-HAB (**XIX**).[78] Ferrocene-functionalized reduced graphene oxide (**XX**).[79] Cu-DBC (**XXI**).[80]

technologies, molecular structures, material morphologies, electrochemical mechanism, current trends, challenges, and future opportunities of the metal-organic compounds of the first transition metal series in the development of SCs.

2 | MONOMETALLIC METAL-ORGANIC COMPOUNDS AND THEIR COMPOSITES

2.1 | Manganese

Manganese is one of the attractive metals in the first transition metal series for ESS applications due to its rich valence states. To date, various pure manganese oxides (MnO$_x$) have been directly used as electrode materials.[94-96] Meanwhile, the pseudocapacitive properties of manganese-organic compounds and their

composites (**1-11**) make them attractive materials for SC applications,[87-93] which may result from the surface redox reactions of manganese ions in different valence states.[88] This conversion process in aqueous electrolytes can be expressed by the following equations:

$$Mn(II)_s + OH^- \leftrightarrow Mn(II)(OH)_{ad} + e^-, \quad (15)$$

$$Mn(II)(OH)_{ad} \leftrightarrow Mn(III)(OH)_{ad} + e^-. \quad (16)$$
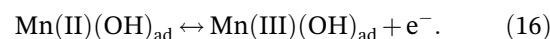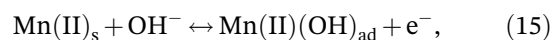
The electrodes and SC performances of manganese-organic compounds are summarized in Tables 1 and 2. MOFs with polycarboxylate ligands (Figure 4A), which generally exhibit 2D or 3D layered structures with [M$_m$(COO)$_n$] nodes of paddle-wheel secondary building units and π-conjugated bridging ligands (Figure 4B),[73,97] have aroused wide research interest as electrode

(A)
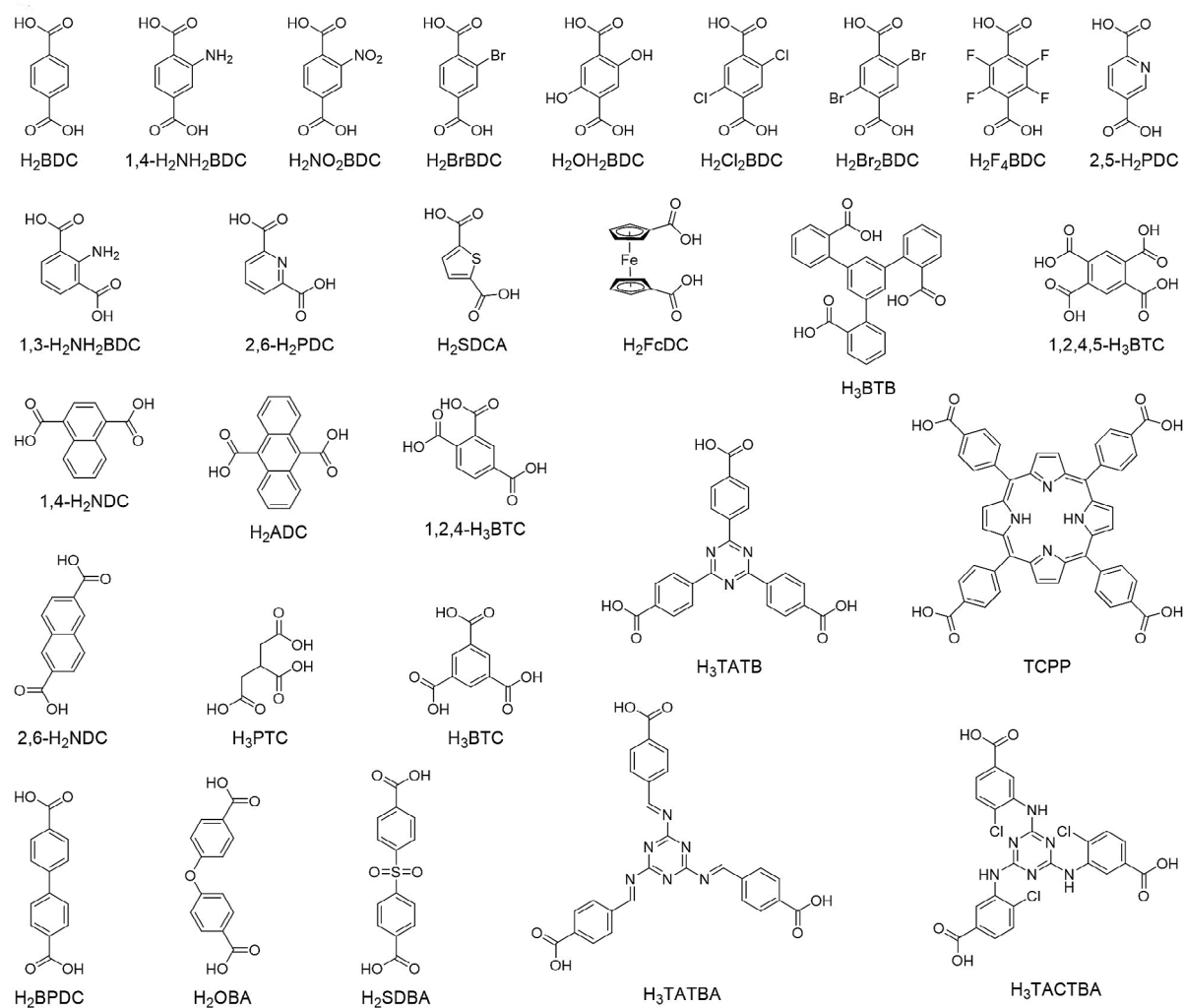
(B)

FIGURE 4 A, Polycarboxylate and B, bridging ligands used to construct metal-organic compounds for SC electrode materials

TABLE 1 Summary of SC electrode performances of manganese-organic compounds

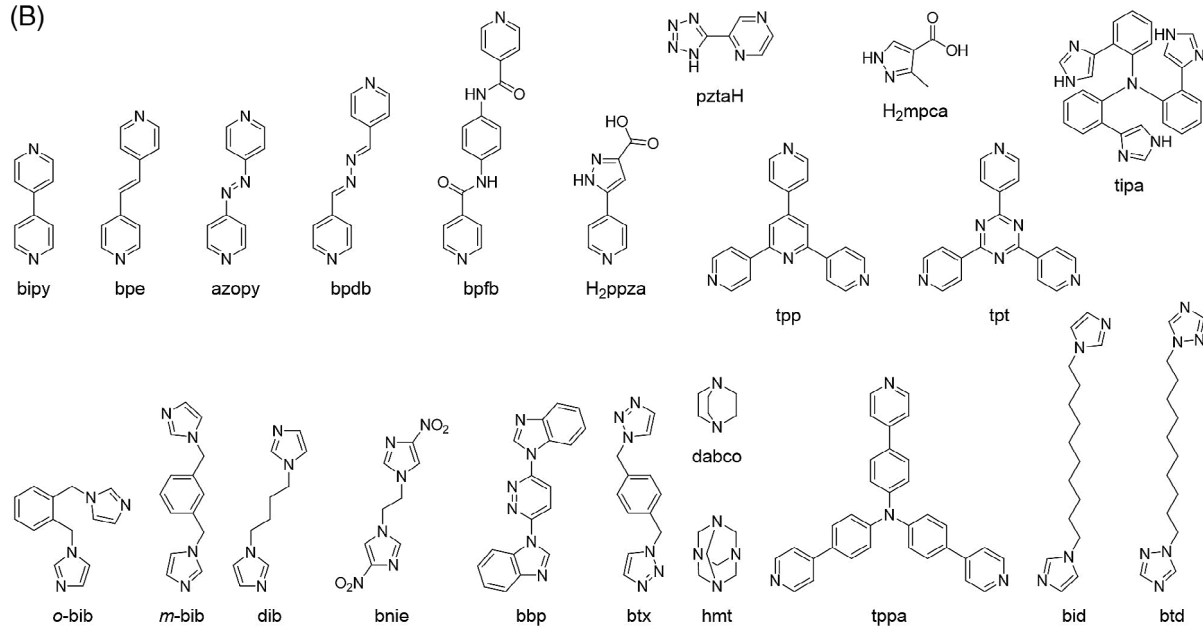|	Metal	Ligand	Composited with	Surface area[a]	Specific capacitance[b]	Cycling stability[b,c]	Electrolyte[d]	Reference
Manganese polycarboxylate MOFs								
1	Mn	H_2BDC	—	—	28.4 F g^{-1} @ 1 A g^{-1}	—	1 M Na_2SO_4	87
					43.2 F g^{-1} @ 5 mV s^{-1}			
2	Mn	H_2BDC	CNT	—	203.1 F g^{-1} @ 1 A g^{-1}	—	1 M Na_2SO_4	87
					206 F g^{-1} @ 5 mV s^{-1}			
3	Mn	H_2F_4BDC, bipy	—	17.08 m^2 g^{-1}	1098 F g^{-1} @ 1 A g^{-1}	92.6% @ 2 A g^{-1} (2000)	1 M KOH	88
					1178 F g^{-1} @ 1 A g^{-1}	94.6% @ 2 A g^{-1} (2000)	1 M LiOH	
4	Mn	H_2BDC	—	32.3 m^2 g^{-1}	177.9 F g^{-1} @ 0.5 A g^{-1}	—	1 M Na_2SO_4	89
					166.4 F g^{-1} @ 1 mV s^{-1}			
5	Mn	H_2BDC, tipa	—	—	1358 F g^{-1} @ 1 A g^{-1}	105% @ — (2000)	6 M KOH	90
6	Mn	H_2BDC	$K_{0.5}Mn_2O_4$	—	611 F g^{-1} @ 1 A g^{-1}	—	1 M Na_2SO_4	91
7	Mn	H_2BDC	$K_{0.5}Mn_2O_4$	—	704 F g^{-1} @ 1 A g^{-1}	—	1 M Na_2SO_4	91
8	Mn	H_2BDC	$K_{0.5}Mn_2O_4$	166.77 m^2 g^{-1}	886.9 F g^{-1} @ 1 A g^{-1}	90.5% @ 2 A g^{-1} (6000)	1 M Na_2SO_4	91
9	Mn	H_2BDC	$K_{0.5}Mn_2O_4$	—	241.5 F g^{-1} @ 1 A g^{-1}	—	1 M Na_2SO_4	91
Others								
10	Mn	THPP-PA	—	—	90.9 F g^{-1} @ 2.5 A g^{-1}	—	1 M Na_2SO_4	92
					81.1 F g^{-1} @ 10 mV s^{-1}			

Abbreviation: CNT, carbon nanotube.

[a]Determined by the Brunauer-Emmett-Teller (BET) method.

[b]Obtained by either CP and GCD method at specific current densities or CV method at specific scan rates.

[c]Evaluated by the capacitance retention after a number of charge/discharge cycles, which are shown in brackets.

[d]Normally in water except for those with special clarification.

materials for SCs. To the best of our knowledge, nearly all reported manganese-organic compounds used as electrode materials for SCs are Mn-MOFs with polycarboxylate ligands (**1-9**) and the highest value of C_g (1358 F g^{-1}) was achieved by a polythreaded Mn-MOF (**5**) based on the ligands of H_2BDC and tipa.[90] The SC electrode based on **5** exhibited no capacitance loss after 2000 charge/discharge cycles in 6 M KOH and an ASC device with **5** as the positive electrode could deliver C_g up to 114.6 F g^{-1}. Another Mn-MOF (**3**) with polycarboxylate ligand (H_2F_4BDC) and bridging ligand (bipy) also showed good SC electrode performance, with C_g over 1000 F g^{-1} in the base solutions (1 M KOH and LiOH). Yao and coworkers presented an accessible strategy to prepare vertically co-oriented $K_{0.5}Mn_2O_4$@Mn-MOF nanosheet arrays (**6-9**), with $K_{0.5}Mn_2O_4$ as both the self-sacrificing template and precursor (Figure 5A), which avoided the extra removal of the template and the use of conductive agents in electrode preparation.[91] $K_{0.5}Mn_2O_4$@Mn-MOF nanosheet arrays were prepared by solvothermal method of different reaction times (4, 6, 8, and 10 hours for composites **6**, **7**, **8** and **9**, respectively), and the optimized C_g reached 886.9 F g^{-1} (**8**). An as-assembled ASC device with **8** as a positive electrode provided the maximum energy density and maximum power density of 42.94 W h kg^{-1} and 6493.51 W kg^{-1}, respectively.

Except for the manganese polycarboxylate MOFs, there are two reports on manganese-organic compounds with ligands of a poly(porphyrin) derivative (**10**)[92] and p-phenylenediamine (**11**).[93] Cheng and coworkers fabricated an ASC device based on a novel Mn(II)-porphyrin polycondensation polymer THPP-PA-Mn (**10**, Figure 5B), which could lighten a light-emitting diode (LED) for ~12 seconds after being charged for 10 seconds by a 2 V direct-current power supply (Figure 5C).[92] Kannangara and coworkers synthesized two layered MOFs, Mn-pPDA (**11**) and Ni-pPDA (**138**), through a liquid-liquid interfacial reaction method.[93] It was found that the ASC devices with **11** and **138** as positive electrodes could deliver C_g of 109.3 and 184.7 F g^{-1}, respectively.

2.2 | Cobalt

For SCs based on monometallic organic compounds, cobalt is the most commonly used metal in the first transition metal series.[25,27,50,67,69,72,73,97-134] Summarized in Tables 3 and 4 are the electrode and SC performances of cobalt-organic compounds and their composites (**12-92**).

TABLE 2 Summary of SC electrode performances of manganese-organic compounds

Positive electrode								
	Metal	Ligand	Composited with	Negative electrode	Specific capacitance[a]	Energy density and power density[b]	Cycling stability[a,c]	Electrolyte[d] Reference
Manganese polycarboxylate MOFs								
2	Mn	H_2BDC	CNT	2	50.3 F g^{-1} @ 0.25 A g^{-1}	$\underline{6.9\ Wh\ kg^{-1}}$ @ $\underline{122.6\ W\ kg^{-1}}$	88% @ 5 A g^{-1} (3000)	1 M Na_2SO_4 87
						1.3 Wh kg^{-1} @ $\underline{2240\ W\ kg^{-1}}$		
4	Mn	H_2BDC	—	4	64.5 F g^{-1} @ 0.25 A g^{-1}	$\underline{4.3\ Wh\ kg^{-1}}$ @ $\underline{176\ W\ kg^{-1}}$	98% @ — (2000)	PVA/Na_2SO_4 89
5	Mn	H_2BDC, tipa	—	AC	114.6 F g^{-1} @ 1 A g^{-1}	$\underline{35.8\ Wh\ kg^{-1}}$ @ $\underline{750\ W\ kg^{-1}}$	85.6% @ 5 A g^{-1} (1000)	6 M KOH 90
8	Mn	H_2BDC	$K_{0.5}Mn_2O_4$	WO_3	—	$\underline{42.94\ Wh\ kg^{-1}}$ @ $\underline{1080.08\ W\ kg^{-1}}$	92.1% @ 2 A g^{-1} (8000)	1 M Na_2SO_4 91
						20.74 Wh kg^{-1} @ $\underline{6493.51\ W\ kg^{-1}}$		
Others								
10	Mn	THPP-PA	—	CNT	—	—	86.3% @ 50 A g^{-1} (3000)	1 M Na_2SO_4 92
11	Mn	pPDA	—	GC	109.3 F g^{-1} @ 0.25 A g^{-1}	$\underline{34.2\ Wh\ kg^{-1}}$ @ $\underline{0.75\ kW\ kg^{-1}}$	97.45% @ 8 A g^{-1} (5000)	1 M KOH 93
						13.3 Wh kg^{-1} @ $\underline{6.0\ kW\ kg^{-1}}$		

Abbreviations: AC, activated carbon; GC, graphite carbon; PVA, polyvinyl alcohol.
[a]Obtained by either CP and GCD method at specific current densities, or CV method at specific scan rates.
[b]Data of maximum energy densities and maximum power densities are underlined.
[c]Evaluated by the capacitance retention after a number of charge/discharge cycles, which are shown in brackets.
[d]Normally in water except for those with special clarification.
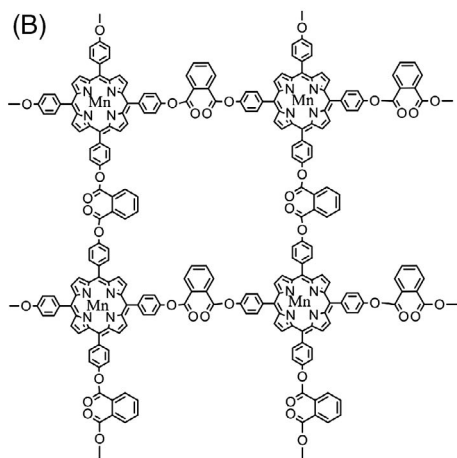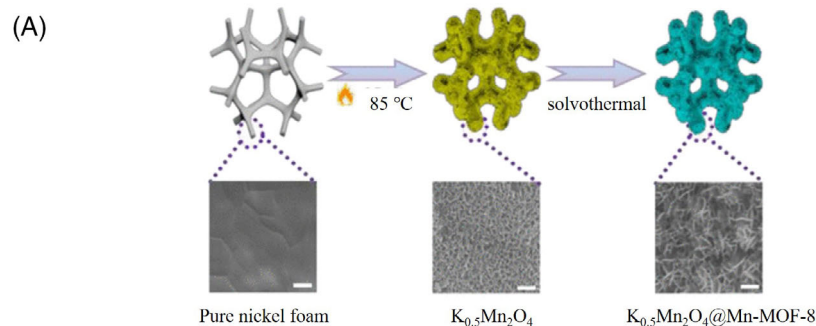
FIGURE 5 A, Schematic illustration of the synthesis of a Mn-MOF composite (**8**). Reproduced with permission: Copyright 2020, American Chemical Society.[91] B, The structure of **10**. Reproduced with permission: Copyright 2019, Elsevier B.V.[92] C, Photograph of a LED driven by an ASC device based on **10**. Reproduced with permission: Copyright 2019, Elsevier B.V[92]

TABLE 3 Summary of SC electrode performances of cobalt-organic compounds

	Metal	Ligand	Composited with	Surface area[a]	Specific capacitance[b]	Cycling stability[b,c]	Electrolyte[d]	Reference
Cobalt organic complex								
12	Co	N_4	PPy	—	$721.9\ F\,g^{-1}$ @ $0.5\ mV\,s^{-1}$	93% @ $0.5\ mA\,cm^{-2}$ (500)	$0.1\ M\ HClO_4$	98
Cobalt polycarboxylate MOFs								
13	Co	H_2BDC	—	—	$206.76\ F\,g^{-1}$ @ $0.6\ A\,g^{-1}$	98.5% @ — (1000)	1 M LiOH	99
14	Co	H_2BDC	rGO	—	$1521.6\ F\,g^{-1}$ @ $0.2\ A\,g^{-1}$	>100% @ $100\ mV\,s^{-1}$ (12 000)	1 M LiOH	100
15	Co	H_2BDC	—	$48.9\ m^2\,g^{-1}$	$2564\ F\,g^{-1}$ @ $1\ A\,g^{-1}$	95.8% @ $2\ A\,g^{-1}$ (3000)	5 M KOH	101
16	Co	H_2BDC	—	—	$1159\ F\,g^{-1}$ @ $0.5\ A\,g^{-1}$	96.7% @ $2\ A\,g^{-1}$ (6000)	3 M KOH	50
17	Co	H_2OH_2BDC	—	—	$182.5\ mF\,cm^{-2}$ @ $0.5\ mA\,cm^{-2}$	91.4% @ $0.5\ A\,cm^{-2}$ (5000)	$1\ M\ TEABF_4$ in ACN	102
					$0.392\ F\,cm^{-2}$ @ $0.88\ mA\,cm^{-3}$	>80% @ $6.3\ mA\,cm^{-3}$ (>10 000)		
					$0.050\ F\,cm^{-3}$ @ $0.88\ mA\,cm^{-3}$			
18	Co	H_2BDC	—	—	$13.6\ mF\,cm^{-2}$ @ $2\ mA\,cm^{-2}$	79.9% @ $50\ mA\,cm^{-2}$ (1000)	2 M KOH	103
19	Co	H_2BDC	—	$9.9\ m^2\,g^{-1}$	$131.8\ F\,g^{-1}$ @ $10\ mV\,s^{-1}$	94.3% @ $100\ mV\,s^{-1}$ (1000)	0.5 M LiOH	67
20	Co	$2,6\text{-}H_2NDC$, bipy	—	$20.29\ m^2\,g^{-1}$	$143.7\ F\,g^{-1}$ @ $10\ mV\,s^{-1}$	95.8% @ $100\ mV\,s^{-1}$ (1000)	0.5 M LiOH	67
21	Co	H_2BPDC	—	$138.35\ m^2\,g^{-1}$	$179.2\ F\,g^{-1}$ @ $10\ mV\,s^{-1}$	77.4% @ $100\ mV\,s^{-1}$ (1000)	0.5 M LiOH	67
22	Co	H_2Br_2BDC	—	—	$1.42\ F\,g^{-1}$ @ $100\ mV\,s^{-1}$	—	$0.1\ M\ Na_2SO_4$	73
23	Co	H_2Br_2BDC	—	—	$1.03\ F\,g^{-1}$ @ $100\ mV\,s^{-1}$	—	$0.1\ M\ Na_2SO_4$	73
24	Co	H_2F_4BDC, hmt	—	$12.15\ m^2\,g^{-1}$	$2474\ F\,g^{-1}$ @ $1\ A\,g^{-1}$	94.3% @ $2\ A\,g^{-1}$ (2000)	1 M KOH	72
					$1768\ F\,g^{-1}$ @ $1\ A\,g^{-1}$	95% @ $2\ A\,g^{-1}$ (2000)	1 M LiOH	
25	Co	H_2BDC, bbp	—	—	$194\ F\,g^{-1}$ @ $1\ A\,g^{-1}$	—	2 M KOH	104
26	Co	$1,2,4\text{-}H_3BTC$, bbp	—	—	$290\ F\,g^{-1}$ @ $0.25\ A\,g^{-1}$	73% @ $2\ A\,g^{-1}$ (2000)	6 M KOH	105
27	Co	$1,2,4,5\text{-}H_4BTC$, bbp	—	—	$157\ F\,g^{-1}$ @ $1\ A\,g^{-1}$	—	2 M KOH	105
28	Co	$1,3\text{-}H_2NH_2BDC$, bbp	—	—	$178\ F\,g^{-1}$ @ $1\ A\,g^{-1}$	—	2 M KOH	105
29	Co	$1,4\text{-}H_2NDC$, bbp	—	—	$108\ F\,g^{-1}$ @ $1\ A\,g^{-1}$	—	2 M KOH	105
					$90\ F\,g^{-1}$ @ $1\ A\,g^{-1}$	—	2 M KOH	
30	Co	H_2OBA, bpfb	—	$170\ m^2\,g^{-1}$	$330\ F\,g^{-1}$ @ $5\ A\,g^{-1}$	—	2 M KOH	106
31	Co	H_2OBA, bpfb	—	$86\ m^2\,g^{-1}$	$636.6\ F\,g^{-1}$ @ $5\ A\,g^{-1}$	94% @ $7\ A\,g^{-1}$ (6000)	2 M KOH	106
32	Co	$1,4\text{-}H_2NH_2BDC$, bpdb	—	—	$325\ F\,g^{-1}$ @ $5\ A\,g^{-1}$	92.03% @ $5\ A\,g^{-1}$ (6000)	6 M KOH	107
					$237.5\ F\,g^{-1}$ @ $5\ A\,g^{-1}$	—	4 M KOH	
					$168.7\ F\,g^{-1}$ @ $5\ A\,g^{-1}$	—	2 M NaOH	
					$106.5\ F\,g^{-1}$ @ $5\ A\,g^{-1}$	—	2 M KOH	
33	Co	$2,5\text{-}H_2PDC$, tpp	—	$1167.3\ m^2\,g^{-1}$	—	78.1% @ $3\ A\,g^{-1}$ (1500)	2 M KOH	108
34	Co	$2,5\text{-}H_2PDC$, tpt	—	$1192.9\ m^2\,g^{-1}$	—	76.1% @ $3\ A\,g^{-1}$ (1500)	2 M KOH	108

(Continues)

TABLE 3 (Continued)

	Metal	Ligand	Composited with	Surface area[a]	Specific capacitance[b]	Cycling stability[b,c]	Electrolyte[d]	Reference
35	Co	H$_2$SDBA, tppa	—	—	75.7 F g^{-1} @ 0.5 A g^{-1}	94% @ 1 A g^{-1} (3000)	3 M KOH	97
36	Co	H$_3$BTC	—	601.7 m^2 g^{-1}	187.3 F g^{-1} @ 0.25 A g^{-1}	72.7% @ 0.25 A g^{-1} (2000)	1 M KOH	109
37	Co	H$_3$BTC	GNS	577.1 m^2 g^{-1}	608.2 F g^{-1} @ 0.25 A g^{-1}	94.9% @ 0.25 A g^{-1} (2000)	1 M KOH	109
38	Co	H$_3$BTC	—	31.98 m^2 g^{-1}	958.1 F g^{-1} @ 2 A g^{-1}	92.3% @ 10 A g^{-1} (3000)	3 M KOH	110
39	Co	H$_3$BTC	—	2.27 m^2 g^{-1}	622.9 F g^{-1} @ 2 A g^{-1}	—	3 M KOH	110
40	Co	H$_3$BTC	—	1.81 m^2 g^{-1}	428.3 F g^{-1} @ 2 A g^{-1}	—	3 M KOH	110
41	Co	H$_3$BTC	—	3.84 m^2 g^{-1}	393.4 F g^{-1} @ 2 A g^{-1}	—	3 M KOH	110
42	Co	H$_3$BTC	—	5.73 m^2 g^{-1}	654.4 F g^{-1} @ 2 A g^{-1}	—	3 M KOH	110
43	Co	H$_3$BTC	—	31.98 m^2 g^{-1}	649.8 F g^{-1} @ 0.25 A g^{-1}	>85% @ 5 A g^{-1} (2000)	3 M KOH	111
44	Co	H$_3$BTC	—	93.61 m^2 g^{-1}	952.5 F g^{-1} @ 0.25 A g^{-1} 1240.4 F g^{-1} @ 5 mV s^{-1}	>85% @ 5 A g^{-1} (2000)	3 M KOH	111
45	Co	H$_3$BTC	—	65.27 m^2 g^{-1}	322.1 F g^{-1} @ 0.25 A g^{-1}	>85% @ 5 A g^{-1} (2000)	3 M KOH	111
46	Co	H$_3$BTC	—	83.47 m^2 g^{-1}	495.6 F g^{-1} @ 0.25 A g^{-1}	>85% @ 5 A g^{-1} (2000)	3 M KOH	111
47	Co	H$_3$TATBA	—	203.7 m^2 g^{-1}	512 F g^{-1} @ 1 A g^{-1}	97.4% @ 10 A g^{-1} (40 000)	3 M KOH	112
48	Co	H$_3$TACTBA	—	—	300 F g^{-1} @ 1 A g^{-1}	94% @ 1 A g^{-1} (1000)	0.1 M TEABF$_4$ in ACN	113
49	Co	H$_3$TATB, dib	—	6.96 m^2 g^{-1}	323 F g^{-1} @ 0.75 A g^{-1} 262 F g^{-1} @ 10 mV s^{-1}	—	6 M KOH	114
50	Co	H$_3$TATB, dib	—	13.66 m^2 g^{-1}	1394 F g^{-1} @ 0.75 A g^{-1} 1443 F g^{-1} @ 2 mV s^{-1}	92.2% @ 10 mV s^{-1} (3000)	6 M KOH	114
					2405 F g^{-1} @ 0.75 A g^{-1}	93.5% @ 10 mV s^{-1} (3000)	4 M KOH	
					497 F g^{-1} @ 0.75 A g^{-1}	81.5% @ 10 mV s^{-1} (3000)	1 M KOH	
51	Co	H$_3$TATB, o-bib	—	13.5 m^2 g^{-1}	2572 F g^{-1} @ 2 A g^{-1} 1757 F g^{-1} @ 2 mV s^{-1}	89.5% @ 25 A g^{-1} (3000) 90.8% @ 50 mV s^{-1} (3000)	6 M KOH	115
52	Co	H$_3$TATB, m-bib	—	9.8 m^2 g^{-1}	502 F g^{-1} @ 2 A g^{-1} 620 F g^{-1} @ 2 mV s^{-1}	91.4% @ 6 A g^{-1} (3000) 93.9% @ 50 mV s^{-1} (3000)	6 M KOH	115
53	Co	H$_3$TATB, m-bib	—	12.6 m^2 g^{-1}	1069 F g^{-1} @ 2 A g^{-1} 1023 F g^{-1} @ 2 mV s^{-1}	93.6% @ 20 A g^{-1} (3000) 95.8% @ 50 mV s^{-1} (3000)	6 M KOH	115
54	Co	TCPP	CNT	—	1016 F g^{-1} @ 2 A g^{-1}	—	6 M KOH	116
55	Co	TCPP	GO	—	668 F g^{-1} @ 2 A g^{-1}	—	6 M KOH	116
Cobalt 3-methylimidazolate MOFs (ZIF-67)								
56	Co	mIM	—	1521 m^2 g^{-1}	—	—	—	117
57	Co	mIM	Ni$_2$CO$_3$(OH)$_2$	232.0 m^2 g^{-1}	1029 F g-1 @ 5 mA cm^{-2} 1037 F g^{-1} @ 5 mV s^{-1}	79.8% @ 10 mV s^{-1} (1600)	6 M KOH	69

TABLE 3 (Continued)

	Metal	Ligand	Composited with	Surface area[a]	Specific capacitance[b]	Cycling stability[b,c]	Electrolyte[d]	Reference
58	Co	mIM	NiC_2O_4	261.1 m² g⁻¹	1019.7 F g⁻¹ @ 5 mV s⁻¹	73% @ 10 mV s⁻¹ (2000)	6 M KOH	118
59	Co	mIM	—	450 m² g⁻¹	1.47 mF cm⁻² @ 10 mV s⁻¹	—	3 M KCl	119
60	Co	mIM	PANI	73 m² g⁻¹	371 F g⁻¹ @ 10 mV s⁻¹ 2146 mF cm⁻² @ 10 mV s⁻¹	—	3 M KCl	119
61	Co	mIM	rGO	—	210 F g⁻¹ @ 1 A g⁻¹	80% @ 10 A g⁻¹ (1000)	6 M KOH	120
62	Co	mIM	—	—	219.7 mF cm⁻² @ 10 mV s⁻¹ 36.62 mF g⁻¹ @ 10 mV s⁻¹	—	3 M KCl	121
63	Co	mIM	PANI	—	1922 mF cm⁻² @ 10 mV s⁻¹ 427.11 mF g⁻¹ @ 10 mV s⁻¹	—	3 M KCl	121
64	Co	mIM	CNT	1194 m² g⁻¹	578.3 mF cm⁻² @ 10 mV s⁻¹ 128.5 mF g⁻¹ @ 10 mV s⁻¹	—	3 M KCl	121
65	Co	mIM	PANI, CNT	—	162.5 mF cm⁻² @ 0.5 mA cm⁻² 3511 mF cm⁻² @ 10 mV s⁻¹ 585.17 mF g⁻¹ @ 10 mV s⁻¹	83% @ 0.5 mA cm⁻² (1000)	3 M KCl	121
66	Co	mIM	PPy	1545.2 m² g⁻¹	417.5 F g⁻¹ @ 0.5 A g⁻¹	—	1 M Na₂SO₄	122
67	Co	mIM	PPy	1168.1 m² g⁻¹	554.4 F g⁻¹ @ 0.5 A g⁻¹ 2.33 F cm⁻² @ 0.4 mA cm⁻²	90.7% @ 20 A g⁻¹ (10 000)	1 M Na₂SO₄	122
68	Co	mIM	PPy	877.4 m² g⁻¹	514.5 F g⁻¹ @ 0.5 A g⁻¹	—	1 M Na₂SO₄	122
69	Co	mIM	PPy	518.8 m² g⁻¹	470.8 F g⁻¹ @ 0.5 A g⁻¹	—	1 M Na₂SO₄	122
70	Co	mIM	POAP	—	724 F g⁻¹ @ —	>90% @ — (1000)	0.1 M HClO₄	123
71	Co	mIM	GO	—	825 F g⁻¹ @ 2 A g⁻¹	90% @ 10 A g⁻¹ (1000)	0.1 M HClO₄	124
72	Co	mIM	rGO	571 m² g⁻¹	1543 F g⁻¹ @ 4.5 A g⁻¹ 562 F g⁻¹ @ 5 mV s⁻¹ 46.5 F g⁻¹ @ 5 mV s⁻¹	90.5% @ — (1000)	0.2 M $K_3[Fe(CN)_6]$ in 1 M Na₂SO₄	125
73	Co	mIM	—	—	66 mF cm⁻² @ 20 mA cm⁻² 37 F g⁻¹ @ 20 mA cm⁻²	—	1 M Na₂SO₄	126
74	Co	mIM	PPy	—	180.2 mF cm⁻² @ 20 mA cm⁻² 284.3 F g⁻¹ @ 20 mA cm⁻²	100.7% @ 5 mA cm⁻² (40 000)	6 M KOH	126
75	Co	mIM	GO	763.06 m² g⁻¹	70.76 F g⁻¹ @ 1 A g⁻¹ 100.41 F g⁻¹ @ 5 mV s⁻¹	150% @ 10 A g⁻¹ (1000)	6 M KOH	127
76	Co	mIM	PPy, BC	11.40 m² g⁻¹	1.15 F cm⁻² @ 0.4 mA cm⁻² 163.3 F cm⁻³ @ 0.4 mA cm⁻²	—	1 M H₂SO₄	128
77	Co	mIM	PPy, BC, polydopamine	12.58 m² g⁻¹	209.09 F g⁻¹ @ 1.82 A g⁻¹	71.04% @ 2 mA cm⁻² (5000)	1 M H₂SO₄	128

(Continues)

TABLE 3 (Continued)

Metal	Ligand	Composited with	Surface area[a]	Specific capacitance[b]	Cycling stability[b,c]	Electrolyte[d]	Reference
78 Co	mIM	PEDOT	$1926\ m^2\ g^{-1}$	$1.71\ F\ cm^{-2}$ @ $0.4\ mA\ cm^{-2}$ $244.29\ F\ cm^{-3}$ @ $0.4\ mA\ cm^{-2}$ $107\ F\ g^{-1}$ @ $1\ A\ g^{-1}$ $107\ F\ g^{-1}$ @ $5\ mV\ s^{-1}$	85% @ $20\ A\ g^{-1}$ (2000)	$1\ M\ H_2SO_4$	129
Others							
79 Co	L-ascorbic acid,$PMo_{10}V_2O_{40}$	—	—	—	79.5% @ $10\ A\ g^{-1}$ (5000)	$6\ M\ KOH$	130
80 Co	L-ascorbic acid, $H_5PMo_{10}V_2O_{40}$	rGO	$13.8\ m^2\ g^{-1}$	—	83% @ $10\ A\ g^{-1}$ (5000)	$6\ M\ KOH$	130
81 Co	L-ascorbic acid, $H_5PMo_{10}V_2O_{40}$	rGO	$18.2\ m^2\ g^{-1}$	$178\ F\ g^{-1}$ @ $0.5\ A\ g^{-1}$	94% @ $10\ A\ g^{-1}$ (5000)	$6\ M\ KOH$	130
82 Co	TBImPc	—	—	$11.04\ F\ g^{-1}$ @ $5\ mV\ s^{-1}$	—	$0.5\ M\ H_2SO_4$	131
83 Co	TBImPc	rGO	—	$25.95\ F\ g^{-1}$ @ $5\ mV\ s^{-1}$	—	$0.5\ M\ H_2SO_4$	131
84 Co	TAPBImPc	—	—	$11.33\ F\ g^{-1}$ @ $5\ mV\ s^{-1}$	—	$0.5\ M\ H_2SO_4$	131
85 Co	TAPBImPc	rGO	—	$34.91\ F\ g^{-1}$ @ $5\ mV\ s^{-1}$	—	$0.5\ M\ H_2SO_4$	131

Abbreviations: ACN, acetonitrile; BC, bacterial cellulose; GNS, graphene nanosheet; GO, graphene oxide; mIM, 2-methylimidazole; PANI, polyaniline; PEDOT, poly(3,4-ethylene dioxythiophene); POAP, poly(ortho-aminophenol); PPy, polypyrrole; rGO, reduced graphene oxide; TEABF$_4$, tetraethylammonium tetrafluoroborate.

[a]Determined by BET method.

[b]Obtained by either CP and GCD method at specific current densities or CV method at specific scan rates.

[c]Evaluated by the capacitance retention after a number of charge/discharge cycles, which are shown in brackets.

[d]Normally in water except for those with special clarification.

TABLE 4 Summary of SC electrode performances of cobalt-organic compounds

Positive electrode Metal	Ligand	Composited with	Negative electrode	Specific capacitance[a]	Energy density and power density[b]	Cycling stability[a,c]	Electrolyte[d]	Reference
Cobalt polycarboxylate MOFs								
18 Co	H_2BDC	—	AC	265 F g^{-1} @ 0.5 A g^{-1}; 13.6 mF g^{-1} @ 2 mA cm^{-2}	1.7 mWh cm^{-2} @ 4.0 mW cm^{-2}	69.7% @ 50 mA cm^{-2} (2000)	2 M KOH	103
31 Co	H_2OBA, bpfb	—	AC	64.1 F g^{-1} @ 5 A g^{-1}	25.73 Wh kg^{-1} @ 849.8 W kg^{-1}; 13.45 Wh kg^{-1} @ 2549.3 W kg^{-1}	91.8% @ 5 A g^{-1} (6000)	2 M KOH	25
32 Co	1,4-H_2NH_2BDC, bpdb	—	AC	39.1 F g^{-1} @ 3 A g^{-1}	50.30 Wh kg^{-1} @ 2.31 kW kg^{-1}; 32 Wh kg^{-1} @ 8 kW kg^{-1}	90.7% @ 5 A g^{-1} (6000)	6 M KOH	104
37 Co	H_3BTC	GNS	37	183.2 F g^{-1} @ 0.25 A g^{-1}	49.8 Wh kg^{-1} @ 1025.8 W kg^{-1}; 26.7 Wh kg^{-1} @ 2049.7 W kg^{-1}	92.2% @ 0.25 A g^{-1} (5000)	1 M KOH	27
86 Co	TCPP, bipy	—	86	184.2 F cm^{-2} @ 1 mA cm^{-2}	—	—	1 M H_2SO_4	132
87 Co	TCPP, bipy	—	87	656.6 F cm^{-2} @ 1 mA cm^{-2}	11.7 mWh cm^{-2} @ 986 mW cm^{-2}	92.5% @ 1 mA cm^{-2} (2600)	1 M H_2SO_4	132
88 Co	TCPP, bipy	—	88	419.6 F cm^{-2} @ 1 mA cm^{-2}	—	—	1 M H_2SO_4	132
89 Co	TCPP, bipy	—	89	426.5 mF cm^{-2} @ 1.2 mA cm^{-2}; 22.45 F cm^{-3} @ 1.2 mA cm^{-2}	1.87 mWh cm^{-3} @ 0.25 W cm^{-3}	93.3% @ 2.4 mA cm^{-2} (3000) (flat); 93.9% @ 2.4 mA cm^{-2} (3000) (bending 180°)	PVA/H_2SO_4	132
Cobalt 3-methylimidazolate MOFs (ZIF-67)								
56 Co	mIM	—	56	2.61 mF cm^{-2} @ 0.42 mA cm^{-2}; 10.45 mF cm^{-2} @ 10 mV s^{-1}	0.42 mWh cm^{-2} @ 1.60 mW cm^{-2}; 0.18 mWh cm^{-2} @ 2.08 mW cm^{-2}	67% @ 0.2 mA cm^{-2} (600)	1 M TBMAMS in ACN	117

(Continues)

TABLE 4 (Continued)

Positive electrode

Metal	Ligand	Composited with	Negative electrode	Specific capacitance[a]	Energy density and power density[b]	Cycling stability[a,c]	Electrolyte[d]	Reference
60 Co	mIM	PANI	**60**	35 mF cm^{-2} @ 0.05 mA cm^{-2} 116 mF cm^{-3} @ 0.05 mA cm^{-2}	0.0044 mWh cm^{-2} @ — @ 0.245 W cm^{-2} 0.0161 mWh cm^{-3} @ — @ 0.833 W cm^{-3}	80% @ 0.05 mA cm^{-2} (2000)	PVA/H$_2$SO$_4$	119
67 Co	mIM	PPy	**67**	225.8 mF cm^{-2} @ 0.4 mA cm^{-2}	0.0113 mWh cm^{-2} @ 0.12 mW cm^{-2} 0.0076 mWh cm^{-2} @ 1.44 mW cm^{-2}	—	PVA/Na$_2$SO$_4$	122
72 Co	mIM	rGO	**72**	326 F g^{-1} @ 3 A g^{-1}	25.5 Wh kg^{-1} @ 2.7 kW kg^{-1}	88.8% @ — (1000)	0.2 M K$_3$[Fe(CN)$_6$] in 1 M Na$_2$SO$_4$	125
77 Co	mIM	PPy, BC, polydopamine	**77**	1.12 F cm^{-2} @ 0.8 mA cm^{-2}	89.8 µWh cm^{-2} @ 0.31 mW cm^{-2}	68.9% @ 10 mA cm^{-2} (5000)	PVA/H$_2$SO$_4$	128
78 Co	mIM	PEDOT	**78**	123 F g^{-1} @ 0.5 A g^{-1}	11 Wh kg^{-1} @ 200 W kg^{-1}	93% @ 20 A g^{-1} (2000)	PVA/H$_2$SO$_4$	129
Others								
81 Co	L-ascorbic acid, H$_5$PMo$_{10}$V$_2$O$_{40}$	rGO	AC	44.6 F g^{-1} @ 10 A g^{-1}	20.1 Wh kg^{-1} @ 927 W kg^{-1} — @ 9071 W kg^{-1}	90.1% @ 10 A g^{-1} (5000)	2 M KOH	130
90 Co	BTA	—	**90**	23.1 F cm^{-3} @ 50 mV s^{-1}	1.6 mWh cm^{-3} @ — @ 1056 W cm^{-3}	96.3% @ 50 V s^{-1} (10 000)	PVA/H$_2$SO$_4$	133
91 Co	BTA	—	**91**	22.0 F cm^{-3} @ 50 mV s^{-1}	—	—	PVA/H$_2$SO$_4$	133
92 Co	iCBA	—	**92**	34.1 F cm^{-3} @ 50 mV s^{-1}	4.7 mWh cm^{-3} @ — @ 1323 W cm^{-3}	86.4% @ 50 mV s^{-1} (350)	PVA/H$_2$SO$_4$	134

Abbreviation: TBMAMS, tributylmethylammonium methyl sulphate.

[a]Obtained by either CP and GCD method at specific current densities, or CV method at specific scan rates.

[b]Data of maximum energy densities and maximum power densities are underlined.

[c]Evaluated by the capacitance retention after a number of charge/discharge cycles, which are shown in brackets.

[d]Normally in water except for those with special clarification.
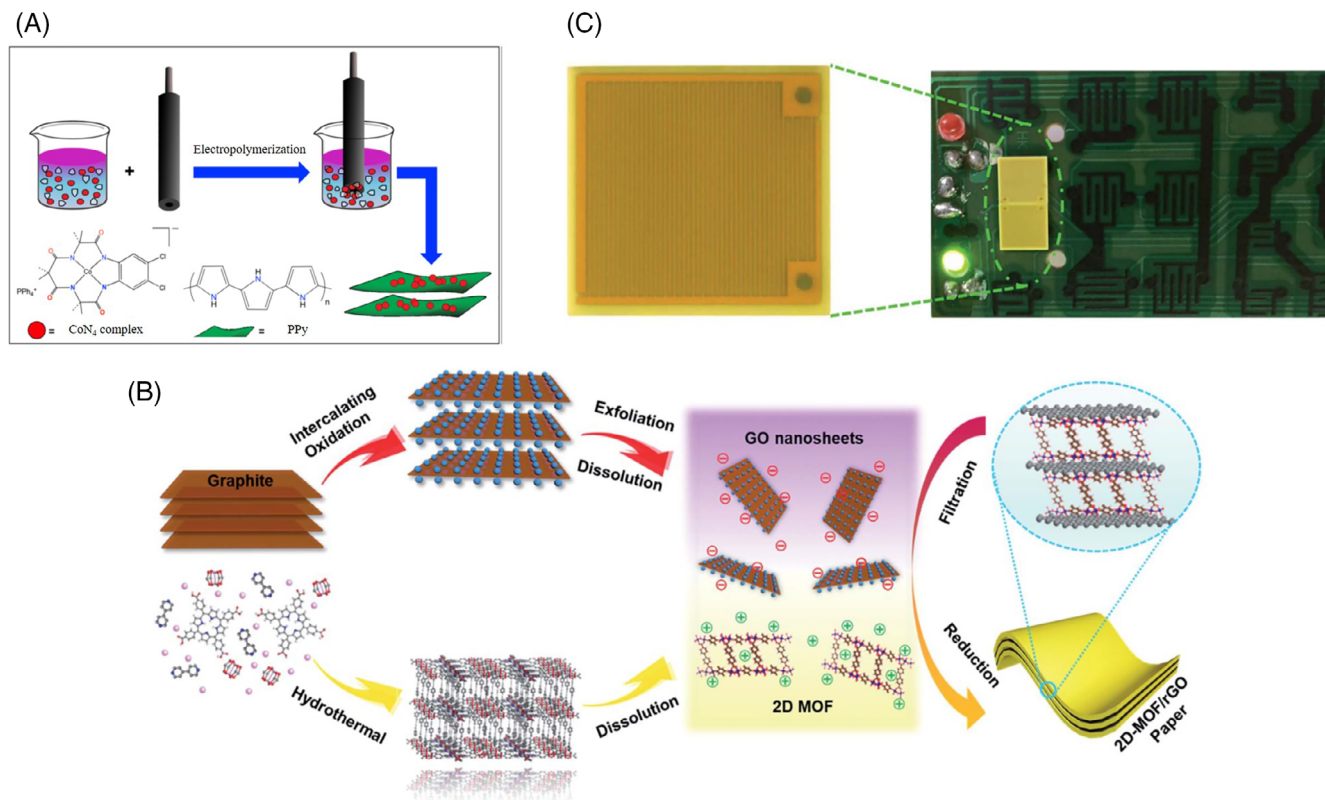
FIGURE 6 A, Schematic illustration of electrochemical deposition of PPy films using pyrrole and CoN$_4$ complex (**12**). Reproduced with permission: Copyright 2021, Springer Nature Limited.[98] B, Schematic illustration of the synthesis route of the 2D-MOF/rGO (**86-89**) and fabrication of the flexible 2D-MOF/rGO hybrid through an electrostatic self-assembly route. Reproduced with permission: Copyright 2018, The Royal Society of Chemistry.[132] C, Integrated micro-SCs and two SCs mounted into a printed circuit board to power up an LED. Reproduced with permission: Copyright 2018, The Royal Society of Chemistry[132]

Polycarboxylate ligands (**13-55, 86-89**) and 3-methylimidazole (**56-78**) are two species of the most common ligands used in cobalt-organic compounds which exhibit SC properties. Similar to manganese-organic compounds, the pseudocapacitance of cobalt-organic compounds can also be ascribed by their surface redox reactions,[72] and their conversion process in aqueous electrolytes can be expressed by the following equations:

$$Co(II)_s + OH^- \leftrightarrow Co(II)(OH)_{ad} + e^-, \quad (17)$$

$$Co(II)(OH)_{ad} \leftrightarrow Co(III)(OH)_{ad} + e^-. \quad (18)$$
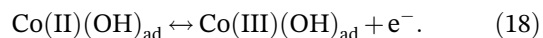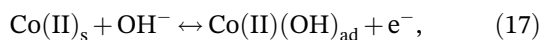
Parnell and coworkers first studied a conductive electrode film (Figure 6A) using macrocyclic Co(III) N$_4$ complex (**12**) and PPy by electrodeposition which demonstrated a superior SC performance,[98] which reached a high C_g value of 721.9 F g^{-1} in acid electrolyte and exhibited high cycling stability with 93% retention after 500 cycles. So far, this was the only work which reported the application of molecular cobalt-organic complex in SCs.

Cobalt polycarboxylate MOFs are the most popular cobalt-organic compounds as electrode materials in SCs.[25,27,50,67,72,73,97,99-116,132] H$_2$BDC (Figure 4A) is one of the most typical polycarboxylate ligands and has been widely used to fabricate SC electrodes based on Co-MOFs and their composites (**13-16, 18, 19, 25**). In 2012, Lee and coworkers first reported Co-BDC MOF (**14**) which showed the high cycling stability with only 1.5% capacitance loss after 1000 cycles.[99] They further extended the ligands to H$_2$NDC (**20**) and H$_2$BPDC (**21**) in 2013 and revealed that the molecular length of organic linkers can be used to manipulate the pore size, surface area and C_g value of MOFs.[67] More impressively, Yang and coworkers reported a layered Co-BDC MOF (**15**) with nanosheet morphology showing an ultrahigh C_g of 2564 F g^{-1}.[101] To further evaluate the practicality of Co-BDC MOF, Zhu and coworkers fabricated an ASC (Co-MOF/NF//AC) by employing Co-BDC (**18**) as the positive electrode and AC as the negative electrode, which delivered a high energy density of 1.7 mW h cm^{-2} at a power density of 4.0 mW cm^{-2} with a capacitance retention of nearly 69.70% after 2000 cycles.[103] Another typical polycarboxylate ligand is H$_3$BTC (**36-46**). Punde and coworkers

synthesized highly porous Co-BTC MOF (**36**) and prepared their hybrid composites (**37**) with graphene nanosheet.[109] A SSC device was assembled from two identical electrodes made of **37** and provided a maximum energy density of 49.8 Wh kg^{-1} at a power density of 1025.8 kW kg^{-1}, while the energy density remained to be 26.7 Wh kg^{-1} along with a higher power density of 2049.7 W kg^{-1}.[109] Ramachandran and coworkers demonstrated a systematic investigation on the synthesis of Co-BTC MOFs (**38-42**) of different structures and sizes in various solvents,[110] and Xuan and coworkers conducted another systematic study of temperature influence on the synthesis of Co-BTC MOF (**43-46**).[111] Among the systematic studies on Co-BTC MOFs, it manifested that there is a positive correlation between specific capacitance and surface area of the MOFs when they were synthesized under similar conditions.

Meanwhile, H$_2$BDC and H$_3$BTC derivatives (Figure 4A) also have attracted wide research interest as ligands for the synthesis of Co-MOFs, which exhibited excellent SC performances (**17**, **20-24**, **26-35**, **47-55**). A 2D layered Co-MOF (**24**) with H$_2$F$_4$BDC (Figure 4A) ligand reported by Liu and coworkers reached a high C_g value of 2474 F g^{-1}.[72] Dong and coworkers synthesized five Co-MOFs (**26-29**) based on 3,6-bis(benzimidazol-1-yl) pyridazine and different polycarboxylate ligands by changing the reaction conditions and studied their molecular structures and electrochemical behaviors.[105] Wang and coworkers reported another Co-MOF with H$_3$TATB (Figure 4A) ligand and found that the electrode with nanorod Co-MOF (**50**) could deliver a higher C_g (2405 F g^{-1}) than that of the bulk crystal state (**49**, 323 F g^{-1}).[114] Wang's group also synthesized a series of interpenetrated and extended 2D layered Co-MOFs (**51-53**) by using H$_3$TATB and varying the flexible N-donor ligands and inorganic anions.[115] The maximum C_g of the electrode based on **51** reached 2572 F g^{-1}, which, to the best of our knowledge, has been the highest value so far among all the cobalt- and other metal-organic compounds. The capacitance of pristine **51** was comparable to the recently reported Fe-, Ni- and Co-coordination polymer electrodes, and also superior to those of the reported metal oxide electrodes and hybrid electrodes which were derived from metal-coordination polymers. Cheng and coworkers fabricated bending-tolerant and highly conductive 2D-MOF/rGO papers through the electrostatic self-assembly of intrinsically electronegative GO sheets and electropositive MOF sheets (**86-89**, Figure 6B).[132] More importantly, the all-solid-state ASCs based on **86** to **89** offer high editability and bending-tolerance properties, and perform very well under various severe conditions, for example, when they are being seriously cut, bent and heavily loaded. In this work, two integrated

devices composed of the comb-like ASCs were connected with a LED in series, and the SCs could power up the LEDs to deliver a dazzling light after being charged for several seconds (Figure 6C).

Another popular type of Co-MOFs is ZIFs which show an attractive electrochemical property. They are ideal for the storage of charges in the electrical double layer due to their intrinsically high surface area and the combination of the advantages of MOFs with high stability and framework diversity.[69,117] ZIF-67, a Co-MOF with the linker of 3-methylimidazolate (mIM), and its composites (**56-78**) have gained an increasing attention in recent years for the application in SCs.[69,117-128] In 2016, Worrall and coworkers reported the pristine ZIF-67 (**56**) with a high surface area of 1521 m^2 g^{-1} as electrode materials for SC application,[117] which has exceeded the surface areas for other Co-polycarboxylate MOFs from 1.81 to 1192.9 m^2 g^{-1}. Gao and coworkers first reported the SC electrode performance of two ZIF-67 composites (**57** and **58**) with nickel-based inorganic salts (Ni$_2$CO$_3$(OH)$_2$ and NiC$_2$O$_4$), both of which had the surface areas over 200 m^2 g^{-1} and delivered the C_g values over 1000 F g^{-1}.[69,118] Wang and coworkers developed the flexible composites (**63-65**) of PANI, CNT and ZIF-67 as SC electrodes, which owned the advantages of good electroactivity, high electroconductivity and hierarchical porous nanostructures.[121] Notably, **65** as electrode materials presented an ultrahigh C_a of 3511 mF cm^{-2} at 10 mV s^{-1}, which are so far the highest C_a value among all reported Co-MOFs. Another ZIF-67 composite without the CNT component, abbreviated as PANI-ZIF-67-CC (**60**), also delivered a high C_a value of 2146 mF cm^{-2}.[119] Xu and coworkers synthesized a series of ZIF-PPy composites (**66-69**, Figure 7C) with different mass ratios of ZIF-67 and PPy tubes.[122] Although the surface areas of these composites decreased (1545.2, 1168.1, 877.4 and 518.8 m^2 g^{-1} for **66**, **67**, **68** and **69**, respectively) with the increase of PPy tube mass ratios (17, 28, 37 and 49% for **66**, **67**, **68** and **69**, respectively), the sample with the highest C_g (**67**) was not the composites with the highest surface area (**66**). It was assumed that the pseudocapacitance of PPy tubes would be hardly affected before and after interweaving the ZIF particles, because the ZIF-67 particles do not change the structural and intrinsic properties of PPy tubes as the PPy tubes just serve as the support for the growth of ZIF-67 particles, and there are no strong chemical interfacial interactions between PPy tubes and ZIF-67 particles.[122] This work demonstrated that the capacitance of ZIF-67 can be increased remarkably after integrating with PPy tubes, and the value can be maximized by adjusting the proportion of the PPy substrates. Another ZIF-67 and PPy composites were reported by Liu and coworkers, where the CC/ZIF-67/PPy composite (**74**) electrodes were prepared through electrochemical deposition technology.[126] Impressively, the capacitance retention of electrode based on

FIGURE 7 A, The structure of the monomers CoTBImPc (**82**) and CoTAPBImPc (**84**).[131] B, Synthesis of PiCBA (**92**) through the coordination reaction between isocyanide and cobalt ions ($R = COOC_2H_5$) and TEM image of **92** on a copper grid. Reproduced with permission: Copyright 2017, Wiley-VCH Verlag GmbH & Co. KGaA, Weinheim.[134] C, Schematic illustration of LBL fabrication of **92** on Au interdigital electrodes. Reproduced with permission: Copyright 2017, Wiley-VCH Verlag GmbH & Co. KGaA, Weinheim[134]
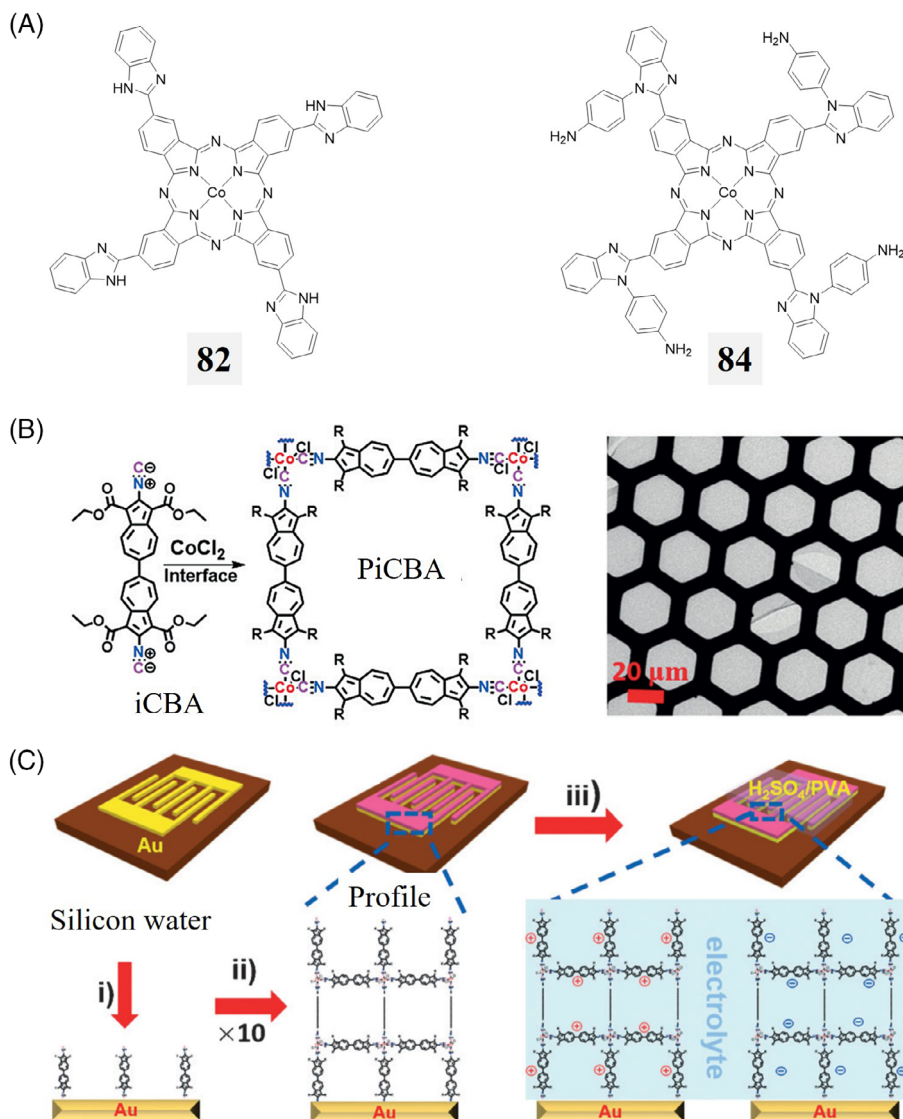
74 was found to be 100.7% after 40 000 cycles, exceeding their original capacitance. An optimized specific capacitance after ~5000 cycles and high long-term cycling stability after 40 000 cycles for **74** as the electrode materials can be realized. The PPy not only firmly adheres to the interspace of CC/ZIF-67 particles, but also forms a thin film on the surfaces of ZIF-67 successfully. The relatively low capacitance before cycles can be explained by the assumption that some Co^{2+} may be entrapped by the PPy film in a deep position and released as the charge/discharge test begins.[126] Sundriyal and coworkers found that the ZIF-67/rGO composites (**72**) could deliver over 10 times higher capacitances with an optimized redox additive electrolyte (562 F g^{-1} at 5 mV s^{-1}) than that in the simple aqueous electrolyte (46.5 F g^{-1} at 5 mV s^{-1}).[125] Moreover, **72** can realize a high C_g value more than 1500 F g^{-1} when tested by the CP method at a current density of 4.5 A g^{-1}.

Besides Co-MOFs with polycarbonate and imidazolate ligands, there are also reports on cobalt coordination polymers based on POMs (**79-81**),[130] phthalocyanine-derivatives (**82-85**, Figure 7A),[131] 1,2,4,5-benzenetetramine (BTA, Figure 9; **90** and **91**),[133] and diisocyano (**92**, Figure 7B)[134] ligands. Hua and coworkers reported that a facile method can be used to construct large scale and highly oriented uniform coordination polymer (Co-BTA, **90** and **91**) thin films.[133] The symmetric micro-SC based on Co-BTA showed a high C_v of 23.1 F cm^{-3} on rigid Si substrates (**90**) and 22.0 F cm^{-3} on flexible polyethylene terephthalate substrates (**91**). Another attempt to fabricate on-chip micro-SCs based on Co-MOF was conducted by Yang and coworkers.[134] The micro-SC based on cobalt coordination polymer frameworks PiCBA (**92**, Figure 7B) prepared by a layer-by-layer approach (Figure 7C) exhibited an ultrahigh C_v of 34.1 F cm^{-3}, which are the highest C_v among all SC devices based on metal-organic compounds, as well as the highest C_v among all reported polymer-based micro-SCs.

TABLE 5 Summary of SC electrode performances of nickel-organic compounds

	Metal	Ligand	Composited with	Surface area[a]	Specific capacitance[b]	Cycling stability[b,c]	Electrolyte[d]	Reference
Nickel polycarboxylate MOFs								
93	Ni	H_2BDC	—	—	1127 F g^{-1} @ 0.5 A g^{-1}	91% @ 2 A g^{-1} (3000)	6 M KOH	135
94	Ni	H_2BDC	—	41.5 m^2 g^{-1}	1765 F g^{-1} @ 0.5 A g^{-1}	93% @ 100 mV s^{-1} (3000)	6 M KOH	136
95	Ni	H_2BDC	—	117.42 m^2 g^{-1}	1021 F g^{-1} @ 0.7 A g^{-1}	96.5% @ 1.4 A g^{-1} (5000)	3 M KOH	137
96	Ni	H_2BDC	—	126.0 m^2 g^{-1}	1457.7 F g^{-1} @ 1 A g^{-1}; 1152.7 F g^{-1} @ 0.01 V s^{-1}	83.4% @ 10 A g^{-1} (3000)	2 M KOH	138
97	Ni	H_2BDC	GO	74.2 m^2 g^{-1}	2192.4 F g^{-1} @ 1 A g^{-1}	85.1% @ 1 A g^{-1} (3000)	2 M KOH	138
98	Ni	H_2BDC	GO	43.37 m^2 g^{-1}	1132.1 F g^{-1} @ 1 A g^{-1}	—	2 M KOH	138
99	Ni	H_2BDC	—	6.578 m^2 g^{-1}	804 F g^{-1} @ 1 A g^{-1}	56.6% @ 10 A g^{-1} (5000)	2 M KOH	139
100	Ni	H_2BDC	—	1904.447 m^2 g^{-1}	432 F g^{-1} @ 1 A g^{-1}	60.5% @ 10 A g^{-1} (5000)	2 M KOH	139
101	Ni	H_2BDC	—	462.35 m^2 g^{-1}	559.42 F g^{-1} @ 1 A g^{-1}	—	3 M KOH	140
102	Ni	H_2BDC	MoS$_2$	857.45 m^2 g^{-1}	1590.24 F g^{-1} @ 1 A g^{-1}	87.97% @ 5 A g^{-1} (20 000)	3 M KOH	140
103	Ni	H_3BTC	—	—	726 F g^{-1} @ 1 A g^{-1}	94.5% @ 1 A g^{-1} (1000)	2 M KOH	141
104	Ni	H_3BTC	—	40.36 m^2 g^{-1}	1057.2 F g^{-1} @ 1 A g^{-1}	70% @ 10 A g^{-1} (2500)	3 M KOH	142
105	Ni	H_3BTC	—	28.28 m^2 g^{-1}	828.2 F g^{-1} @ 1 A g^{-1}	—	3 M KOH	142
106	Ni	H_3BTC	—	23.36 m^2 g^{-1}	581.2 F g^{-1} @ 1 A g^{-1}	—	3 M KOH	142
107	Ni	H_3BTC	—	5.24 m^2 g^{-1}	554.3 F g^{-1} @ 1 A g^{-1}	—	3 M KOH	142
108	Ni	H_3BTC, bipy	S	537.47 m^2 g^{-1}	1453.5 F g^{-1} @ 1 A g^{-1}	89.23% @ 5 A g^{-1} (5000)	3 M KOH	143
109	Ni	H_2OH_2BDC	—	—	0.415 F cm^{-2} @ 0.88 mA cm^{-3}; 0.052 F cm^{-3} @ 0.88 mA cm^{-3}	>80% @ 6.3 mA cm^{-3} (4000)	1 M TEABF$_4$ in ACN	102
110	Ni	H_2ADC, dabco	—	783 m^2 g^{-1}	552 F g^{-1} @ 1 A g^{-1}	—	2 M KOH	74
111	Ni	H_3TATB, bid	—	5.5 m^2 g^{-1}	750 F g^{-1} @ 1 A g^{-1}; 441 F g^{-1} @ 5 mV s^{-1}; 601 F g^{-1} @ 1 A g^{-1}	—	6 M KOH; 1 M KOH	144
112	Ni	H_3TATB, btd	—	3.6 m^2 g^{-1}	666 F g^{-1} @ 1 A g^{-1}; 392 F g^{-1} @ 5 mV s^{-1}; 230 F g^{-1} @ 1 A g^{-1}	—	6 M KOH; 1 M KOH	144
113	Ni	2,5-H_2PDC, tpp	—	1179.5 m^2 g^{-1}	523 F g^{-1} @ 1 A g^{-1}	67.7% @ 3 A g^{-1} (1500)	2 M KOH	108
114	Ni	2,5-H_2PDC, tpt	—	1017.3 m^2 g^{-1}	—	60.1% @ 3 A g^{-1} (1500)	2 M KOH	108
115	Ni	TCPP	CNT	—	2280 F g^{-1} @ 5 A g^{-1}	—	6 M KOH	116
116	Ni	TCPP	GO	—	1490 F g^{-1} @ 5 A g^{-1}	—	6 M KOH	116

TABLE 5 (Continued)

	Metal	Ligand	Composited with	Surface area[a]	Specific capacitance[b]	Cycling stability[b,c]	Electrolyte[d]	Reference
Nickel polyamine/polyphenol MOFs								
117	Ni	CAT	LSG	212 m² g⁻¹	8.5 mF cm⁻² @ 1 mA cm⁻²	81% @ 2 mA cm⁻² (5000)	3 M LiCl	145
118	Ni	CAT	—	—	253 mF cm⁻² @ 1 mA cm⁻² 320 F g⁻¹ @ 1 mA cm⁻²	67% @ — (1000)	1 M KOH	146
119	Ni	CAT	NiCo-LDH	—	3200 mF cm⁻² @ 1 mA cm⁻² 2133 F g⁻¹ @ 1 mA cm⁻²	80% @ — (1000)	1 M KOH	146
120	Ni	CAT	—	—	321.95 F g⁻¹ @ 0.5 A g⁻¹	57% @ 5 A g⁻¹ (5000)	2 M KOH	147
121	Ni	CAT	CNF	543.80 m² g⁻¹	502.95 F g⁻¹ @ 0.5 A g⁻¹	73% @ 5 A g⁻¹ (5000)	2 M KOH	147
122	Ni	EA	—	—	1050 F g⁻¹ @ 0.5 A g⁻¹	89% @ 10 A g⁻¹ (1000)	1 M KOH	148
123	Ni	CAT	CNF	203 m² g⁻¹	75 F g⁻¹ @ 0.2 A g⁻¹	—	3 M KCl	149
124	Ni	HITP	CNF	195 m² g⁻¹	125 F g⁻¹ @ 0.33 A g⁻¹	—	3 M KCl	149
125	Ni	HITP	—	630 m² g⁻¹	111 F g⁻¹ @ 0.05 A g⁻¹ 18 µF cm⁻² @ 0.05 A g⁻¹ 118 F cm⁻³ @ 0.05 A g⁻¹	—	1 M TEABF₄ in ACN	150
126	Ni	HAB	—	—	427 F g⁻¹ @ 0.2 mV s⁻¹ 23 F cm⁻² @ 0.2 mV s⁻¹ 760 F cm⁻³ @ 0.2 mV s⁻¹	90% @ 10 A g⁻¹ (12 000)	1 M KOH	78
127	Ni	HITP	—	732 m² g⁻¹	84 F g⁻¹ @ 5 mV s⁻¹ 11.5 µF cm⁻² @ 5 mV s⁻¹	—	[EMIM][BF₄]	151
				641 m² g⁻¹	75 F g⁻¹ @ 5 mV s⁻¹ 11.7 µF cm⁻² @ 5 mV s⁻¹	—	[EMIM][BF₄]	
				556 m² g⁻¹	66 F g⁻¹ @ 5 mV s⁻¹ 11.9 µF cm⁻² @ 5 mV s⁻¹	—	[EMIM][BF₄]	
Others								
128	Ni	isonicotinic acid	—	148 m² g⁻¹	634 F g⁻¹ @ 5 mV s⁻¹	84% @ 50 mV s⁻¹ (2000)	6 M KOH	152
129	Ni	SA	—	186.8 m² g⁻¹	1698 F g⁻¹ @ 1 A g⁻¹	94.8% @ 1 A g⁻¹ (1000)	6 M KOH	153
130	Ni	H₂ppza	—	—	125 F g⁻¹ @ 0.5 A g⁻¹ 184 F g⁻¹ @ 5 mV s⁻¹	65% @ 1 A g⁻¹ (1000)	2 M KOH	154
131	Ni	TEMPO	—	264 m² g⁻¹	124 F g⁻¹ @ 0.1 A g⁻¹	—	0.1 M TBAP in ACN	155
132	Ni	TEMPO	—	5.2 m² g⁻¹	167 F g⁻¹ @ 0.1 A g⁻¹	—	0.1 M TBAP in ACN	155
133	Ni	salphen	MWCNT	—	200 µF cm⁻² @ 0.1 mA cm⁻²	—	1 M TEMABF₄ in ACN	75

Abbreviations: [EMIM][BF₄], 1-ethyl-3-methylimidazolium tetrafluoroborate; CNF, carbon nanofiber; LDH, layered double hydroxide; LSG, laser scribed graphene; MWCNT, multiwalled carbon nanotube; TBAP, butylammonium perchlorate; TEMABF₄, riethylmethylammonium tetrafluoroborate. SA, salicylic acid.

[a]Determined by BET method.

[b]Obtained by either CP and GCD method at specific current densities or CV method at specific scan rates.

[c]Evaluated by the capacitance retention after a number of charge/discharge cycles, which are shown in brackets.

[d]Normally in water except for those with special clarification.

TABLE 6 Summary of SC electrode performances of nickel-organic compounds

	Positive electrode			Negative electrode	Specific capacitance[a]	Energy density and power density[b]	Cycling stability[a,c]	Electrolyte[d]	Reference
	Metal	Ligand	Composited with						
Nickel polycarboxylate MOFs									
94	Ni	H_2BDC	—	rGO/C_3N_4	103 F g⁻¹ @ 0.5 A g⁻¹	36.6 Wh kg⁻¹ @ 480 W kg⁻¹ / 16 Wh kg⁻¹ @ 19.2 kW kg⁻¹	95% @ 2 A g⁻¹ (5000)	6 M KOH	136
95	Ni	H_2BDC	—	AC	230 mF cm⁻² @ 1.0 mA cm⁻²	4.18 mWh cm⁻³ @ — / — @ 231.2 mW cm⁻³	92.8% @ 5.0 mA cm⁻² (5000)	PVA/KOH	137
99	Ni	H_2BDC	—	AC	95 F g⁻¹ @ 1 A g⁻¹	31.5 Wh kg⁻¹ @ 800 W kg⁻¹ / 16 Wh kg⁻¹ @ 8000 W kg⁻¹	50% @ 4 A g⁻¹ (5000)	2 M KOH	139
102	Ni	H_2BDC	MoS_2	AC	233.4 F g⁻¹ @ 0.5 A g⁻¹	72.93 Wh kg⁻¹ @ 375 W kg⁻¹	94.61% @ 8 A g⁻¹ (10 000)	3 M KOH	140
134	Ni	H_2BDC	CNT	AC	898 mF cm⁻² @ 1 mA cm⁻²; 359 F g⁻¹ @ 1 mA cm⁻²	0.3396 mWh cm⁻² @ — / 4.85 mWh cm⁻³ @ — / 135.84 Wh kg⁻¹ @ —	93% @ 5 mA cm⁻² (4000)	PVA/KOH	156
135	Ni	H_2BDC, btd	—	AC	80.6 F g⁻¹ @ 0.5 A g⁻¹	28.7 Wh kg⁻¹ @ 400 W kg⁻¹	87% @ 3 A g⁻¹ (4000)	—	25
103	Ni	H_3BTC	—	AC	—	16.5 Wh kg⁻¹ @ 2078 W kg⁻¹	—	2 M KOH	141
105	Ni	H_3BTC	—	AC	87 F g⁻¹ @ 0.5 A g⁻¹	21.05 Wh kg⁻¹ @ 0.44 kW kg⁻¹ / 5.36 Wh kg⁻¹ @ 6.03 kW kg⁻¹	70% @ 5 A g⁻¹ (2000)	3 M KOH	142
108	Ni	H_3BTC, bipy	S	AC	136.5 F g⁻¹ @ 1 A g⁻¹	56.86 Wh kg⁻¹ @ 480 W kg⁻¹ / 48.54 Wh kg⁻¹ @ 800 W kg⁻¹	86.67% @ 5 A g⁻¹ (20 000)	3 M KOH	143
136	Ni	H_3BTC	CNT	AC	97.6 F g⁻¹ @ 1 A g⁻¹	44.4 Wh kg⁻¹ @ 440 W kg⁻¹ / 26.1 Wh kg⁻¹ @ 5255 W kg⁻¹	—	3 M KOH	32
110	Ni	H_2ADC, dabco	—	AC	—	—	98% @ 10 A g⁻¹ (16 000)	2 M KOH	74
113	Ni	2,5-H_2PDC, tpp	—	AC	48.4 F g⁻¹ @ 0.5 A g⁻¹	15.1 Wh kg⁻¹ @ 375.8 W kg⁻¹ / 7.2 Wh kg⁻¹ @ 7.5 kW kg⁻¹	—	2 M KOH	108
Nickel polyamine/polyphenol MOFs									
117	Ni	CAT	LSG	117	0.76 mF cm⁻² @ 0.2 mA cm⁻²	4.1 μWh cm⁻² @ — / — @ 7 mW cm⁻²	87% @ 2 mA cm⁻² (5000)	PVA/LiCl	145
119	Ni	CAT	NiCo-LDH	AC	435 mF cm⁻² @ 1 mA cm⁻²	93 μWh cm⁻² @ 18 mW cm⁻²	74% @ 25 mA cm⁻² (1000)	1 M KOH	146
121	Ni	CAT	CNF	AC	68.58 F g⁻¹ @ 0.5 A g⁻¹	18.67 Wh kg⁻¹ @ 297.12 W kg⁻¹ / 12.22 Wh kg⁻¹ @ 6982.86 W kg⁻¹	106.19% @ 5 A g⁻¹ (5000)	2 M KOH	147

TABLE 6 (Continued)

Positive electrode			Negative electrode	Specific capacitance[a]	Energy density and power density[b]	Cycling stability[a,c]	Electrolyte[d]	Reference
Metal	Ligand	Composited with						
				9.53 F cm⁻³ @ 0.5 A g⁻¹	9.53 mWh cm⁻³ @ 41.27 mW cm⁻³	—	PVA/KOH	
122 Ni	EA	—	AC	87.8 F g⁻¹ @ 1 A g⁻¹	31.22 Wh kg⁻¹ @ 800 W kg⁻¹ / 20.6 Wh kg⁻¹ @ 8017 W kg⁻¹	91.8% @ 10 A g⁻¹ (4000)	1 M KOH	148
124 Ni	HITP	CNF	124	141.5 F g⁻¹ @ 0.075 A g⁻¹; 96 mF cm⁻² @ 0.2 mA cm⁻²; 2800 mF cm⁻³ @ 0.2 mA cm⁻²	6.5 mWh cm⁻² @ —; 185.7 mWh cm⁻³ @ —; — @ 0.013 mW cm⁻²; — @ 0.37 mW cm⁻³	90% @ 1 A g⁻¹ (10 000)	PVA/KCl	149
125 Ni	HITP	—	125	117 F g⁻¹ @ 0.1 A g⁻¹	—	90% @ 2 A g⁻¹ (10 000)	Celgard 3501 membrane[150]	150
137 Ni	HITP	—	137	170.36 F g⁻¹ @ 0.1 mA cm⁻²; 15.69 mF cm⁻² @ 0.1 mA cm⁻²	0.049 mWh cm⁻² @ 0.046 W cm⁻²	84.14% @ 1 mA cm⁻² (100 000)	0.5 M Na₂SO₄	157
138 Ni	pPDA	—	GC	184.7 F g⁻¹ @ 1 A g⁻¹	57.5 Wh kg⁻¹ @ 0.75 kW kg⁻¹ / 6.39 Wh kg⁻¹ @ 5.98 kW kg⁻¹	80% @ 8 A g⁻¹ (5000)	1 M KOH	93
Others								
129 Ni	SA	—	graphene	166 F g⁻¹ @ 1 A g⁻¹	—	—	6 M KOH	153
139 and PPy[e] Ni	salen	rGO	poly(C_{60}Pd) and PPy[e]	153 F g⁻¹ @ 0.4 A g⁻¹; 27.2 mF cm⁻² @ 0.07 mA cm⁻²	102.60 Wh kg⁻¹ @ 12.21 kW kg⁻¹; 18.2 μWh cm⁻² @ 2.2 μW cm⁻²	91% @ 5.2 A g⁻¹ (10 000)	0.1 M TBAPF₆ in ACN	158

Abbreviation: TBAPF₆, tetrabutylammonium hexafluorophosphate.

[a]Obtained by either CP and GCD method at specific current densities, or CV method at specific scan rates;
[b]Data of maximum energy densities and maximum power densities are underlined;
[c]Evaluated by the capacitance retention after a number of charge/discharge cycles, which are shown in brackets.
[d]Normally in water except for those with special clarification.
[e]Dual electrodes.
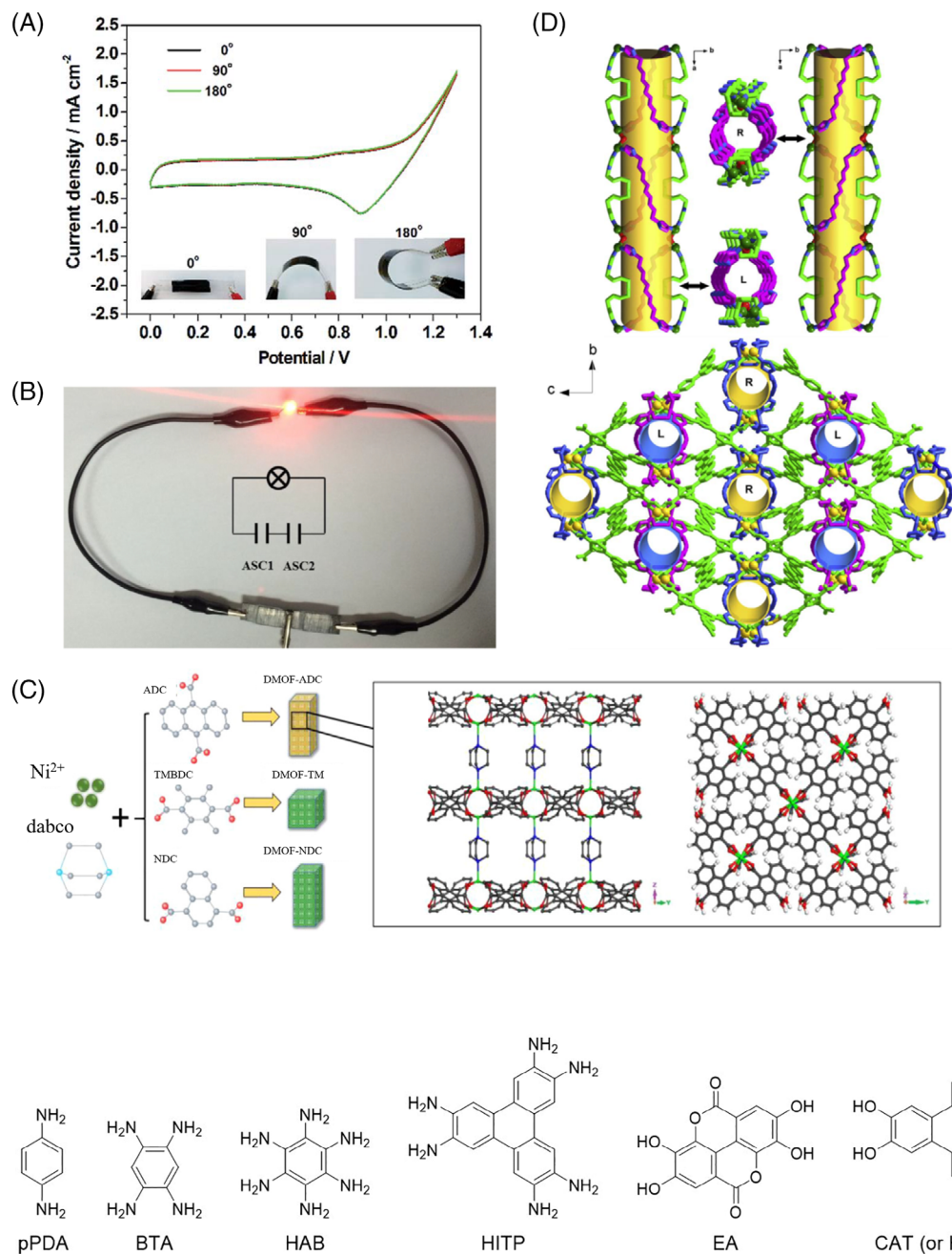
FIGURE 8 A, Cyclic voltammetry of an ASC (**95**) with three bending modes (insets). Reproduced with permission: Copyright 2016, The Royal Society of Chemistry.[137] B, Photograph of a red LED powered by two ASC devices in series. Reproduced with permission: Copyright 2018, Elsevier Inc.[142] C, Schematic illustration of the synthesis process of Ni-MOFs and wireframe view of 3D Ni-DMOF-ADC (**110**). Reproduced with permission: Copyright 2016, Elsevier Ltd.[74] D, Schematic illustration of the left and right helical channels in different directions and the 3D framework helical channels of Ni-MOFs (**111** and **112**). Reproduced with permission: Copyright 2017, Elsevier B.V[144]

FIGURE 9 Polyamine and polyphenol ligands used to construct metal-organic compounds as SC electrode materials

2.3 | Nickel

Nickel-organic compounds and their composites with polycarboxylate (**93-116**), polyamine or polyphenol (**117-127**, **134-138**) and others (**128-133**, **139**) have drawn increasing attention in the field of SCs in recent years.[25,32,74,75,78,93,102,108,116,135-158] Tables 5 and 6 list the electrode and SC performances of nickel-organic compounds. The conversion process of surface redox reactions for nickel-organic compounds can be expressed by the following equations[141]:

$$Ni(II)_s + OH^- \leftrightarrow Ni(II)(OH)_{ad} + e^-, \quad (19)$$

$$Ni(II)(OH)_{ad} \leftrightarrow Ni(III)(OH)_{ad} + e^-. \quad (20)$$
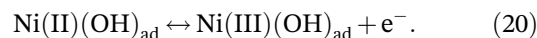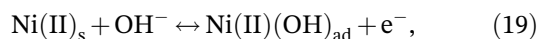
So far, there are still no reports on the SC properties of nickel-organic molecular complexes. Similar to Co-MOFs, Ni-MOFs with polycarboxylate ligands (Figure 4A) and their composites (**93-116**) are the most studied and reported. A Ni-BDC-based ASC (**128**) showed high gravimetric energy density of 135.84 Wh kg^{-1}, and another Ni-BDC-based ASC (**94**) achieved a high

FIGURE 10 A, Schematic illustration of the fabrication process of LSG/Ni-CAT MOF hybrid SC and structure of LSG/Ni-CAT MOF (**117**). Reproduced with permission: Copyright 2019, WILEY-VCH Verlag GmbH & Co. KGaA, Weinheim.[145] B, Schematic illustration of the molecular structure of $Ni_3(HITP)_2$ (**125**) and relative size of pores[150]
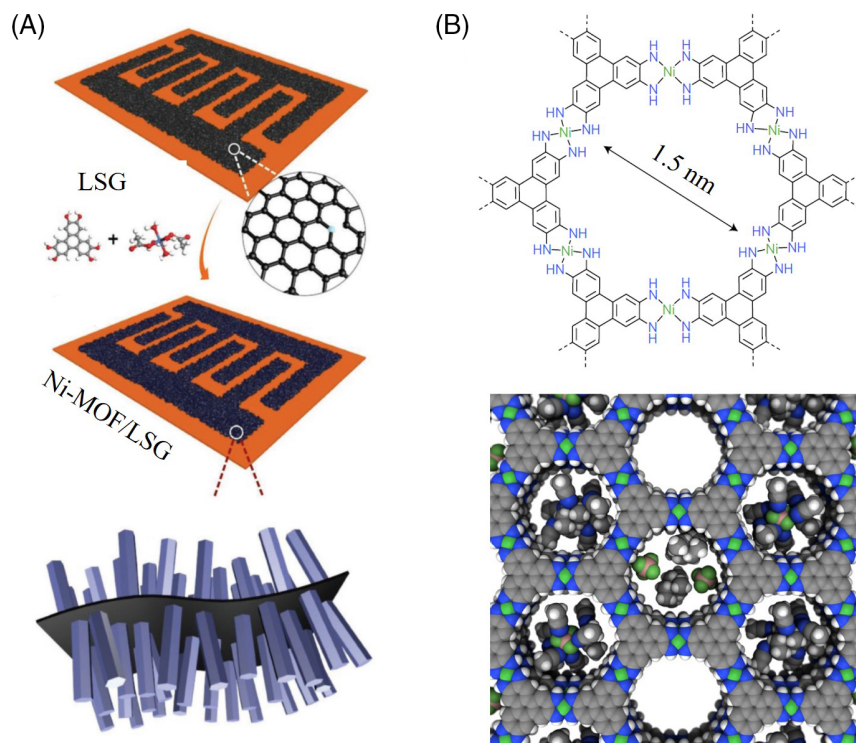
FIGURE 11 A, Synthesis of radical COFs (**131** and **132**). Reproduced with permission: Copyright 2015, WILEY-VCH Verlag GmbH & Co. KGaA, Weinheim.[155] B, The structure of [Ni(salphen)]$_n$ (**133**)[75] and [Ni(salen)]$_n$ (**139**).[158] C, A dual anode and dual cathode setup proposed for the assembled ASC laboratory model. The dual anode: **139** (1) and PPy (2). The dual cathode: poly(C$_{60}$-Pd) (3) and PPy (2′). Reproduced with permission: Copyright 2018, Elsevier Ltd.[158]
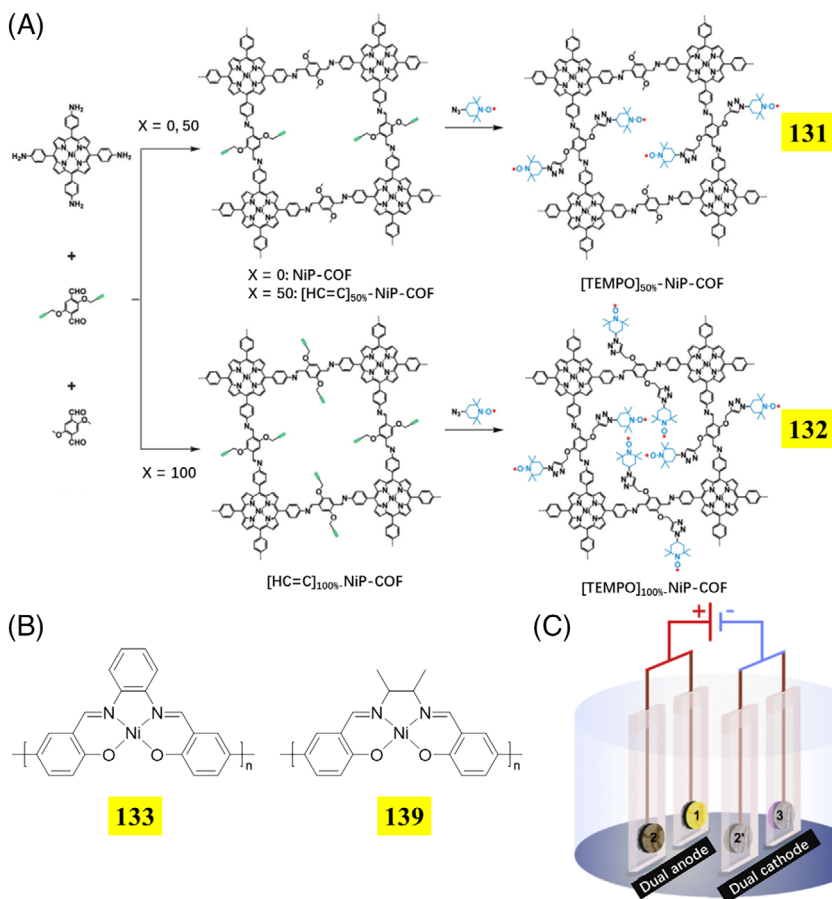
TABLE 7 Summary of SC electrode performances of copper-organic compounds

	Metal	Ligand	Composited with	Surface area[a]	Specific capacitance[b]	Cycling stability[b,c]	Electrolyte[d]	Reference
Copper polycarboxylate MOFs								
140	Cu	H_3BTC	rGO	$1214 \ m^2 \ g^{-1}$	$385 \ F \ g^{-1}$ @ $1 \ A \ g^{-1}$ / $377 \ F \ g^{-1}$ @ $100 \ mV \ s^{-1}$	—	$0.5 \ M \ Na_2SO_4$	159
141	Cu	H_3BTC	PEDOT	—	$81 \ mF \ cm^{-2}$ @ $10 \ mV \ s^{-1}$	—	$3 \ M \ KCl$	160
142	Cu	H_3BTC	PEDOT, GO	—	$105 \ mF \ cm^{-2}$ @ $0.4 \ mA \ cm^{-2}$ / $128 \ mF \ cm^{-2}$ @ $10 \ mV \ s^{-1}$	—	$3 \ M \ KCl$	160
143	Cu	H_3BTC	PPy, GO	—	$111.5 \ mF \ cm^{-2}$ @ $10 \ mV \ s^{-1}$	—	$3 \ M \ KCl$	160
144	Cu	H_3BTC	—	$1316.24 \ m^2 \ g^{-1}$	$85 \ F \ g^{-1}$ @ $1.6 \ A \ g^{-1}$	—	$1 \ M \ Na_2SO_4$	161
145	Cu	H_3BTC	rGO	$1038.71 \ m^2 \ g^{-1}$	$685.33 \ F \ g^{-1}$ @ $1.6 \ A \ g^{-1}$	91.91% @ $1.6 \ A \ g^{-1}$ (1000)	$1 \ M \ Na_2SO_4$	161
146	Cu	H_3BTC	POAP	$36.24 \ m^2 \ g^{-1}$	$422 \ F \ g^{-1}$ @ $400 \ mV \ s^{-1}$	93% @ $1 \ mA \ g^{-1}$ (1000)	$0.1 \ M \ HClO_4$	162
147	Cu	H_3BTC	—	$190 \ m^2 \ g^{-1}$	$70 \ F \ g^{-1}$ @ $1 \ A \ g^{-1}$	—	$6 \ M \ KOH$	163
148	Cu	H_3BTC	PANI	—	$270 \ F \ g^{-1}$ @ $1 \ A \ g^{-1}$	—	$6 \ M \ KOH$	163
149	Cu	H_3BTC	—	$12.2 \ m^2 \ g^{-1}$	$122.8 \ F \ g^{-1}$ @ $1.5 \ A \ g^{-1}$ / $282 \ F \ g^{-1}$ @ $5 \ mV \ s^{-1}$	>84% @ $3 \ A \ g^{-1}$ (3000)	$3 \ M \ KOH$	164
150	Cu	H_3BTC	—	$12.9 \ m^2 \ g^{-1}$	$228 \ F \ g^{-1}$ @ $1.5 \ A \ g^{-1}$ / $462.4 \ F \ g^{-1}$ @ $5 \ mV \ s^{-1}$	89.7% @ $3 \ A \ g^{-1}$ (3000)	$3 \ M \ KOH$	164
151	Cu	H_3BTC	—	$12.4 \ m^2 \ g^{-1}$	$167.6 \ F \ g^{-1}$ @ $1.5 \ A \ g^{-1}$ / $330 \ F \ g^{-1}$ @ $5 \ mV \ s^{-1}$	>84% @ $3 \ A \ g^{-1}$ (3000)	$3 \ M \ KOH$	164
152	Cu	H_3BTC	—	$12.7 \ m^2 \ g^{-1}$	$142.6 \ F \ g^{-1}$ @ $1.5 \ A \ g^{-1}$ / $312.2 \ F \ g^{-1}$ @ $5 \ mV \ s^{-1}$	>84% @ $3 \ A \ g^{-1}$ (3000)	$3 \ M \ KOH$	164
153	Cu	H_3BTC	MnO_2	$1055.2 \ m^2 \ g^{-1}$	$667 \ F \ g^{-1}$ @ $1 \ A \ g^{-1}$	—	$1 \ M \ Na_2SO_4$	165
154	Cu	H_2F_4BDC, hmt	—	—	$1274 \ F \ g^{-1}$ @ $1 \ A \ g^{-1}$ / $1102 \ F \ g^{-1}$ @ $1 \ A \ g^{-1}$	88% @ $2 \ A \ g^{-1}$ (2000) / 88% @ $2 \ A \ g^{-1}$ (2000)	$1 \ M \ LiOH$ / $1 \ M \ KOH$	166
155	Cu	H_2Br_2BDC	—	—	$0.42 \ F \ g^{-1}$ @ —	—	$0.1 \ M \ Na_2SO_4$	73
156	Cu	H_2F_4BDC, H_2mpca	—	—	$735 \ F \ g^{-1}$ @ $1 \ A \ g^{-1}$	71% @ $2 \ A \ g^{-1}$ (1500)	$1 \ M \ KOH$	167
157	Cu	$1,2,4,5-H_4BTC$	POAP	—	$241 \ F \ g^{-1}$ @ —	90% @ — (1000)	$0.5 \ M \ HClO_4$	168
Cu-POMOFs								
158	Cu	$\alpha-K_6P_2W_{18}O_{62}$, pztaH, bpe	—	—	$168 \ F \ g^{-1}$ @ $5 \ A \ g^{-1}$	90.7% @ $2 \ mA \ cm^{-2}$ (1000)	$1 \ M \ H_2SO_4$	77
159	Cu	$H_4SiW_{12}O_{40}$, btx	—	—	$110.3 \ F \ g^{-1}$ @ $3 \ A \ g^{-1}$ / $77.6 \ mF \ cm^{-2}$ @ $2.1 \ mA \ cm^{-2}$	87% @ $25 \ A \ g^{-1}$ (1000)	$1 \ M \ H_2SO_4$	169

TABLE 7 (Continued)

	Metal	Ligand	Composited with	Surface area[a]	Specific capacitance[b]	Cycling stability[b,c]	Electrolyte[d]	Reference
160	Cu	$(NH_4)_6W_{12}O_{40}$, btx	—	—	50 F g⁻¹ @ 3 A g⁻¹; 35.2 mF cm⁻² @ 2.1 mA cm⁻²	87.5% @ 18 A g⁻¹ (1000)	1 M H_2SO_4	169
161	Cu	$H_3PMo_{12}O_{40}$, H_3BTC	PPy	21.57 m² g⁻¹	313 mF cm⁻² @ 0.5 mA cm⁻²; 1354 mF cm⁻² @ 10 mV s⁻¹; 281.9 F g⁻¹ @ 10 mV s⁻¹	—	3 M KCl	170
162	Cu	$H_3PMo_{12}O_{40}$, H_3BTC	PPy	50.72 m² g⁻¹	1090 mF cm⁻² @ 0.5 mA cm⁻²; 5147 mF cm⁻² @ 10 mV s⁻¹; 779.8 F g⁻¹ @ 10 mV s⁻¹	—	3 M KCl	170
163	Cu	$H_3PMo_{12}O_{40}$, H_3BTC	PPy	104.64 m² g⁻¹	277 mF cm⁻² @ 0.5 mA cm⁻²; 1383 mF cm⁻² @ 10 mV s⁻¹; 244.3 F g⁻¹ @ 10 mV s⁻¹	—	3 M KCl	170
164	Cu	$H_3PW_{12}O_{40}$, btx	—	—	100 F g⁻¹ @ 2 A g⁻¹	—	1 M H_2SO_4	171
165	Cu	$H_3PMo_{12}O_{40}$, btx	—	—	237 F g⁻¹ @ 2 A g⁻¹	92% @ 10 A g⁻¹ (1000)	1 M H_2SO_4	171
166	Cu	$H_4SiMo_{12}O_{40}$, btx	—	—	138.4 F g⁻¹ @ 2 A g⁻¹	—	1 M H_2SO_4	171
167	Cu	$H_3PMo_{12}O_{40}$, btx	—	—	249 F g⁻¹ @ 3 A g⁻¹	93.5% @ 10 A g⁻¹ (1000)	1 M H_2SO_4	172
168	Cu	$H_4PMo^{VI}_9Mo^V_3O_{39}$, btx	—	—	154.5 F g⁻¹ @ 3 A g⁻¹	91.1% @ 10 A g⁻¹ (1000)	1 M H_2SO_4	172
169	Cu	$H_3PMo_{12}O_{40}$, H_3BTC	PPy	—	508.62 F g⁻¹ @ 2 mA cm⁻²; 2034.51 mF cm⁻² @ 2 mA cm⁻²	70.86% @ 20 mA cm⁻² (9000)	1 M H_2SO_4	173
170	Cu	$H_3PMo_{12}O_{40}$, H_3BTC	PPy	—	500.61 F g⁻¹ @ 2 mA cm⁻²; 2753.45 mF cm⁻² @ 2 mA cm⁻²	—	1 M H_2SO_4	173
171	Cu	$(NH_4)_6Mo_7O_{24}$, bnie	—	—	800 F g⁻¹ @ 1 A g⁻¹; 538 F g⁻¹ @ 4 A g⁻¹	52.1% @ 30 mV s⁻¹ (5000)	4 M KOH	174
172	Cu	$(NH_4)_6Mo_7O_{24}$, bnie	—	—	828 F g⁻¹ @ 1 A g⁻¹	45.3% @ 30 mV s⁻¹ (5000)	4 M KOH	174
173	Cu	$(NH_4)_6Mo_7O_{24}$, bnie	CNT	—	564 F g⁻¹ @ 4 A g⁻¹	>100% @ 30 mV s⁻¹ (8000)	4 M KOH	174
174	Cu	$(NH_4)_6Mo_7O_{24}$, bnie	CNT	—	424 F g⁻¹ @ 4 A g⁻¹	97.7% @ 30 mV s⁻¹ (8000)	4 M KOH	174
175	Cu	$(NH_4)_6Mo_7O_{24}$, bnie	GO	—	482 F g⁻¹ @ 4 A g⁻¹	98.2% @ 30 mV s⁻¹ (8000)	4 M KOH	174
176	Cu	$(NH_4)_6Mo_7O_{24}$, bnie	GO	—	548 F g⁻¹ @ 4 A g⁻¹	>100% @ 30 mV s⁻¹ (8000)	4 M KOH	174
Copper polyamine/polyphenol MOFs								
177	Cu	CAT	—	540 m² g⁻¹	202 F g⁻¹ @ 0.5 A g⁻¹	80% @ 800 mV s⁻¹ (5000)	3 M KCl	175
178	Cu	CAT	—	475 m² g⁻¹	215.9 F g⁻¹ @ 0.5 A g⁻¹	79.7% @ 10 A g⁻¹ (5000)	1 M KCl	176
179	Cu	CAT	—	468 m² g⁻¹	94 mF cm⁻² @ 1.25 mA cm⁻²	—	3 M KCl	177

(Continues)

TABLE 7 (Continued)

	Metal	Ligand	Composited with	Surface area[a]	Specific capacitance[b]	Cycling stability[b,c]	Electrolyte[d]	Reference
180	Cu	CAT	—	—	$116\ \mathrm{F\ g^{-1}}$ @ $1.25\ \mathrm{mA\ cm^{-2}}$ $463\ \mathrm{mF\ cm^{-2}}$ @ $1.25\ \mathrm{mA\ cm^{-2}}$ $484\ \mathrm{mF\ cm^{-2}}$ @ $10\ \mathrm{mV\ s^{-1}}$	87% @ $100\ \mathrm{mV\ s^{-1}}$ (5000)	3 M KCl	177
181	Cu	CAT	—	—	$44.6\ \mathrm{mF\ cm^{-2}}$ @ $5\ \mathrm{mV\ s^{-1}}$	69% @ $0.4\ \mathrm{mA\ cm^{-1}}$ (1000)	1 M KCl	178
182	Cu	DBCO	—	$271\ \mathrm{m^2\ g^{-1}}$	$479\ \mathrm{F\ g^{-1}}$ @ $0.2\ \mathrm{A\ g^{-1}}$	72% @ $5\ \mathrm{A\ g^{-1}}$ (2000)	1 M NaCl	80
183	Cu	HAB	—	—	$215\ \mathrm{F\ g^{-1}}$ @ $1\ \mathrm{mV\ s^{-1}}$ $0.86\ \mathrm{F\ cm^{-2}}$ @ $1\ \mathrm{mV\ s^{-1}}$	—	1 M KOH	78
Copper porphyrin compounds								
184	Cu	TCPP	PPy	$22\ \mathrm{m^2\ g^{-1}}$	$496\ \mathrm{F\ g^{-1}}$ @ $1\ \mathrm{A\ g^{-1}}$	70% @ $20\ \mathrm{A\ g^{-1}}$ (3000)	0.5 M H$_2$SO$_4$	179
185	Cu	TCPP	CNT	—	$833.3\ \mathrm{F\ g^{-1}}$ @ $1\ \mathrm{A\ g^{-1}}$	—	1 M H$_2$SO$_4$	116
186	Cu	TCPP	GO	—	$831.7\ \mathrm{F\ g^{-1}}$ @ $1\ \mathrm{A\ g^{-1}}$	—	1 M H$_2$SO$_4$	116
187	Cu	TCPP	MXene	—	$326.1\ \mathrm{F\ g^{-1}}$ @ $0.1\ \mathrm{A\ g^{-1}}$ $1.64\ \mathrm{F\ cm^{-2}}$ @ $1\ \mathrm{mA\ cm^{-2}}$ $694.2\ \mathrm{F\ cm^{-3}}$ @ $1\ \mathrm{mA\ cm^{-3}}$	~100% @ $50\ \mathrm{mV\ s^{-1}}$ (30 000)	0.5 M H$_2$SO$_4$	180
188	Cu	TCPP	PPy	—	$163.34\ \mathrm{F\ g^{-1}}$ @ $0.2\ \mathrm{A\ g^{-1}}$ $340.6\ \mathrm{mF\ cm^{-2}}$ @ $1\ \mathrm{mA\ cm^{-2}}$ $71.14\ \mathrm{F\ cm^{-3}}$ @ $1\ \mathrm{mA\ cm^{-3}}$	91% @ $2\ \mathrm{mA\ cm^{-2}}$ (20 000)	0.5 M H$_2$SO$_4$	181
Others								
189	Cu	DPA	—	—	$217.3\ \mathrm{F\ g^{-1}}$ @ $0.4\ \mathrm{mA\ cm^{-2}}$ $869.3\ \mathrm{mF\ cm^{-2}}$ @ $0.4\ \mathrm{mA\ cm^{-2}}$ $23.3\ \mathrm{F\ g^{-1}}$ @ $10\ \mathrm{mV\ s^{-1}}$ $93.3\ \mathrm{mF\ cm^{-2}}$ @ $10\ \mathrm{mV\ s^{-1}}$	95.5% @ $6.7\ \mathrm{mA\ cm^{-2}}$ (2000)	1 M NaOH	182

[a]Determined by BET method.
[b]Obtained by either CP and GCD method at specific current densities or CV method at specific scan rates.
[c]Evaluated by the capacitance retention after a number of charge/discharge cycles, which are shown in brackets.
[d]Normally in water except for those with special clarification.

TABLE 8 Summary of SC electrode performances of copper-organic compounds

Positive electrode			Negative electrode	Specific capacitance[a]	Energy density and power density[b]	Cycling stability[a,c]	Electrolyte[d]	Reference
Metal	Ligand	Composited with						
Copper polycarboxylate MOFs								
140 Cu	H_3BTC	rGO	**140**	193 F g⁻¹ @ —	$\underline{42\,\text{Wh kg}^{-1}}$ @ — — @ 3100 W kg⁻¹	98.5% @ — (4000)	PVA/NaNO₃	159
142 Cu	H_3BTC	PPy, GO	**142**	35.5 mF cm⁻² @ 0.4 mA cm⁻² / 37.8 mF cm⁻² @ 5 mV s⁻¹	51 mWh cm⁻³ @ 2.1 mW cm⁻³	89.8% @ 80 mV s⁻¹ (4000)	PVA/H₃PO₄	160
148 Cu	H_3BTC	PANI	rGO	19.93 F g⁻¹ @ 0.5 A g⁻¹	$\underline{6.22\,\text{Wh kg}^{-1}}$ @ 374.52 W kg⁻¹ / $\underline{1.58\,\text{Wh kg}^{-1}}$ @ 7497.07 W kg⁻¹	87% @ 3 A g⁻¹ (2000)	6 M KOH	163
153 Cu	H_3BTC	MnO₂	AC	340 F g⁻¹ @ 1 A g⁻¹	—	95% @ 4 A g⁻¹ (6000)	1 M Na₂SO₄	165
Cu-POMOFs								
162 Cu	$H_3PMo_{12}O_{40}$, H_3BTC	PPy	**162**	1879 mF cm⁻² @ 25 mA cm⁻²	$\underline{0.316\,\text{mWh cm}^{-2}}$ @ 6.4 mW cm⁻² 0.0496 mWh cm⁻² @ 52.5 mW cm⁻²	—	PVA/H₂SO₄	170
169 Cu	$H_3PMo_{12}O_{40}$, H_3BTC	PPy	FeMo/C	—	$\underline{16.67\,\text{Wh kg}^{-1}}$ @ 419.75 W kg⁻¹ / 1.12 mWh cm⁻³ @ 27.78 mW cm⁻³	80.62% @ — (10 000)	1 M H₂SO₄	173
Copper polyamine/polyphenol MOFs								
177 Cu	CAT	—	**177**	120 F g⁻¹ @ 0.5 A g⁻¹ / 22 µF cm⁻² @ 0.5 A g⁻¹	2.6 Wh kg⁻¹ @ 200 W kg⁻¹	>85% @ 50 mV s⁻¹ (5000)	PVA/KCl	175
178 Cu	CAT	—	**178**	239.1 F g⁻¹ @ 0.25 A g⁻¹ / 50.3 µF cm⁻² @ 0.25 A g⁻¹	4.3 Wh kg⁻¹ @ 200 W kg⁻¹	79,9% @ 5 A g⁻¹ (5000)	1 M KCl	176
180 Cu	CAT	—	**180**	252.1 mF cm⁻² @ 1.25 mA cm⁻²	$\underline{22.4\,\text{µWh cm}^{-2}}$ @ — — @ 1.1 mW cm⁻²	90% @ 100 mV s⁻¹ (5000)	PVA/LiCl	177
190 Cu	CAT	—	**190**	20.3 mF cm⁻² @ 2 mV s⁻¹	0.51 mWh cm⁻² @ 2.54 mW cm⁻²	—	1 M KCl	178

(Continues)

TABLE 8 (Continued)

| Positive electrode | | Composited with | Negative electrode | Specific capacitance[a] | Energy density and power density[b] | Cycling stability[a,c] | Electrolyte[d] | Reference |
Metal	Ligand							
182 Cu	DBCO	—	**182**	396 F g^{-1} @ 0.2 A g^{-1} 879 mF cm^{-2} @ 0.2 A g^{-1} 22 F cm^{-3} @ 0.2 A g^{-1}	$\underline{13.8\,\text{Wh kg}^{-1}}$ @ 0.1 kW kg^{-1} 7.6 Wh kg^{-1} @ $\underline{5.0\,\text{W kg}^{-1}}$	80% @ 5 A g^{-1} (2000)	1 M NaCl	80
Copper porphyrin compounds								
191 Cu	DEPP	—	graphite	216 F g^{-1} @ 1 A g^{-1}	$\underline{345\,\text{Wh kg}^{-1}}$ @ 29 kW kg^{-1}	85% @ 4 A g^{-1} (2000) 60% @ 4 A g^{-1} (8000)	1 M LiPF$_6$ in EC/DMC (v:v = 1:1)	183
184 Cu	TCPP	PPy	**184**	240 F g^{-1} @ 2 A g^{-1} 48 mF cm^{-2} @ 1.6 mA cm^{-2}	$\underline{0.29\,\text{mWh cm}^{-3}}$ @ 270 mW cm^{-3}	68.5% @ 5 A g^{-1} (3000)	PVA/H$_2$SO$_4$	179
187 Cu	TCPP	MXene	**187**	40.7 F g^{-1} @ 0.01 A g^{-1} 408 mF cm^{-2} @ 0.5 mA cm^{-2} 10.2 F cm^{-3} @ 2.5 mA cm^{-3}	$\underline{20.4\,\mu\text{Wh cm}^{-2}}$ @ 152.2 μW cm^{-2}	95.9% @ 5 mA cm^{-2} (7000)	PVA/H$_2$SO$_4$	180
188 Cu	TCPP	PPy	**188**	65.4 mF cm^{-2} @ 0.2 mA cm^{-2}	$\underline{2.27\,\mu\text{Wh cm}^{-2}}$ @ 50 μW cm^{-2}	~100% @ — (20 000)	PVA/H$_2$SO$_4$	181

Abbreviation: EC/DMC, ethylene carbonate and dimethyl carbonate.

[a]Obtained by either CP and GCD method at specific current densities, or CV method at specific scan rates;

[b]Data of maximum energy densities and maximum power densities are underlined;

[c]Evaluated by the capacitance retention after a number of charge/discharge cycles, which are shown in brackets.

[d]Normally in water except for those with special clarification.

FIGURE 12 A, A spinning motor powered by rGO/HKUST-1 SSC (**140**) over 9 minutes. Reproduced with permission: Copyright 2015, Elsevier Ltd.[159] B, Schematic synthesis of the HUST-1/rGO hybrid (**145**). Reproduced with permission: Copyright 2016, The Royal Society of Chemistry.[161] C, A green and a red LED lightened by an ASC (**148**) for 3 and 5 minutes, respectively. Reproduced with permission: Copyright 2018, Elsevier B.V.[163] D, Schematic diagram of the formation mechanism of HUST-1 (**149-152**) at different temperatures. Reproduced with permission: Copyright 2017, Elsevier B.V[164]
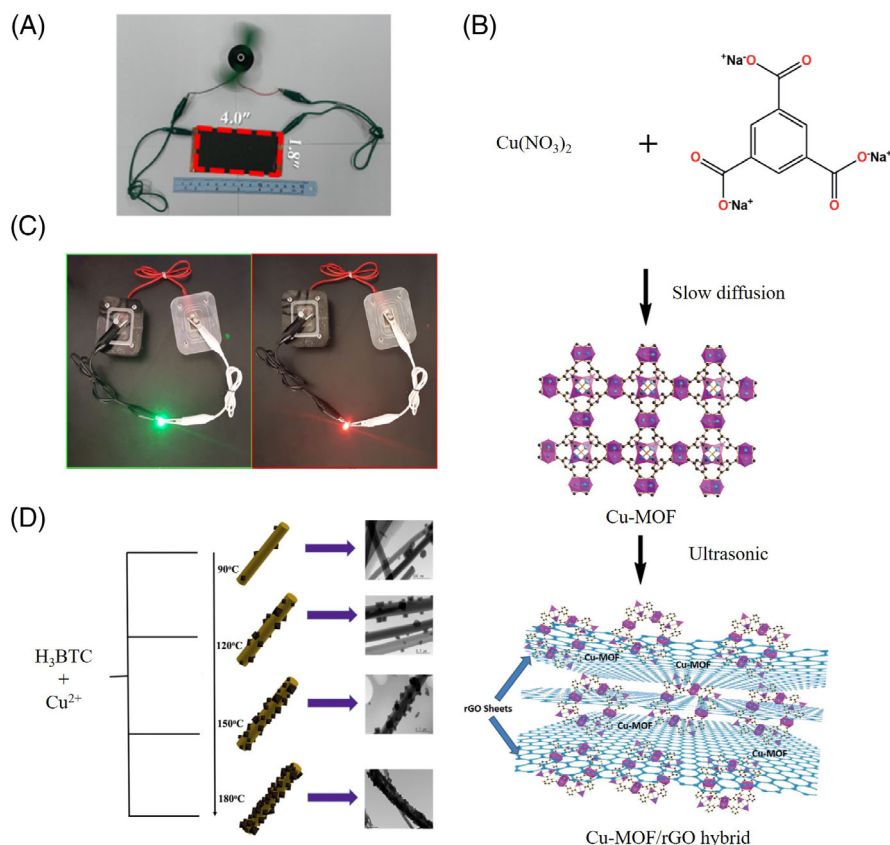
gravimetric power density of 19.2 kW kg^{-1}.[136,156] These are the best performance data among all the SCs with the electrode materials made of nickel-organic compounds, and are far higher than the highest gravimetric energy density (50.30 Wh kg^{-1}) and power density (9071 W kg^{-1}) of the Co-MOFs.[107,130] Yan and coworkers assembled a flexible solid-state accordion-like ASC device on Ni-BDC MOF (**95**), which exhibited excellent mechanical flexibility with a bending angle in the range of 0° to 180° (Figure 8A).[137] Du and coworkers fabricated a series of novel hierarchical porous Ni-BTC MOFs (**104-107**) by a facile hydrothermal process with different ratios of H$_3$BTC and nickel ions, and the ASC device based on **105** could light up a red LED (Figure 8B).[142] Qu and coworkers synthesized three novel water-stable pillared Ni-MOFs (**110**, Figure 8C) with good stability heritage and directly applied as SC electrodes without morphology modification.[74] The ASC device with **110** as the positive electrode exhibited high cycling stability, with only 2% loss of capacitance after 16 000 cycles. Wang and coworkers introduced two topological and isostructural 3D Ni-MOFs (**111** and **112**) with novel 1D helical channels as the SC electrodes, which were synthesized by a rigid tripodal ligand (H$_3$TATB, Figure 4A) and a flexible secondary linker (Figure 8D).[144] The highest C_g of nickel polycarboxylate MOFs reached 2280 F g^{-1} (**115**), which is also the highest value for the nickel-organic compounds.[116] Another Ni-MOF (**97**) with H$_2$BDC ligand also afforded a high C_g value of 2192.4 F g^{-1}.[138] These values are comparable to the highest C_g of Co-MOFs (2572 F g^{-1}, **51**).

The ligands of polyamine and polyphenol (Figure 9) are also popularly used to construct 2D Ni-MOFs (**117-127**, **134-138**) in recent years.[78,93,145-151,157] In addition to the common properties of ultrahigh surface areas and larger interior layer-spaces and so forth, these sheet-like 2D materials deliver versatile performances owing to their distinctive inner structures and compositions.[57] Wu and coworkers prepared MSCs by using Ni-CAT MOF (**117**) to grow selectively on patterned 3D laser-scribed graphene (LSG) electrodes through a combined laser-scribing and a selective solvothermal deposition process (Figure 10A).[145] Li and coworkers fabricated a hierarchical electrode material with Ni-CAT/NiCo-LDH/NF (**119**), which delivered a high C_a (3200 mF cm^{-2}) by taking advantage of the regular nanostructure and making full use of the high porosity and excellent conductivity of the material.[146] Zhou and coworkers fabricated continuous Ni$_3$(HITP)$_2$ MOF (**123** and **124**) nanolayers on the surface of CNFs by the interfacial synthesis, and a SSC based on CNF@Ni-HITP (**124**) provided an ultrahigh C_v of 2800 mF cm^{-3}.[149] Sheberla and coworkers reported a highly conductive Ni$_3$(HITP)$_2$ MOF (**125**), which is penetrated
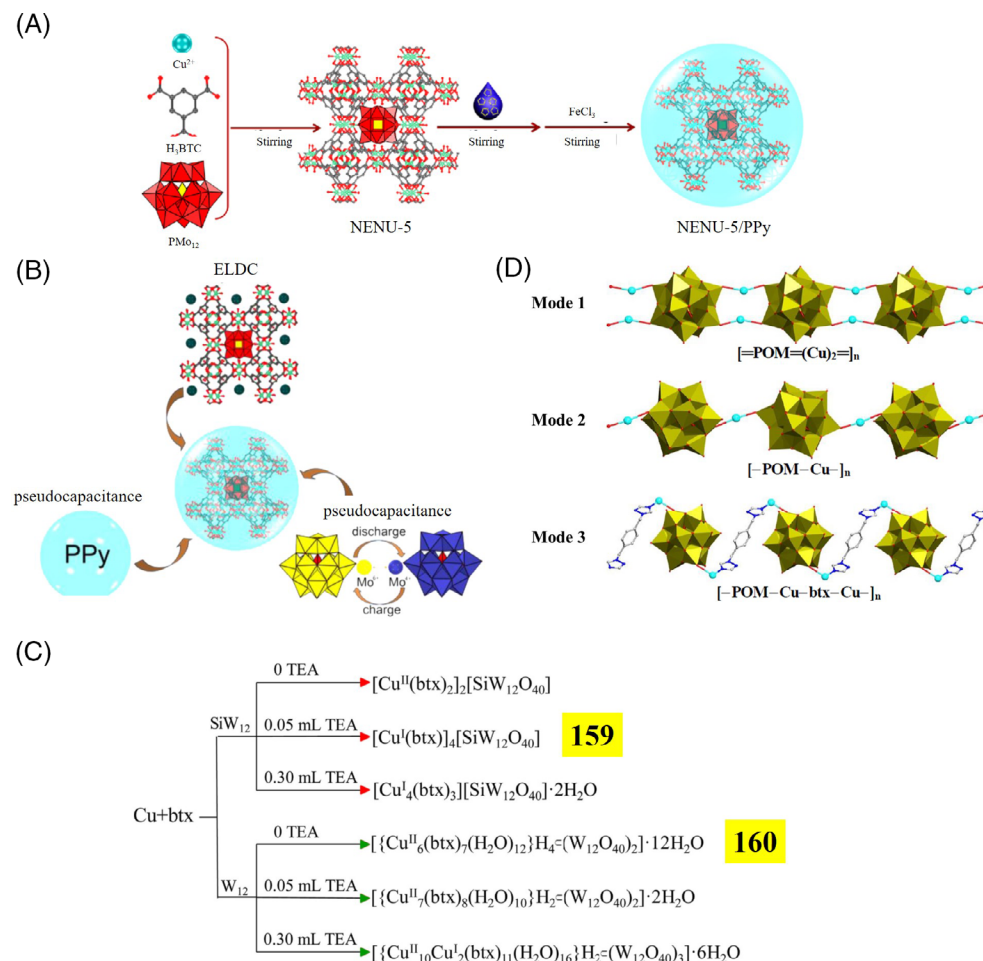
by 1D cylindrical channels of ~1.5 nm diameter.[150] The $Ni_3(HITP)_2$ combined the advantages of high surface area, excellent electrical conductivity and large open channels that could enable the swift movement of electrolytes, suffering only minimal volume changes on repeated charge/discharge cycles (Figure 10B). Feng and coworkers developed a highly conductive and dense 2D Ni-HAB MOF (**126**), which exhibited exceptionally high C_v of 760 F cm^{-3}, superior to those of all metal-organic compounds.[78] Thanks to the small particle size of Ni-HAB, even with an increase in the thickness of the electrodes up to 360 μm, the C_a value did not show a plateau and reached a value of 23 F cm^{-2}. To clarify how the ions transport and to predict the corresponding potential-dependent capacitance in characteristic shapes, Bi and coworkers performed the constant-potential molecular dynamics (MD) simulations to analyze the double-layer structure and capacitive performance of SCs composed of Ni-MOFs electrodes (**127**) and room temperature ionic liquids (RTILs).[151] Modeling results revealed that these MOF/RTIL-based cells could exhibit superior performance to most carbon-based devices, which suggests promising avenues for designing SCs with both

high energy and power density. Nguyen and coworkers developed a new approach for the fabrication of $Ni_3(HITP)_2$ SC material (**137**) by electrophoretic deposition technology, and the assembled SSC showed exceptionally ultrahigh cycling stability with a retention of about 84% after 10^7 cycles.[157]

Except for Ni-MOFs with polycarboxylate, polyamine and polyphenol ligands, there are also some reports on other nickel-organic compounds in the SC application (**128-133**, **139**). Xu and coworkers synthesized 1D nickel hydroxide nanorods (**129**) based on SA via a facile hydrothermal process and used as electrode materials for SCs,[153] which provided a high C_g over 1600 F g^{-1}, with only ~5% loss of capacitance after 1000 cycles. A facile and general strategy was developed by Xu and coworkers that enabled the conversion of a conventional nickel-based covalent organic framework (COF) into an outstanding redox-active energetic framework (**131** and **132**, Figure 11A) by the channel-wall functionalization.[155] The conventional imine-linked COFs **131** and **132**, as a scaffold with nickel-porphyrin at the vertices and ethynyl units on the channel walls, turned out to be electrochemically inactive. Accomplishment of the click reactions

FIGURE 14 A, Chemical and crystal structure of CuDEPP (191).[183] B, Mesomeric transformations of 191. Reproduced with permission: Copyright 2017, Wiley-VCH Verlag GmbH & Co. KGaA, Weinheim.[183] C, Schematic illustration of the electrophoretic deposition of Cu-TCPP and electropolymerization of PPy (188). Reproduced with permission: Copyright 2019, The Royal Society of Chemistry.[181] D, Schematic illustration of the synthesis of MXene/MPFs (187) films through a vacuum filtration method. Reproduced with permission: Copyright 2019, WILEY-VCH Verlag GmbH & Co. KGaA, Weinheim[180]
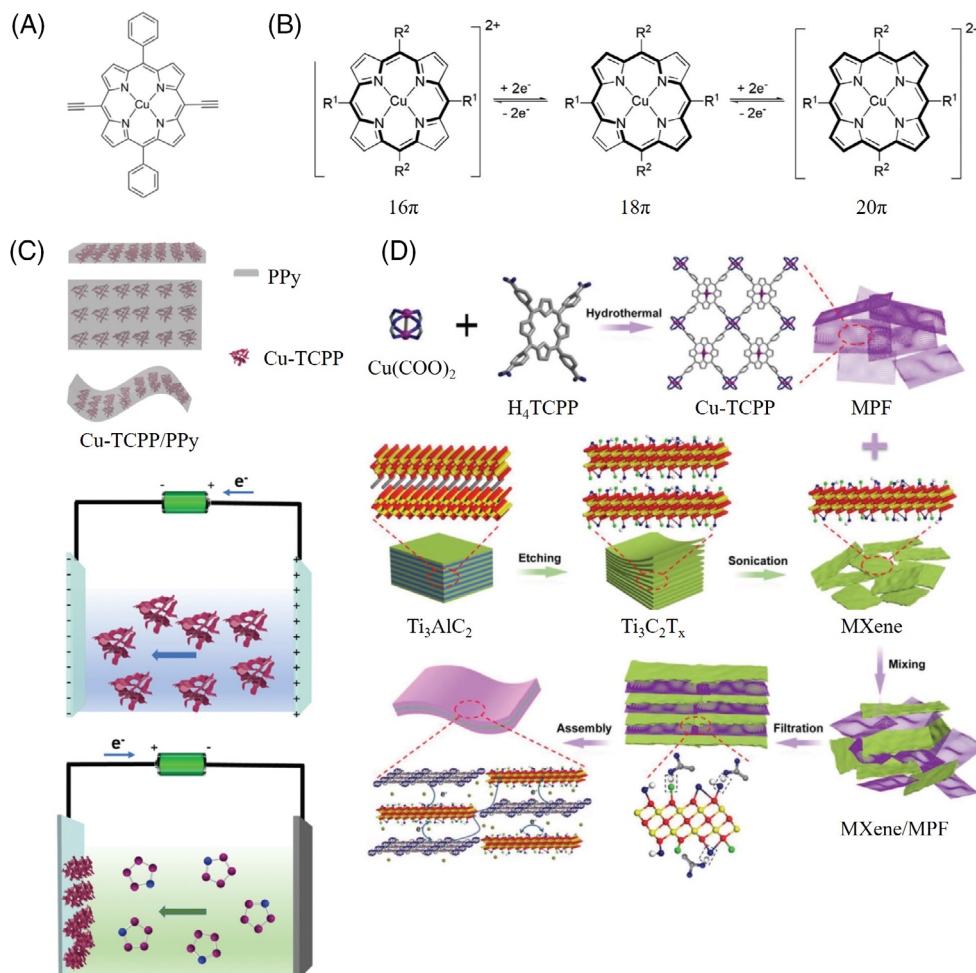
functionalized the $[HC\equiv C]_{X\%}$-NiP-COF with organic radicals into $[TMEPO]_{X\%}$-NiP-COF that enhanced the electrochemical activities. These results indicate that the strategy of post-synthetic wall engineering is useful to convert a conventional COF into radical frameworks, in which open accessible polyradicals are covalently immobilized on the channel walls in a controlled manner. Łępicka and coworkers prepared a redox conducting polymer (139, Figure 11B) by electropolymerization under potentiodynamic conditions.[158] The polymer 139, together with two polymers (poly(C_{60}-Pd) and PPy), were combined to devise a laboratory model of a new ASC with a dual anode and a dual cathode (Figure 11C). This ASC exhibited a largely extended voltage operation in the range of 0 to 2.2 V.

2.4 | Copper

The electrode and SC performances of copper-organic compounds are listed in Tables 7 and 8. So far, reported copper-organic compounds and their composites with SC properties can be divided into copper carboxylate

MOFs (140-157), copper polyoxometalate organic frameworks (Cu-POMOFs, 158-176), copper polyamine or polyphenol MOFs (177-183), copper porphyrin compounds (184-188), etc. Copper can exhibit electrochemical activity through the redox reaction between Cu(0), Cu(I), and Cu(II), and its organic compounds have been widely studied in SCs.[73,77,78,80,116,159-183] Relevant conversion process can be expressed by the following equations[164,167,174]:

$$Cu(I)_s + OH^- \leftrightarrow Cu(I)(OH)_{ad} + e^-, \quad (21)$$

$$Cu(II)_s + OH^- \leftrightarrow Cu(II)(OH)_{ad} + e^-, \quad (22)$$

$$Cu(I)(OH)_{ad} \leftrightarrow Cu(II)(OH)_{ad} + e^-, \quad (23)$$

$$Cu(II)(OH)_{ad} \leftrightarrow Cu(III)(OH)_{ad} + e^-. \quad (24)$$
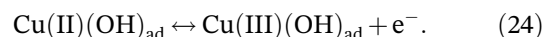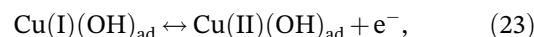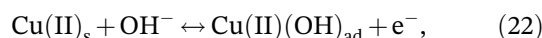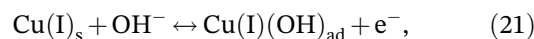
Among copper polycarboxylate MOFs (140-157), HUST-1 (also known as MOF-199, 140-153) with H_3BTC ligand showed interesting behavior in the electrochemically based SCs due to its large surface area and high pore

TABLE 9 Summary of SC electrode performances of zinc-organic compounds

	Metal	Ligand	Composited with	Surface area[a]	Specific capacitance[b]	Cycling stability[b,c]	Electrolyte[d]	Reference
Zinc 3-methylimidazolate MOFs (ZIF-8)								
192	Zn	mIM		—	99 F g^{-1} @ 5 mV s^{-1}	—	6 M KOH	68
193	Zn	mIM	SnO_2	—	931 F g^{-1} @ 5 mV s^{-1}	—	6 M KOH	68
194	Zn	mIM	PANI, ZnO, graphene	—	1.378 F cm^{-2} @ 1 mA cm^{-2}	73% @ 8 mA cm^{-2} (400)	3 M KCl	196
195	Zn	mIM	ZnO	$185.6 \text{ m}^2 \text{ g}^{-1}$	61.4 F g^{-1} @ 10 mV s^{-1} 325.6 mF cm^{-2} @ 10 mV s^{-1}	—	3 M KCl	197
196	Zn	mIM	PANI, ZnO	$136.8 \text{ m}^2 \text{ g}^{-1}$	652.2 F g^{-1} @ 10 mV s^{-1} 4370 mF cm^{-2} @ 10 mV s^{-1} 4839 mF cm^{-2} @ 5 mA cm^{-2}	—	3 M KCl	197
Others								
197	Zn	mTCPP	—	$1450 \text{ m}^2 \text{ g}^{-1}$	142 F g^{-1} @ 5 A g^{-1}	—	0.1 M TBAPF6 in DCM	71

Abbreviation: DCM, dichloromethane.

[a]Determined by BET method;

[b]Obtained by either CP and GCD method at specific current densities or CV method at specific scan rates;

[c]Evaluated by the capacitance retention after a number of charge/discharge cycles, which are shown in brackets;

[d]Normally in water except for those with special clarification.

volume.[73,159-168,184] Srimuk and coworkers firstly studied the HUST-1 as the active material for SC electrodes.[159] The as-assembled flexible all-solid-state SSC based on rGO/HUST-1 composites (**140**) exhibited a high C_g of 193 F g^{-1} and could supply the electricity to a spinning motor over a 9-minute discharging time (Figure 12A). Saraf and coworkers further improved the SC performance with rGO/HUST-1 (**145**) by using a facile ultra-sonication assisted synthetic method (Figure 12B).[161] The slow diffusion grown powder of HUST-1 showed a remarkable surface area of $1316.246 \text{ m}^2 \text{ g}^{-1}$ and their rGO composites provided a maximum C_g of 685.33 F g^{-1}. Moreover, Jafari and coworkers assembled an ASC device with HUST-1/PANI composite (**148**) as the positive electrode, which could lighten up LEDs over 3 minutes without recharging (Figure 12C).[163] A systematic investigation of mixed phases of HUST-1 was carried out by Ramachandran and coworkers, in which the HUST-1 (**149**-**152**) were prepared by water as the only solvent at different temperatures ($90°C$, $120°C$, $150°C$, and $180°C$ for **149**, **150**, **151,** and **152**, respectively).[164] It was found that the higher temperature weakened the electrochemical performance due to the less faradaic redox reaction from the surface of a specific phase, and the large void space in HUST-1 electrode could improve effectively the electrolyte ions transport and furnish the superior electrochemical performance (Figure 12D). Besides, Liu and coworkers prepared a 2D copper-based layered coordination polymer (**154**) with H_2F_4BDC and hmt as mixed bridging ligands.[166] The C_g of **154** were found to be 1274 and 1102 F g^{-1} in 1 M LiOH and KOH, respectively, and similar CV curves with a pair of similar redox peaks were observed from the CV curves in both aqueous electrolytes, which indicated that the pseudocapacitive behaviors were mainly associated with the redox reactions.

Another important type of copper-organic compounds is the POMOFs that has attracted recent research interests in the field of SC (**158**-**176**).[28,38,77,169-174] POMOFs have many exceptional advantages for SC applications, such as long cycling life due to their poor solubility in water and in common inorganic and/or organic solvents, and crystalline forms which are suitable for investigating their effect on SC properties. Wang and coworkers first realized the modification of SC electrodes by using POM-based coordination polymers (**158**). It was assumed that the improvement of conductivity of Cu-MOFs with mixed N-donor ligands (pztaH and bpe, Figure 4B) was realized by the introduction of Wells-Dawson-type POM ($\alpha\text{-}K_6P_2W_{18}O_{62}$) into the long range order structure, because part of the electrons on the localized state may turn into the extended state so that the conductivity mechanism is transformed from

TABLE 10 Summary of SC electrode performances of zinc-organic compounds

	Positive electrode			Negative electrode	Specific capacitance[a]	Energy density and power density[b]	Cycling stability[a,c]	Electrolyte[d]	Reference
	Metal	Ligand	Composited with						
Zn polycarboxylate MOFs									
198	Zn	H_2BDC	—	198	0.341 F cm^{-2} @ 0.88 mA cm^{-3} / 0.043 F cm^{-3} @ 0.88 mA cm^{-3}	—	>80% @ 6.3 mA cm^{-3} (3500)	1 M TEABF$_4$ in ACN	102
199	Zn	H_2BDC, 1,4-H_2NH_2BDC	—	199	0.232 F cm^{-2} @ 0.88 mA cm^{-3} / 0.029 F cm^{-3} @ 0.88 mA cm^{-3}	—	>80% @ 6.3 mA cm^{-3} (10 000)	1 M TEABF$_4$ in ACN	102
200	Zn	H_2BDC, H_2BrBDC	—	200	0.478 F cm^{-2} @ 0.88 mA cm^{-3} / 0.060 F cm^{-3} @ 0.88 mA cm^{-3}	—	>80% @ 6.3 mA cm^{-3} (1600)	1 M TEABF$_4$ in ACN	102
201	Zn	H_2BDC, H_2Cl_2BDC	—	201	0.566 F cm^{-2} @ 0.88 mA cm^{-3} / 0.072 F cm^{-3} @ 0.88 mA cm^{-3}	—	>80% @ 6.3 mA cm^{-3} (>10 000)	1 M TEABF$_4$ in ACN	102
202	Zn	H_2BDC, H_2NO_2BDC	—	202	0.913 F cm^{-2} @ 0.88 mA cm^{-3} / 0.122 F cm^{-3} @ 0.88 mA cm^{-3}	—	>80% @ 6.3 mA cm^{-3} (3000)	1 M TEABF$_4$ in ACN	102
203	Zn	H_2BDC, 2, 6-H_2NDC	—	203	0.195 F cm^{-2} @ 0.88 mA cm^{-3} / 0.025 F cm^{-3} @ 0.88 mA cm^{-3}	—	>80% @ 6.3 mA cm^{-3} (>10 000)	1 M TEABF$_4$ in ACN	102
204	Zn	H_2BDC, 1,4-H_2NH_2BDC, H_2BrBDC	—	204	0.790 F cm^{-2} @ 0.88 mA cm^{-3} / 0.100 F cm^{-3} @ 0.88 mA cm^{-3}	—	>80% @ 6.3 mA cm^{-3} (3500)	1 M TEABF$_4$ in ACN	102
205	Zn	H_2BDC, 1,4-H_2NH_2BDC,	—	205	0.891 F cm^{-2} @ 0.88 mA cm^{-3}	—	>80% @ 6.3 mA cm^{-3} (>10 000)	1 M TEABF$_4$ in ACN	102

(Continues)

TABLE 10 (Continued)

Positive electrode

	Metal	Ligand	Composited with	Negative electrode	Specific capacitance[a]	Energy density and power density[b]	Cycling stability[a,c]	Electrolyte[d]	Reference
		H_2BrBDC, H_2Cl_2BDC			$0.113\ F\ cm^{-3}$ @ $0.88\ mA\ cm^{-3}$				
206	Zn	H_2BDC, 1,4-H_2NH_2BDC, H_2BrBDC, H_2Cl_2BDC, H_2NO_2BDC	—		$0.752\ F\ cm^{-2}$ @ $0.88\ mA\ cm^{-3}$; $0.095\ F\ cm^{-3}$ @ $0.88\ mA\ cm^{-3}$	—	>80% @ $6.3\ mA\ cm^{-3}$ (2500)	1 M TEABF$_4$ in ACN	102
207	Zn	H_2BDC, 1,4-H_2NH_2BDC, H_2BrBDC, H_2Cl_2BDC, H_2NO_2BDC, 2,6-H_2NDC	—		$0.501\ F\ cm^{-2}$ @ $0.88\ mA\ cm^{-3}$; $0.063\ F\ cm^{-3}$ @ $0.88\ mA\ cm^{-3}$	—	>80% @ $6.3\ mA\ cm^{-3}$ (1500)	1 M TEABF$_4$ in ACN	102
208	Zn	H_3BTB	—		$0.713\ F\ cm^{-2}$ @ $0.88\ mA\ cm^{-3}$; $0.090\ F\ cm^{-3}$ @ $0.88\ mA\ cm^{-3}$	—	>80% @ $6.3\ mA\ cm^{-3}$ (4000)	1 M TEABF$_4$ in ACN	102
		Zinc 3-methylimidazolate MOFs (ZIF-8)							
209	Zn	mIM	—		$0.268\ F\ cm^{-2}$ @ $0.88\ mA\ cm^{-3}$; $0.034\ F\ cm^{-3}$ @ $0.88\ mA\ cm^{-3}$	—	>80% @ $6.3\ mA\ cm^{-3}$ (2500)	1 M TEABF$_4$ in ACN	102
194	Zn	mIM	PANI, ZnO, graphene		—	$\dfrac{235\ \mu Wh\ cm^{-3}}{1542\ \mu W\ cm^{-3}}$	—	PVA/H$_2$SO$_4$	196
196	Zn	mIM	PANI, ZnO		$226.9\ mF\ cm^{-2}$ @ $0.5\ mA\ cm^{-2}$; $986.5\ mF\ cm^{-3}$ @ $0.5\ mA\ cm^{-2}$	$\dfrac{0.0315\ mWh\ cm^{-2}}{0.327\ W\ cm^{-2}}$; $\dfrac{0.0205\ mWh\ cm^{-2}}{5.435\ W\ cm^{-2}}$; $\dfrac{0.137\ mWh\ cm^{-3}}{1.421\ W\ cm^{-3}}$; $\dfrac{0.089\ mWh\ cm^{-3}}{23.629\ W\ cm^{-2}}$	—	PVA/KCl	197

TABLE 10 (Continued)

Positive electrode		Composited with	Negative electrode	Specific capacitance[a]	Energy density and power density[b]	Cycling stability[a,c]	Electrolyte[d]	Reference
Metal	Ligand							
Others								
210 Zn	pPDA	—	GC	200.86 F g^{-1} @ 1 A g^{-1}	62.75 Wh kg^{-1} @ — — @ 4501.1 W kg^{-1}	96.2% @ — (2000)	1 M KOH	198
211 Zn	pPDA	—	GC	184.1 F g^{-1} @ 1 A g^{-1}	57.52 Wh kg^{-1} @ — — @ 4499.03 W kg^{-1}	96.81% @ — (2000)	1 M KOH	198
212 Zn	pPDA	—	GC	167.3 F g^{-1} @ 1 A g^{-1}	52.25 Wh kg^{-1} @ — — @ 4498.92 W kg^{-1}	96.79% @ — (2000)	1 M KOH	198

[a]Obtained by either CP and GCD method at specific current densities, or CV method at specific scan rates;
[b]Data of maximum energy densities and maximum power densities are underlined;
[c]Evaluated by the capacitance retention after a number of charge/discharge cycles, which are shown in brackets.
[d]Normally in water except for those with special clarification.

the hopping to the drifting transport.[77] A series of HUST-1-based POMOF composites (NENU-5/PPy-n, **161-163**) with different PPy doping ratios were reported by Wang and coworkers.[170] Figure 13A,B illustrate the synthetic process and possible mechanism for the cooperative capacity of NENU-5/PPy-n composites, respectively. More impressively, the electrode materials of NENU-5/PPy-0.15 composite (**162**) exhibited a high C_a of 5147 mF cm^{-2}, and the as-assembled all-solid-state SSC device can provide a C_a value of 1879 mF cm^{-2}. To our best knowledge, these C_a values are the highest among all the SC electrodes and devices based on the metal-organic compounds. Meanwhile, introduction of proper organic nitrogen elements into the Cu-based POMOF is believed to improve its conductivity.[185,186] One of the popular N-donor ligands is btx (Figure 4A).[169,171,172] Chai and coworkers synthesized two Cu-POMOFs (**159** and **160**) based on Keggin-type POM $H_4SiW_{12}O_{40}$ and $(NH_4)_6W_{12}O_{40}$ via regulating the amount of triethylamine in the POM/Cu/btx reaction system (Figure 13C).[169] They also studied the relationship between crystal structure on the molecular level and their capacitance performance. It is deduced that the different capacitances may be dominated by the modes of direct connection between POM building blocks and covalent networks. Figure 13D shows three direct modes of POM building blocks in the two series of POMOFs. For the modes 1 and 2, two isolated polyoxoanions are linked together through sharing Cu cations to form extended 1D lines or 2D sheets, which can effectively promote the electron transfer between adjacent POMs. However, electrons cannot transfer effectively between POMs in mode 3 due to the additional insertion of the non-conjugative Cu-btx subunits.[169] Afterwards, Chai's group further synthesized three new POMOFs (**164-166**) based on Keggin-type POMs with different Cu(I)/Cu(II) complexes and the btx ligand.[171] It was found that the POMOFs with fully oxidized metal atoms ($[PW^{VI}_{12}O_{40}]^{3-}$ in compound 1 and $[PMo^{VI}_{12}O_{40}]^{3-}$ in compound 4) tended to produce higher capacitance than that of the POMOFs with partially reduced metal atoms ($[PW^{VI}_{10}W^V_2O_{40}]^{5-}$ in compound 2, $[PW^{VI}_9W^V_3O_{40}]^{6-}$ in compound 3 and $[SiMo^{VI}_{11}Mo^VO_{40}]^{5-}$ in compound 5). Similar phenomenon was also found in Chai's other work (**167** and **168**),[172] and these results indicate that the fully oxidized Keggin POMs can provide a higher oxidation capacity. Wang and coworkers constructed two layered Cu(I)-based POMOFs (**171** and **172**) with β-$[Mo_8O_{26}]^{4-}$ polyoxoanions and flexible bnie (Figure 4A) linker.[174] Both SC electrodes fabricated with **171** and **172** showed a poor cycling stability with nearly half of the
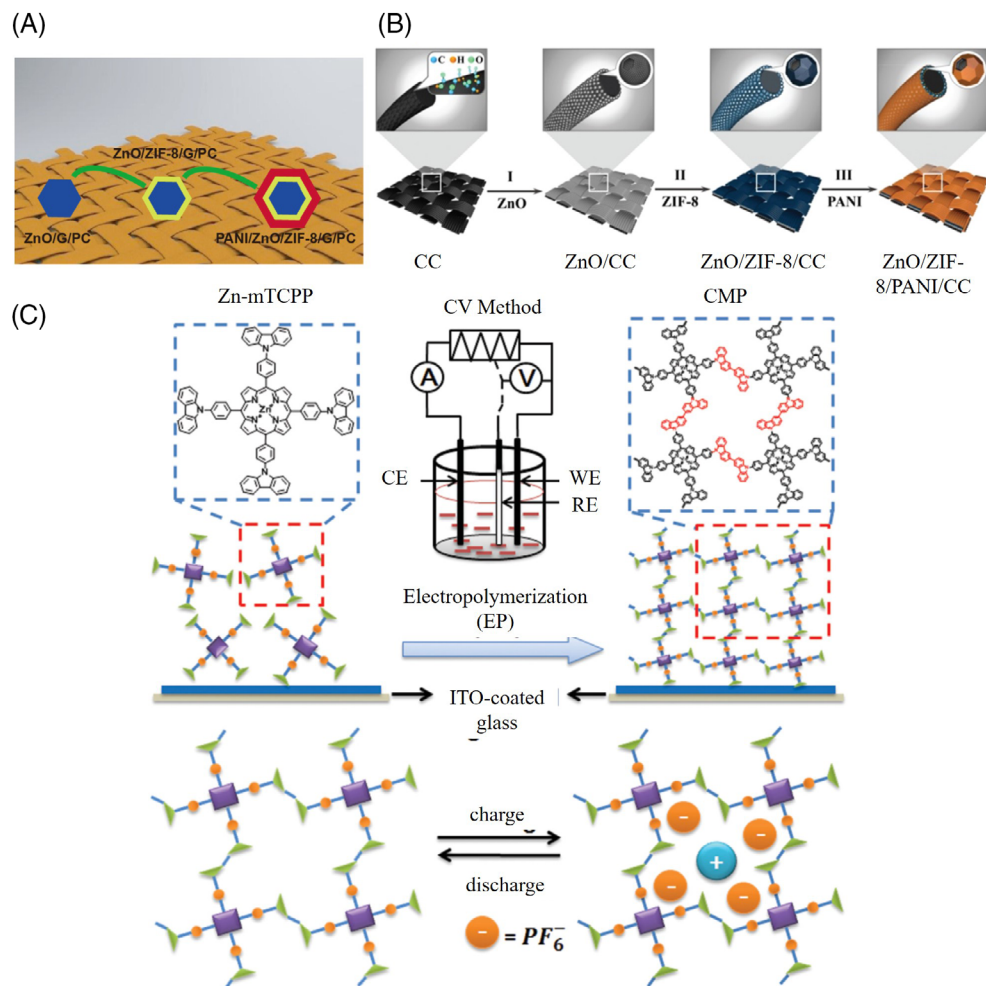
FIGURE 15 Schematic illustration of A, the fabrication process of the PANI/ZnO/ZIF-8/G/PC electrode material (**194**). Reproduced with permission: Copyright 2018, Elsevier Inc.[196] B, the fabrication process of the PANI/ZnO@ZIF-8-CC electrode material (**196**). Reproduced with permission: Copyright 2019, The Royal Society of Chemistry.[197] C, The electropolymerization process and the possible ion transmission mechanism of the poly(Zn-mTCPP) (**197**). Reproduced with permission: Copyright 2015, WILEY-VCH Verlag GmbH & Co. KGaA, Weinheim[71]

capacitance loss after 5000 cycles. In order to solve this problem, the conductive carbon-based matrix (such as CNT or GO) was introduced to POMOF materials (**173-176**). The resulting four composites with POMOF/carbon all exhibited high capacitance retention exceeding 100% after 5000 cycles, and the capacitance still remained ~100% after 8000 cycles.

There are also several SC reports on Cu-MOFs with polyamine and polyphenol ligands (**177-183**).[78,80,175-178] However, the SC electrode performances of these Cu-MOFs are not comparable to those of the Ni-MOFs with the same polyamine or polyphenol ligands. For instance, the highest C_g and C_a of Ni-CAT-based electrodes are 2133 F g^{-1} (**119**) and 3200 mF cm^{-2} (**119**), respectively, while those of Cu-CAT-based electrodes are only 215.9 F g^{-1} (**178**) and 484 mF cm^{-2} (**119**), respectively.[146,176,177] However, a SSC, based on a 4-fold interpenetrated 3D Cu-MOF (**182**), could afford an ultrahigh C_g of 396 F g^{-1}, which is the highest mass capacitance among all SC devices based on metal-organic compounds.[80]

Among a diversity of MOFs, ultrathin 2D metal-porphyrin framework (MPF) nanosheets have drawn extensive attention as electrode materials for SCs due to their π-conjugated skeletons, large surface areas, inherent porosities and abundant accessible active sites.[71,92,116,131,132,179-181,187-194] Moreover, porphyrins generally present small HOMO-LUMO gaps that enable the facile uptake and release of electrons, thus leading to fast redox kinetics.[195] Gao and coworkers developed a copper complex CuDEPP (**191**, Figure 14A) with 18π porphyrin as potential electrode materials for EES.[183] In contrast to the slow discharge/charge processes in conventional lithium ion batteries, the CuDEPP electrode exhibited a rapid redox conversion involving the transfer of electrons (up to four) (Figure 14B). More impressively, the ASC device with CuDEPP could deliver a high energy density of 345 Wh kg^{-1}, which is the highest among all SC devices based on metal-organic compounds. Despite many advantages mentioned above, the poor electrical conductivity and low chemical stability of MPFs are still inevitable obstacles which limit their electrochemical performance. One way to circumvent these problems is to carbonize the MPF precursors into conductive carbon-based composites, destroying their initial

TABLE 11 Summary of SC electrode performances of vanadium-, chromium- and iron-organic compounds

	Metal	Ligand	Composited with	Surface area[a]	Specific capacitance[b]	Cycling stability[b,c]	Electrolyte[d]	Reference
Vanadium-organic compound								
213	V	H_2BDC	—	116.8 m² g⁻¹	572.5 F g⁻¹ @ 0.5 A g⁻¹	92.8% @ 1 A g⁻¹ (10 000)	1 M Na_2SO_4	199
Chromium-organic compound								
214	Cr	H_2BDC	PANI	318.95 m² g⁻¹	1197 F g⁻¹ @ 1 A g⁻¹	90% @ 20 A g⁻¹ (10 000)	1 M H_2SO_4	200
Iron-organic compounds								
215	Fe	H_3BTC	—	—	57.5 F g⁻¹ @ 0.1 A g⁻¹	—	0.1 M K_2SO_4	70
216	Fe	H_2BDC	—	408.34 m² g⁻¹	353 F g⁻¹ @ 20 mV s⁻¹	74.4% @ 1 A g⁻¹ (10 000)	1 M H_2SO_4	201
217	Fe	(ferrocene)	GO	—	178 F g⁻¹ @ 20 mV s⁻¹	—	0.01 M ferrocene and 1 M $TEABF_4$ in ACN	202
218	Fe	(ferrocene-derivative)	GO	—	200 F g⁻¹ @ 1 A g⁻¹	96% @ 50 mV s⁻¹ (2000)	1 M H_2SO_4	81
219	Fe	(ferrocene-derivative)	rGO	—	—	89% @ 50 mV s⁻¹ (2000)	1 M H_2SO_4	79
220	Fe	(ferrocene-derivative)	CNT	—	695 F g⁻¹ @ 1 A g⁻¹	99.93% @ 50 mV s⁻¹ (2000)	1 M H_2SO_4	82

[a]Determined by BET method;
[b]Obtained by either CP and GCD method at specific current densities or CV method at specific scan rates;
[c]Evaluated by the capacitance retention after a number of charge/discharge cycles, which are shown in brackets;
[d]Normally in water except for those with special clarification.

structures inevitably.[192] Another way is to coat MPF with conductive polymers or intercalate other 2D conductive nanosheets into MPF structures.[116,179-181] Zhao and coworkers fabricated a Cu-TCPP/PPy composite (**188**) as flexible and free-standing film through a direct surface oxidation polymerization of PPy on the surface of a wrinkled 2D ultrathin Cu-TCPP film with the combination of the electrophoretic deposition method and electrochemical polymerization technology (Figure 14C).[181] The electrode **188** exhibited a high cycling stability with 91% capacitance retention after 20 000 cycles in 0.5 M H_2SO_4, and there was even no obvious capacitance loss after 20 000 cycles for the as-assembled all-solid-state SSC. Subsequently, Zhao's group developed an interlayer MXene/MPFs hybrid (**187**) film through the vacuum-assisted filtration method (Figure 14D).[180] The surface terminations (—O, —OH, and —F) on MXene nanosheets were found to bond to the hydrogen atom in carboxy groups of Cu-TCPP nanosheets through hydrogen bonds. It is believed that this synergistic effect prevents the self-restacking of both nanosheets and affords 3D interconnected conductive network with porous architecture efficiently, which facilitates the rapid ionic and electronic transport and shortens the transmission path. Besides, serious volume changes of **187** electrode during fast charge/discharge process can be alleviated by the interlayer hydrogen bonds, thus realizing an ultrahigh cycling stability (with ~100% capacitance retention after 30 000 cycles) and even maintaining a great electrode structural integrity under bending and folding.

2.5 | Zinc

The SC electrode and device performances of zinc-organic compounds and their composites (**192**-**212**)[68,71,102,196-198] are summarized in Tables 9 and 10. Similar to ZIF-67 discussed in Section 2.2, Zn-MOFs with 3-methylimidazole ligands (known as ZIF-8, **192**-**196**, **209**) have also attracted wide research interest in the field of SC.[68,102,196,197] Gao and coworkers prepared a composite (**193**) of ZIF-8 with SnO_2 quantum dots via a simple in-situ epoxide precipitation method. The obtained composite could deliver almost 10 times higher C_g than that of pure ZIF-8 (**192**).[68] ZIF-8 is also an attractive MOF to construct a flexible film electrode after forming composites with conductive polymers. Figure 15A,B demonstrate two fabrication processes of the PANI/ZnO/ZIF-8 composites (**194** and **196**).[196,197] Each of the two as-assembled all-solid-state SSCs based on **194** and **196** exhibited good mechanical stability and high capacitance retention under various mechanical bending angles, suggesting that the MOF composites are suitable for developing

TABLE 12 Summary of SC performances of vanadium-, chromium-, and iron-organic compounds

Positive electrode			Negative electrode	Specific capacitance[a]	Energy density and power density[b]	Cycling stability[a,c]	Electrolyte[d]	Reference
Metal	Ligand	Composited with						
Vanadium-organic compound								
213 V	H₂BDC	—	AC	131.6 F g⁻¹ @ 0.5 A g⁻¹	—	92.1% @ 1 A g⁻¹ (10 000)	1 M Na₂SO₄	199
				146.5 mF cm⁻² @ 0.5 mA cm⁻²	6.72 mWh cm⁻³ @ —	93.6% @ 2 mA cm⁻² (10 000)	PVA/Na₂SO₄	
Chromium-organic compound								
214 Cr	H₂BDC	PANI	**214**	371 F g⁻¹ @ 0.5 A g⁻¹	7 Wh kg⁻¹ @ — / — @ 2000 W kg⁻¹	81% @ 2.5 A g⁻¹ (10 000)	PVA/Na₂SO₄	200
Iron-organic compounds								
217 Fe	(ferrocene)	GO	**217**	178 F g⁻¹ @ 1 A g⁻¹	—	>96% @ 5 A g⁻¹ (8000)	—	202

[a]Obtained by either CP and GCD method at specific current densities, or CV method at specific scan rates;
[b]Data of maximum energy densities and maximum power densities are underlined;
[c]Evaluated by the capacitance retention after a number of charge/discharge cycles, which are shown in brackets.
[d]Normally in water except for those with special clarification.

high-capacitive and mechanically durable SCs. On the other hand, Choi and coworkers synthesized 10 Zn-MOFs (n(MTV-)MOF-5 series, **198**-**207**) with diverse structures, sizes, and functionalities of pores, based on various mixed polycarboxylate ligands (Figure 4A).[102] The C_a and C_v of these SSCs ranged from 25 to 122 mF cm⁻² and from 195 to 913 mF cm⁻³, respectively. Some Zn-MOFs exhibited high cycling stability with over 80% capacitance retention after more than 10 000 cycles. Zhang and coworkers demonstrated a high-performance film-state SSC based on a novel conjugated microporous poly(zinc-porphyrin) (CMP, **197**) films. The SC electrodes were prepared by the electropolymerization of the zinc-porphyrin monomer Zn-mTCPP (Figure 15C) on (indium tin oxide)-coated glass, and the specific surface area of the polymer reached 1450 m² g⁻¹. Figure 15C also illustrates the electropolymerization process and the possible ion transmission mechanism of **197**.

2.6 | Other metals

Tables 11 and 12 list the SC electrode and device performances of vanadium- (**213**), chromium- (**214**), and iron-organic (**215**-**220**) compounds and their composites. So far, there are still no SC reports on the scandium- and titanium-organic compounds among the first transition metal series, and only one report for vanadium- and chromium-organic compounds, respectively.[199,200] Yan and coworkers prepared a uniform rod-like V-MOF (V^{IV}(O)(BDC), also known as MIL-47, **213**) which exhibited an ultrahigh cycling stability with over 92% capacitance retention after 10 000 cycles in both three-electrode system and aqueous/all-solid-state ASC device.[199] Wang and coworkers fabricated nanocomposites (**214**) based on PANI and a Cr-MOF (MIL-101) via in situ polymerization method (Figure 16A), which provided a high C_g of 1197 F g⁻¹ and retained 90% capacitance after 10 000 cycles.[200] The as-assembled flexible all-solid-state SSC device reached a high C_g of 371 F g⁻¹ and exhibited extraordinary mechanical stability with no obvious capacitance loss at the bending angle from 0° to 180° and 90% capacitance retention after being bent at 180° for 1000 times. Figure 16B shows that four connected SSC devices could light up a red LED for 90 seconds at a voltage of 1.8 V.

Compared to vanadium- and chromium-organic compounds, iron-organic compounds are more attractive in the field of SCs due to the presence of two common oxidation states (Fe(II) and Fe(III)) of iron element. Apart from two reported iron polycarboxylate MOFs (**215** and **216**),[70,201] ferrocene is a well-known organometallic compound in the design and preparation of electrochemical materials, and its derivatives (**218**-**220**) are more

FIGURE 16 A, Schematic illustration of the fabrication process of PANI/MIL-101 composite (**214**). Reproduced with permission: Copyright 2018, Elsevier Ltd.[200] B, Digital photograph of LED powered by a four-connected SSC (**214**). Reproduced with permission: Copyright 2018, Elsevier Ltd.[200] C, Schematic illustration of two preparation processes of the composite LRGO/Fc (**217**). Reproduced with permission: Copyright 2018, The Royal Society of Chemistry.[202] D, Structure of ferrocenyl-modified GO (**218**),[81] rGO (**219**)[79] and chitosan (**220**)[82]
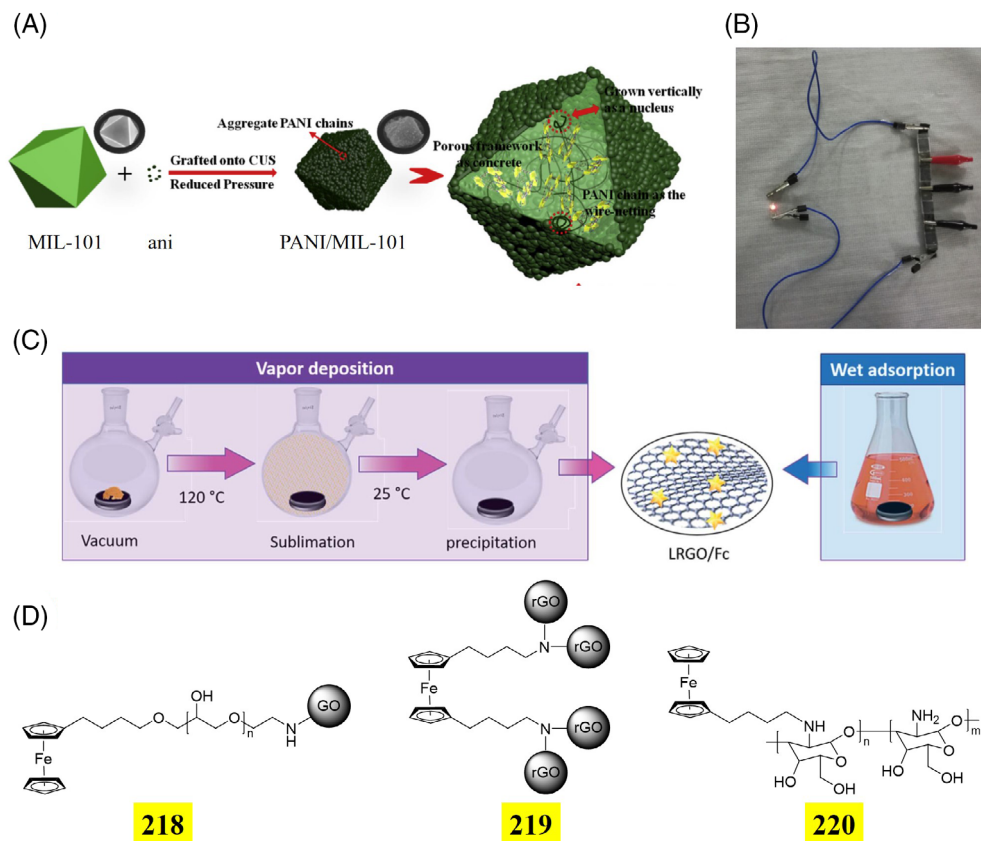
frequently reported in SCs due to their rich electrochemical redox systems and high chemical stability.[79,81,82,202] Borenstein and coworkers presented the fabrication of a laser-reduced GO/ferrocene composite (LRGO/Fc, **217**, Figure 16C) and as-assembled SSC delivered a high C_g of 178 F g^{-1}.[202] Teimuri-Mofrad and coworkers focused on the ferrocenyl compounds (Figure 16D) with functionalized tethers (—O and —N), and used them to modify GO (**218**)[81] and rGO (**219**),[79] via chemical reactions. Teimuri-Mofrad's group also synthesized a ferrocene-modified chitosan (**220**), which could provide a high C_g value close to 700 F g^{-1}.[82] All composites **218-220** showed a good cycling stability in aqueous acid solutions.

2.7 | Summary

So far, for the SC electrodes based on the monometallic metal-organic compounds of the first transition metal series and their composites, C_g, C_a and C_v values have reached 2572 F g^{-1} (**51**),[115] 5147 mF cm^{-2} (**162**),[170] and 760 F cm^{-3} (**126**),[78] respectively, and most electrodes exhibited high cycling stabilities (over 90% capacitance retention) after thousands of consecutive charge-discharge cycles. These desirable performances of the electrode materials pave the way to their practical applications. A few reports showed the application of SCs to power other

devices (LEDs in most cases),[25,80,92,107,119,125,140,175] certifying their bright future as ESSs.

3 | BIMETALLIC METAL-ORGANIC COMPOUNDS AND THEIR COMPOSITES

In the last decade, heterometallic organic compounds (especially bimetallic MOFs) and their composites (**211-264**), also have aroused an increasing attraction due to their unique SC performances.[26,37,66,76,203-222] Owing to the tunable structures resulting from the mole ratios of different metal centers, the properties of bimetallic organic compounds could be adjusted and thus novel and special applications can be obtained on the basis of the monometallic organic compounds.[57] Listed in Tables 13 and 14 are the SC electrode and device performances of bimetallic organic compounds and their composites.

Bimetallic-organic compounds with SC properties are mainly the bimetallic MOFs with either polycarboxylate ligands (**221-245**, **260-264**)[26,37,66,203-216,222] or 3-methylimidazole (**246-256**)[217-220] ligands. As shown in Tables 13 and 14, cobalt, nickel and zinc are the most popular metal elements used to fabricate SC electrodes based on bimetallic-organic compounds. So far, bimetallic-organic compounds have attracted numerous

TABLE 13 Summary of SC electrode performances of bimetallic organic compounds

	Metal	Ligand	Composited with	Surface area[a]	Specific capacitance[b]	Cycling stability[b,c]	Electrolyte[d]	Reference
221	Na, Co	H_2SDCA, azopy	—	$6.02 \ m^2 \ g^{-1}$	$321.8 \ F \ g^{-1}$ @ $4 \ A \ g^{-1}$	97.4% @ $18 \ A \ g^{-1}$ (5000)	0.5 M Na_2SO_4	203
222	Mn, Co	H2BDC	—	$15.8 \ m^2 \ g^{-1}$	$1.318 \ F \ cm^{-2}$ @ $1 \ mA \ cm^{-2}$; $2.375 \ F \ cm^{-2}$ @ $5 \ mV \ s^{-1}$	86% @ $100 \ mV \ s^{-1}$ (3000)	2 M KOH	204
223	Co, Zn	H_2BDC	—	—	$0.30 \ F \ g^{-1}$ @ $10 \ mA \ g^{-1}$; $0.49 \ F \ g^{-1}$ @ $25 \ mV \ s^{-1}$	92% @ $10 \ mA \ g^{-1}$ (1000)	0.1 M $TBAPF_6$ in ACN	66
224	Ni, Zn	H_2BDC	—	$35.5 \ m^2 \ g^{-1}$	—	92% @ $2 \ A \ g^{-1}$ (3000)	6 M KOH	205
225	Ni, Zn	H_2BDC	—	$47.9 \ m^2 \ g^{-1}$	$1620 \ F \ g^{-1}$ @ $0.25 \ A \ g^{-1}$	91% @ $2 \ A \ g^{-1}$ (3000)	6 M KOH	205
226	Ni, Zn	H_2BDC	—	$46.5 \ m^2 \ g^{-1}$	—	88% @ $2 \ A \ g^{-1}$ (3000)	6 M KOH	205
227	Ni, Zn	H_2BDC	—	$171 \ m^2 \ g^{-1}$	$380 \ F \ g^{-1}$ @ $1 \ mV \ s^{-1}$; $0.54 \ F \ cm^{-2}$ @ $1 \ mV \ s^{-1}$	>100% @ — (500)	1 M KOH	206
228	Ni, Zn	H_2BDC	rGO	$58 \ m^2 \ g^{-1}$	$758 \ F \ g^{-1}$ @ $1 \ mV \ s^{-1}$; $1.28 \ F \ cm^{-2}$ @ $1 \ mV \ s^{-1}$	>100% @ — (500)	1 M KOH	206
229	Co, Ni	H_3BTC	—	—	$758 \ F \ g^{-1}$ @ $1 \ A \ g^{-1}$	75% @ $15 \ A \ g^{-1}$ (1000)	2 M KOH	207
230	Co, Ni	H_3BTC	—	—	$1067 \ F \ g^{-1}$ @ $1 \ A \ g^{-1}$	68.4% @ $10 \ A \ g^{-1}$ (2500)	3 M KOH	208
231	Co, Ni	H_2BDC	—	$144.4 \ m^2 \ g^{-1}$	$1300 \ F \ g^{-1}$ @ $1 \ A \ g^{-1}$	71% @ $6 \ A \ g^{-1}$ (3000)	6 M KOH	209
232	Co, Ni	H_2BDC	—	$22 \ m^2 \ g^{-1}$	$2230 \ F \ g^{-1}$ @ $1 \ A \ g^{-1}$	68.5% @ $6 \ A \ g^{-1}$ (6000)	6 M KOH	210
233	Co, Ni	H_2BDC	—	$22 \ m^2 \ g^{-1}$	$1168 \ F \ g^{-1}$ @ $1 \ A \ g^{-1}$	—	6 M KOH	210
234	Co, Ni	H_2BDC	—	$27.19 \ m^2 \ g^{-1}$	$978.9 \ F \ g^{-1}$ @ $1 \ A \ g^{-1}$	78% @ $10 \ A \ g^{-1}$ (3000)	2 M KOH	211
235	Co, Ni	H_2BDC	PPy	$66.5 \ m^2 \ g^{-1}$	$1109 \ F \ g^{-1}$ @ $0.5 \ A \ g^{-1}$	81.4% @ $20 \ A \ g^{-1}$ (5000)	2 M KOH	212
236	Co, Ni	H_2OBA	—	—	$650 \ F \ g^{-1}$ @ $1 \ A \ g^{-1}$	—	6 M KOH	213
237	Co, Ni	H_2OBA	rGO	—	$860 \ F \ g^{-1}$ @ $1 \ A \ g^{-1}$	—	6 M KOH	213
238	Co, Ni	H_2BPDC	—	—	$990.7 \ F \ g^{-1}$ @ $1 \ A \ g^{-1}$	55.8% @ $1 \ A \ g^{-1}$ (3000)	2 M KOH	214
239	Co, Ni	H_2BPDC	—	—	$526 \ F \ g^{-1}$ @ $0.5 \ A \ g^{-1}$	—	2 M KOH	215
240	Co, Ni	H_2BPDC	MWCNT	—	$641 \ F \ g^{-1}$ @ $0.5 \ A \ g^{-1}$	—	2 M KOH	215
241	Co, Ni	H_2BPDC	MWCNT	—	$750 \ F \ g^{-1}$ @ $0.5 \ A \ g^{-1}$	—	2 M KOH	215
242	Co, Ni	H_2BPDC	MWCNT	—	$1010 \ F \ g^{-1}$ @ $0.5 \ A \ g^{-1}$	~100% @ $5 \ A \ g^{-1}$ (3000)	2 M KOH	215
243	Co, Ni	H_2BPDC	MWCNT	—	$638 \ F \ g^{-1}$ @ $0.5 \ A \ g^{-1}$	—	2 M KOH	215
244	Co, Ni	H_2BPDC	MWCNT	—	$610 \ F \ g^{-1}$ @ $0.5 \ A \ g^{-1}$	—	2 M KOH	215
245	Ni, Cu	2,6-H_2PDC	—	$95.37 \ m^2 \ g^{-1}$	$526 \ F \ g^{-1}$ @ $1 \ A \ g^{-1}$	8% @ $1 \ A \ g^{-1}$ (1200)	6 M KOH	216
246	Co, Ni	mIM	—	—	$530.4 \ F \ g^{-1}$ @ $0.5 \ A \ g^{-1}$	99.75% @ $2 \ A \ g^{-1}$ (2000)	1 M LiOH	217
247	Co, Ni	mIM	—	—	$120.0 \ F \ g^{-1}$ @ $1 \ A \ g^{-1}$	81.3% @ $1 \ A \ g^{-1}$ (300)	6 M KOH	218

TABLE 13 (Continued)

	Metal	Ligand	Composited with	Surface area[a]	Specific capacitance[b]	Cycling stability[b,c]	Electrolyte[d]	Reference
248	Co, Ni	mIM	—	—	$230.9\ \mathrm{F\ g^{-1}}$ @ $1\ \mathrm{A\ g^{-1}}$	—	6 M KOH	218
249	Co, Ni	mIM	—	—	$447.2\ \mathrm{F\ g^{-1}}$ @ $1\ \mathrm{A\ g^{-1}}$	99.6% @ $1\ \mathrm{A\ g^{-1}}$ (300)	6 M KOH	218
250	Co, Ni	mIM	—	—	$341.8\ \mathrm{F\ g^{-1}}$ @ $1\ \mathrm{A\ g^{-1}}$	—	6 M KOH	218
251	Co, Ni	mIM	rGO	—	$968\ \mathrm{F\ g^{-1}}$ @ $1\ \mathrm{A\ g^{-1}}$	—	—	219
252	Co, Ni	mIM	rGO	—	$1100\ \mathrm{F\ g^{-1}}$ @ $1\ \mathrm{A\ g^{-1}}$	—	—	219
253	Co, Ni	mIM	rGO	—	$1553\ \mathrm{F\ g^{-1}}$ @ $1\ \mathrm{A\ g^{-1}}$	83.6% @ — (5000)	—	219
254	Co, Ni	mIM	rGO	—	$1451\ \mathrm{F\ g^{-1}}$ @ $1\ \mathrm{A\ g^{-1}}$	—	—	219
255	Co, Zn	mIM	ZnO	—	$9.5\ \mathrm{F\ g^{-1}}$ @ $10\ \mathrm{mV\ s^{-1}}$	—	3 M KCl	220
256	Co, Zn	mIM	ZnO, PANI	—	$340.7\ \mathrm{F\ g^{-1}}$ @ $1\ \mathrm{A\ g^{-1}}$ $389.1\ \mathrm{F\ g^{-1}}$ @ $10\ \mathrm{mV\ s^{-1}}$	~82.5% @ $2\ \mathrm{A\ g^{-1}}$ (5000)	3 M KCl	220
257	Fe, Co	(ferrocene-derivative)	—	—	$446.8\ \mathrm{F\ g^{-1}}$ @ $1.2\ \mathrm{A\ g^{-1}}$	~88.37% @ $4\ \mathrm{A\ g^{-1}}$ (800)	1 M KOH	76
258	Fe, Co	(ferrocene-derivative)	—	—	$1613\ \mathrm{F\ g^{-1}}$ @ $1\ \mathrm{A\ g^{-1}}$	—	$1\ \mathrm{M}\ t\text{-}\mathrm{Bu_3PC_{10}H_{25}BF_4}$	221
259	Fe, Co	(ferrocene-derivative)	—	—	$2517\ \mathrm{F\ g^{-1}}$ @ $1\ \mathrm{A\ g^{-1}}$	90.1% @ $2\ \mathrm{A\ g^{-1}}$ (1000)	$1\ \mathrm{M}\ t\text{-}\mathrm{Bu_3PC_{10}H_{25}BF_4}$	221

[a]Determined by BET method.

[b]Obtained by either CP and GCD method at specific current densities or CV method at specific scan rates.

[c]Evaluated by the capacitance retention after a number of charge/discharge cycles, which are shown in brackets.

[d]Normally in water except for those with special clarification.

TABLE 14 Summary of SC performances of bimetallic organic compounds

	Positive electrode			Negative electrode	Specific capacitance[a]	Energy density and power density[b]	Cycling stability[a,c]	Electrolyte[d]	Reference
	Metal	Ligand	Composited with						
222	Mn, Co	H_2BDC	—	AC	$68.8\ F\ g^{-1}$ @ $0.8\ A\ g^{-1}$ $106.7\ F\ g^{-1}$ @ $10\ mV\ s^{-1}$	$30.85\ Wh\ kg^{-1}$ @ $685\ W\ kg^{-1}$ $22.8\ Wh\ kg^{-1}$ @ $2285.7\ W\ kg^{-1}$	—	2 M KOH	204
260	Co, Ni	H_2BDC	—	AC	$36.8\ F\ g^{-1}$ @ $1\ A\ g^{-1}$	$14.77\ Wh\ kg^{-1}$ @ $8477\ W\ kg^{-1}$	76.8% @ $5\ A\ g^{-1}$ (3000)	2 M KOH	211
261	Co, Ni	H_2BDC	—	CNT	$211.7\ F\ g^{-1}$ @ $1\ A\ g^{-1}$	$61.8\ Wh\ kg^{-1}$ @ $725\ W\ kg^{-1}$ $28.7\ Wh\ kg^{-1}$ @ $7250\ W\ kg^{-1}$	86% @ $10\ A\ g^{-1}$ (5000)	3 M KOH	37
262	Ni, Zn	H_2BDC	—	CNT	$183.4\ F\ g^{-1}$ @ $1\ A\ g^{-1}$	$53.6\ Wh\ kg^{-1}$ @ $725\ W\ kg^{-1}$ $26.1\ Wh\ kg^{-1}$ @ $7250\ W\ kg^{-1}$	80% @ $10\ A\ g^{-1}$ (5000)	3 M KOH	37
263	Co, Ni	H_2BDC	—	Graphene, CNT	$1.43\ F\ cm^{-2}$ @ $6.1\ A\ cm^{-2}$ $100\ F\ cm^{-3}$ @ $0.5\ A\ cm^{-3}$	$31.3\ mWh\ cm^{-3}$ @ $376.6\ mW\ cm^{-3}$ $17.9\ mWh\ cm^{-3}$ @ $3769.4\ mW\ cm^{-3}$	~100% @ $3\ A\ cm^{-3}$ (10 000)	6 M KOH	26
229	Co, Ni	H_3BTC	—	AC	$58.8\ F\ g^{-1}$ @ $1\ A\ g^{-1}$	$20.9\ Wh\ kg^{-1}$ @ $800\ W\ kg^{-1}$ $15.8\ Wh\ kg^{-1}$ @ $4000\ W\ kg^{-1}$	85% @ $3\ A\ g^{-1}$ (5000)	2 M KOH	207
264	Co, Ni	H_3PTC	—	AC	$169.5\ F\ g^{-1}$ @ $0.5\ A\ g^{-1}$	$75.1\ Wh\ kg^{-1}$ @ $900\ W\ kg^{-1}$ $41.5\ Wh\ kg^{-1}$ @ $18\ kW\ kg^{-1}$	85.6% @ $5\ A\ g^{-1}$ (8000)	PBI/KOH	222
231	Co, Ni	H_2BDC	—	AC	—	$25.92\ Wh\ kg^{-1}$ @ $375\ W\ kg^{-1}$	78.1% @ $1\ A\ g^{-1}$ (6000)	6 M KOH	209
232	Co, Ni	H_2BDC	—	AC	$109.9\ F\ g^{-1}$ @ $0.5\ A\ g^{-1}$	$34.3\ Wh\ kg^{-1}$ @ $375\ W\ kg^{-1}$ $20.83\ Wh\ kg^{-1}$ @ $7500\ W\ kg^{-1}$	75.2% @ $1\ A\ g^{-1}$ (6000)	6 M KOH	210
235	Co, Ni	H_2BDC	PPy	AC	$132\ F\ g^{-1}$ @ $0.5\ A\ g^{-1}$	$41.2\ Wh\ kg^{-1}$ @ $375\ W\ kg^{-1}$	79.1% @ $5\ A\ g^{-1}$ (10 000)	2 M KOH	212
237	Co, Ni	H_2OBA	rGO	AC	$181.4\ F\ g^{-1}$ @ $1\ A\ g^{-1}$	$72.8\ Wh\ kg^{-1}$ @ $850\ W\ kg^{-1}$ $15.1\ Wh\ kg^{-1}$ @ $42.5\ kW\ kg^{-1}$	91.6% @ — (6000)	6 M KOH	213
242	Co, Ni	H_2BPDC	MWCNT	Graphite	$142\ F\ g^{-1}$ @ $0.5\ A\ g^{-1}$	$19.7\ Wh\ kg^{-1}$ @ ~$250\ W\ kg^{-1}$ $6.25\ Wh\ kg^{-1}$ @ $28\ 125\ W\ kg^{-1}$	~100% @ $5\ A\ g^{-1}$ (3000)	2 M KOH	215
242	Co, Ni	H_2BPDC	MWCNT	**242**	$146\ F\ g^{-1}$ @ $0.5\ A\ g^{-1}$	$20.2\ Wh\ kg^{-1}$ @ ~$250\ W\ kg^{-1}$ $1.1\ Wh\ kg^{-1}$ @ ~$10\ 000\ W\ kg^{-1}$	—	2 M KOH	215
245	Ni, Cu	$2,6-H_2PDC$	—	AC	$48.7\ F\ g^{-1}$ @ $1\ A\ g^{-1}$	$17.3\ Wh\ kg^{-1}$ @ $798.5\ kW\ kg^{-1}$	63% @ $1\ A\ g^{-1}$ (1000)	6 M KOH	216
253	Co, Ni	mIM	rGO	rGO	—	$44\ Wh\ kg^{-1}$ @ $3168\ W\ kg^{-1}$	—	—	219

Abbreviation: PBI, polybenzimidazole.

[a]Obtained by either CP and GCD method at specific current densities, or CV method at specific scan rates;

[b]Data of maximum energy densities and maximum power densities are underlined;

[c]Evaluated by the capacitance retention after a number of charge/discharge cycles, which are shown in brackets.

[d]Normally in water except for those with special clarification.

FIGURE 17 Schematic illustration of A, the synthetic process of 3D hierarchical bimetallic MOFs (261 and 262). Reproduced with permission: Copyright 2017, The Royal Society of Chemistry.[37] B, Ion and charge transfer in the 261 and 262 electrodes. Reproduced with permission: Copyright 2017, The Royal Society of Chemistry.[37] C, The synthesis process for the Ni/Co-MOF (229). Reproduced with permission: Copyright 2018, Elsevier Inc.[207] D, A possible mode of structural change for the Ni-MOF before and after Zn-doping. Reproduced with permission: Copyright 2014, The Royal Society of Chemistry[205]
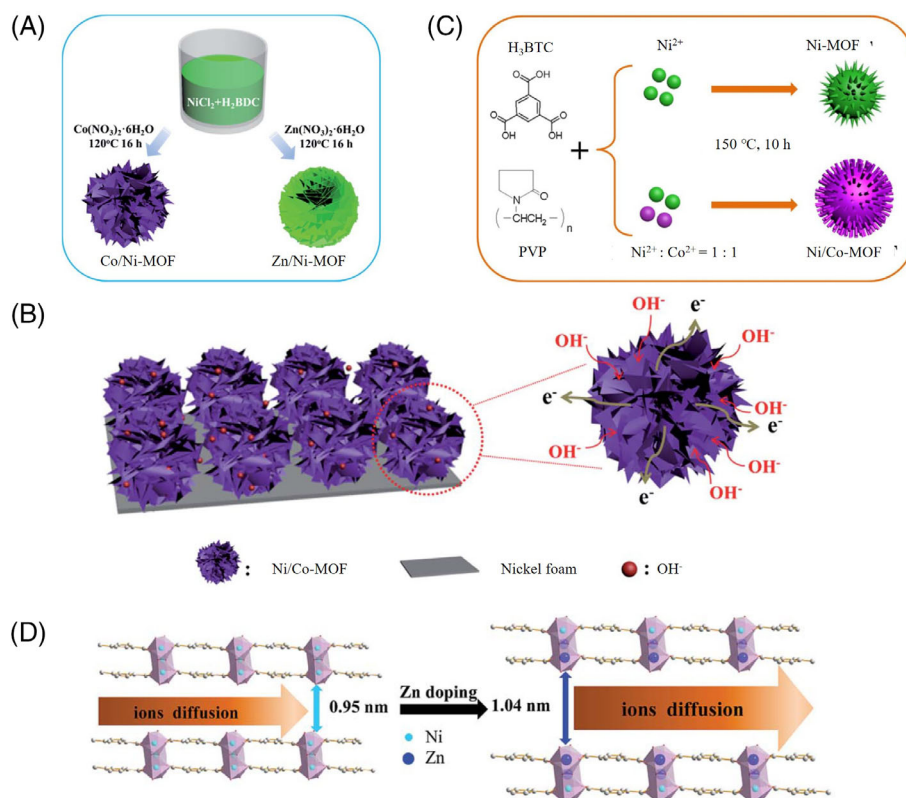
research interest due to their good SC performances. Rajak and coworkers synthesized a new heterometallic Na/Co-based MOF (221) by a facile mixed ligand strategy with slow-diffusion technique at room temperature.[203] For 221, the high cycling stability (with less than 3% capacitance loss after 5000 charge-discharge cycles) was observed at a quite high current density of 18 A g^{-1}. Wang and coworkers synthesized a series of bimetallic MOF nanosheets (232 and 233) with arrays on nickel foams having different nickel-cobalt mole ratios, and 232 gave a high C_g of 2230 F g^{-1}.[210] Rahmanifar and coworkers prepared the composite (237) of Ni/Co-MOF (236) and rGO, and the as-assembled ASC device based on 237 realized a high energy density and power density of 72.8 Wh kg^{-1} and 42.5 kW kg^{-1}, respectively.[213] Beka and coworkers reported a series of 2D Ni/Co-MOF ultrathin nanosheets/rGO hybrid electrode materials (251-254) with different rGO doping weights, and the C_g of composite 253 reached a high value of 1553 F g^{-1}.[219]

Interestingly, higher specific capacitance values have been observed in some bimetallic organic compounds when compared to the monometallic ones with the same ligands. Jiao and coworkers synthesized a Ni-BDC MOF and partially substituted it with Co^{2+} and Zn^{2+} to form two 3D hierarchical bimetallic MOFs, Co/Ni-MOF (261), and Zn/Ni-MOF (262).[37] Figure 17A illustrates the synthetic process of 261 and 262. It was found that the bimetallic MOFs showed higher C_g values (236.1 and 161.5

mAh g^{-1} for Co/Ni-MOF and Zn/Ni-MOF, respectively) than that of Ni-MOF (122 mAh g^{-1}) when they were used as the battery-type electrodes.[37] The ASCs based on 261 and 262 could also provide higher C_g and energy densities than those of the ASC based on the original monometallic Ni-MOF. The fact that these bimetallic MOFs exhibited superior capacitances to the monometallic MOF can be ascribed to the following reasons. On one hand, as demonstrated in Figure 17B, the smaller ionic radius of Co^{2+} (0.65 Å) than that of Ni^{2+} (0.69 Å) helps create more Ni^{2+} vacancies in the Co/Ni-MOF, which may lead to the generation of a larger number of free holes for pseudo-capacitance, thus contributing to the improvement of the electrical conductivity.[223,224] On the other hand, the bigger Zn^{2+} (0.74 Å) partly replaced Ni^{2+} (0. 69 Å) in the Zn/Ni-MOF to form a layered structure with enlarged interlayer distances (1.04 and 0.95 nm for Zn/Ni-MOF and Ni-MOF, respectively), which provides enough space for electrolyte diffusion and ensures more facile OH$^-$ intercalation and deintercalation for electrical double-layer capacitance.[225] The increase of capacitance in bimetallic organic compounds compared to the relevant monometallic ones was also observed in other reports.[210,213,216,217]

Moreover, in several reports, bimetallic organic compounds tend to exhibit a higher cycling stability than the monometallic ones when used as SC electrode materials. A series of Zn-doped Ni-MOFs (224-226) exhibited over 88% capacitance retention after 3000 cycles, which is far
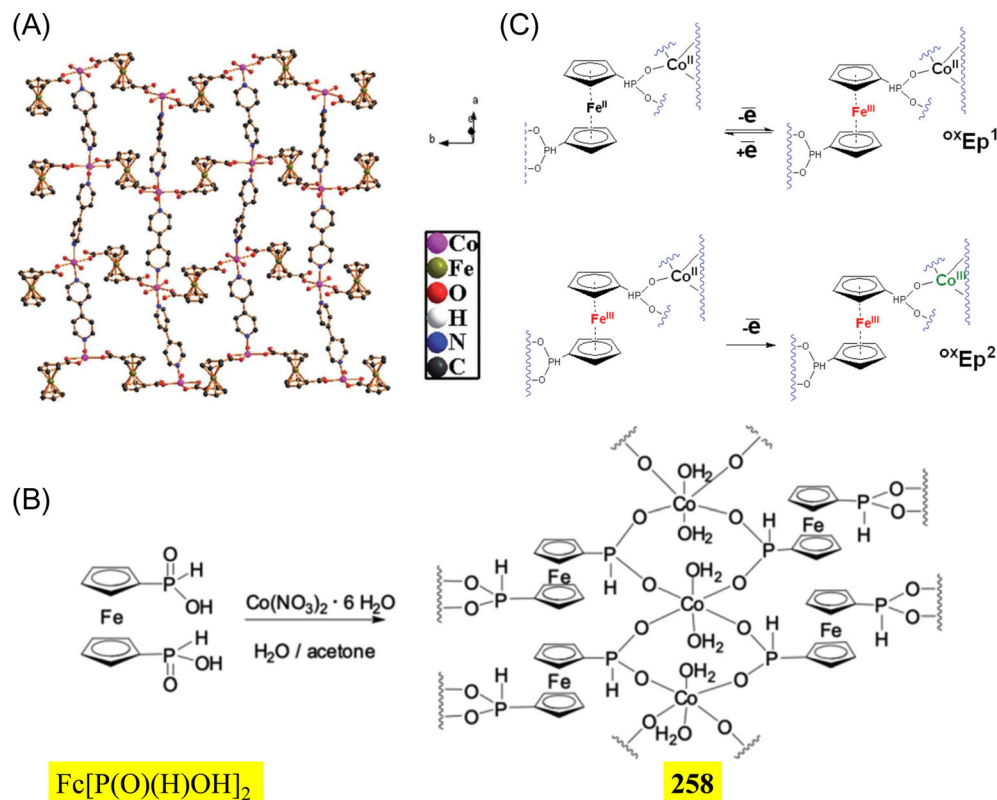
(A)

(C)

(B)

Fc[P(O)(H)OH]$_2$

258

FIGURE 18 A, Ball-stick model of **257** along the *c*-axis. Reproduced with permission: Copyright 2017, The Royal Society of Chemistry.[76] B, Synthesis route of [Co(H$_2$O)$_2$(Fc[P(O)(H)O]$_2$)·2H$_2$O]$_n$ (**258**). Reproduced with permission: Copyright 2019, The Royal Society of Chemistry.[221] C, The oxidation processes of **258** and **259**. Reproduced with permission: Copyright 2019, The Royal Society of Chemistry[221]

larger than that of the non-doped Ni-MOF (66%).[205] The Ni/Co-MOF (**229**) also showed a higher cycling stability than that of Ni-MOF synthesized under the same condition (Figure 17C).[207] The enhancement of cycling stability of bimetallic MOFs can be ascribed to the change of MOF's structure and morphology when they were modified by heterometal elements. It was suggested that the flower-like microspheres of **224 to 226** aggregated by the nanosheets could provide interconnected open pores (Figure 17D),[205] which not only should be favorable for the diffusion of electrolytes but also could effectively help buffer the volume variation during the charge/discharge process.[226,227] For **229**, it was inferred that the interconnected rods would support the structure to alleviate the structure collapse during the charge/discharge process.[207] Besides, it was reported that disordered structure was beneficial to enhance the electrochemical and structure stability. Therefore, the bimetallic MOFs with low-crystalline states are caused by the introduction of heterometal ions, which would possess a higher rate capacitance and a better cycling stability.[74]

Besides using mixed metal salts in the synthetic processes or doping heterometal elements in the post-synthesis, another approach to construct bimetallic organic compounds is to adopt ferrocene-derivatized ligands to coordinate with metal ions directly.[76,221] Rajak and coworkers synthesized a 3D inclined polycatenated Co-MOF (**257**, Figure 18A) with mixed ligands (H$_2$FcDC and

bipy).[76] It was found that, compared to the Co-MOF with bipy ligand only, the introduction of highly electro-active ferrocene based ligand H$_2$FcDC not only enhances the structural integrity and flexibility but also improves the electrochemical performance. Khrizanforov and coworkers synthesized two 2D Co-based coordination polymers, [Co(H$_2$O)$_2$(Fc[P(O)(H)O]$_2$)·2H$_2$O]$_n$ (**258**) and [Co(Fc[P(O)(H)O]$_2$)]$_n$ (**259**) (Figure 18B).[221] Figure 18C illustrates the charge transfer mechanism between different oxidation states of iron and cobalt in two coordination polymers. The C_g of the electrode based on **259** reached 2517 F g^{-1}, which has been the highest C_g among all bimetallic organic compounds so far, and is very close to the highest value (2572 F g^{-1}, **51**) for all metal-organic compounds.[115]

4 | CHALLENGES AND OUTLOOK

In summary, the metal-organic compounds of the first transition metal series have attracted extensive attention for the application in the SC field, by virtue of their rich redox activities, optimizable synthesis protocols, abundant active sites, adjustable porous structures, high surface areas and diverse topological architectures. The performance of partial SC electrodes based on metal-organic compounds has surpassed that of the traditional electrode materials such as carbon-based materials, metal oxides/

nitrides/carbides/sulfides/hydroxides and conductive polymers. In this article, the first-transition-series metal-organic compounds and their composites as SC electrode materials are reviewed comprehensively in terms of ligand selection, synthesis strategy, structural characterization and electrochemical performance. Despite the great progresses in the development of metal-organic compounds as SC electrode materials in the past decade, these materials are still confronted with several challenges. To realize the commercialization of SCs based on metal-organic compounds and satisfy the requirements of practical applications in our daily life, the design and research strategies to overcome the bottlenecks are listed as follows:

1. Most metal-organic compounds lack sufficient conductivity in their pristine forms. A widely adopted approach to fabricate SC electrode from less conductive materials is to introduce the conductive matrices (such as carbon-based materials and conductive polymers). However, in some cases, the composition of metal-organic compounds with conductive matrices could block their inherent porosities, decrease the surface area and the number of active sites, impede the mobility of ions and electrons, and result in enhancing the cycling stability at the cost of sacrificing the specific capacitance and energy density. For composite formation strategy, morphology, structure, reaction mechanism and electrochemical properties of the composites should be optimized in light of the synthetic methods and preparation processes to develop more advanced materials.

2. A more straightforward way to conquer the above issues is to develop metal-organic compounds with inherently high conductivities. Compared to the highly porous but less conductive metal-organic compounds in 3D topologies, those in 2D topologies can achieve sufficiently high levels of conductivities through their planar π-conjugated frameworks without the assistance of conductive matrices. Although the use of π-conjugated building blocks of large formula weight for 2D structures may cause a risk in the loss of the specific gravimetric capacitance, this category of materials and their composites are still promising candidates.

3. To realize higher capacitance, the porous metal-organic compounds can serve as templates for preparing pseudocapacitive materials. The capacitance of these composites can be largely improved due to the extremely high theoretical capacitance values of pseudocapacitive materials such as transition metal oxides. However, it is worth mentioning that the instinctively low structural and chemical stability of pseudocapacitive materials may limit the cycling performances of their electrode composites.

4. As discussed in Section 3, doped monometallic MOFs with heterometal ions to form bimetallic compounds tend to help achieve superior capacitances. Theoretically, the doping ions which have smaller ionic radii may create more vacancies and consequently more holes in the MOF structures for improving the electrical conductivity, while the doping ions which have larger radii could enlarge the interlayer distances to allow more space for electrolyte diffusion. By optimizing the ratio of heterometal ions, the capacitance can be improved significantly.

5. To date, the research of metal-organic compounds as SC electrode materials still mainly focuses on the aqueous electrolytes or gel electrolytes prepared from aqueous solutions. The electrolysis voltage of water (1.23 V) hinders the SCs based on metal-organic compounds from the applications when wide potential windows are required. The limitation of metal-organic compounds in aqueous media may be originated from their solubility in organic conductive ionic liquids. The development of oleophobic metal-organic compounds for the SC electrodes would extend their applications to a wider potential window.

6. There is still a lack of fundamental understanding into the electrochemical mechanism of metal-organic compounds and the interaction effects of each component in the composites. Most researchers believe the electrochemical behaviors of metal-organic compounds to be originated from the pseudocapacitive mechanism, while only a few examples showed the EDLC mechanism. More efforts on exploring the electrochemical mechanism associated with the experimental characterizations and theoretical studies should be made to conduct the targeted improvement of the SC performances.

7. The processes of electrode fabrication and device assembling are yet to be optimized and several important factors are even obscure in most reports, such as current collector variety, binder variety, mass ratios of active materials and binders, the volume of liquid electrolytes, etc. These factors can play a significant role in the electrochemical performance. Optimized design of electrodes and SC devices should be taken into account in future research endeavors.

To conclude, metal-organic compounds are still very promising active materials for SCs in spite of their existing challenges, especially those from the first transition metal series. So far, considerable research efforts have been made to use metal-organic compounds not only in SC devices with high performances, but also diverse SC applications at the laboratory scale, such as on-chip micro-SCs, portable all-solid-state SCs, wearable flexible SCs, AC line-filtering SCs and battery-SC hybrid devices.

With the rapid development of metal-organic compounds in recent years, a bright future is believed to come for this new type of functional materials.

CONFLICT OF INTEREST
There are no conflicts to declare.

ORCID
Bulin Chen https://orcid.org/0000-0002-0553-9107
Linli Xu https://orcid.org/0000-0002-7032-9464
Zhiyuan Xie https://orcid.org/0000-0001-6081-2033
Wai-Yeung Wong https://orcid.org/0000-0002-9949-7525

REFERENCES
1. González A, Goikolea E, Barrena JA, Mysyk R. Review on supercapacitors: technologies and materials. *Renew Sustain Energy Rev*. 2016;58:1189-1206.
2. Christen T, Carlen MW. Theory of Ragone plots. *J Power Sources*. 2000;91(2):210-216.
3. Yu M, Lin D, Feng H, Zeng Y, Tong Y, Lu X. Boosting the energy density of carbon-based aqueous supercapacitors by optimizing the surface charge. *Angew Chem Int Ed*. 2017;56(20):5454-5459.
4. Kandalkar SG, Dhawale DS, Kim C-K, Lokhande CD. Chemical synthesis of cobalt oxide thin film electrode for supercapacitor application. *Synth Met*. 2010;160(11):1299-1302.
5. Shi P, Li L, Hua L, et al. Design of amorphous manganese oxide@multiwalled carbon nanotube fiber for robust solid-state supercapacitor. *ACS Nano*. 2017;11(1):444-452.
6. Yu M, Cheng X, Zeng Y, et al. Dual-doped molybdenum trioxide nanowires: a bifunctional anode for fiber-shaped asymmetric supercapacitors and microbial fuel cells. *Angew Chem Int Ed*. 2016;55(23):6762-6766.
7. Gebresilassie EG, Armand M, Scrosati B, Passerini S. Energy storage materials synthesized from ionic liquids. *Angew Chem Int Ed*. 2014;53(49):13342-13359.
8. Jabeen N, Xia Q, Savilov SV, Aldoshin SM, Yu Y, Xia H. Enhanced pseudocapacitive performance of α-MnO_2 by cation preinsertion. *ACS Appl Mater Interfaces*. 2016;8(49):33732-33740.
9. Dong L, Xu C, Li Y, et al. Flexible electrodes and supercapacitors for wearable energy storage: a review by category. *J Mater Chem A*. 2016;4(13):4659-4685.
10. Zeng Y, Lin Z, Meng Y, et al. Flexible ultrafast aqueous rechargeable Ni//Bi battery based on highly durable single-crystalline bismuth nanostructured anode. *Adv Mater*. 2016;28(41):9188-9195.
11. Ozkan S, Nguyen NT, Hwang I, Mazare A, Schmuki P. Highly conducting spaced TiO_2 nanotubes enable defined conformal coating with nanocrystalline Nb_2O_5 and high performance supercapacitor applications. *Small*. 2017;13(14):1603821.
12. Wang S, Liu N, Su J, et al. Highly stretchable and self-healable supercapacitor with reduced graphene oxide based fiber springs. *ACS Nano*. 2017;11(2):2066-2074.
13. Simon P, Gogotsi Y. Materials for electrochemical capacitors. *Nat Mater*. 2008;7(11):845-854.
14. Zhang H, Nai J, Yu L, Lou XW. Metal-organic-framework-based materials as platforms for renewable energy and environmental applications. *Joule*. 2017;1(1):77-107.
15. Li X, Zhao Y, Bai Y, et al. A non-woven network of porous nitrogen-doping carbon nanofibers as a binder-free electrode for supercapacitors. *Electrochim Acta*. 2017;230:445-453.
16. Huang P, Lethien C, Pinaud S, et al. On-chip and freestanding elastic carbon films for micro-supercapacitors. *Science*. 2016;351(6274):691-695.
17. Deka BK, Hazarika A, Kim J, Park Y-B, Park HW. Recent development and challenges of multifunctional structural supercapacitors for automotive industries. *Int J Energy Res*. 2017;41(10):1397-1411.
18. Largeot C, Portet C, Chmiola J, Taberna P-L, Gogotsi Y, Simon P. Relation between the ion size and pore size for an electric double-layer capacitor. *J Am Chem Soc*. 2008;130(9):2730-2731.
19. Wang G, Zhang L, Zhang J. A review of electrode materials for electrochemical supercapacitors. *Chem Soc Rev*. 2012;41(2):797-828.
20. Huang C, Zhang J, Young NP, Snaith HJ, Grant PS. Solid-state supercapacitors with rationally designed heterogeneous electrodes fabricated by large area spray processing for wearable energy storage applications. *Sci Rep*. 2016;6(1):25684.
21. González-Gaitán C, Ruiz-Rosas R, Nishihara H, Kyotani T, Morallón E, Cazorla-Amorós D. Successful functionalization of superporous zeolite templated carbon using aminobenzene acids and electrochemical methods. *Carbon*. 2016;99:157-166.
22. Wang Y, Shi Z, Huang Y, et al. Supercapacitor devices based on graphene materials. *J Phys Chem C*. 2009;113(30):13103-13107.
23. Hu X, Shao W, Hang X, Zhang X, Zhu W, Xie Y. Superior electrical conductivity in hydrogenated layered ternary chalcogenide nanosheets for flexible all-solid-state supercapacitors. *Angew Chem Int Ed*. 2016;55(19):5733-5738.
24. Sundriyal S, Kaur H, Bhardwaj SK, Mishra S, Kim K-H, Deep A. Metal-organic frameworks and their composites as efficient electrodes for supercapacitor applications. *Coord Chem Rev*. 2018;369:15-38.
25. Wang K, Li Q, Ren Z, et al. 2D metal–organic frameworks (MOFs) for high-performance batcap hybrid devices. *Small*. 2020;16(30):2001987.

26. Hong M, Zhou C, Xu S, et al. Bi-metal organic framework nanosheets assembled on nickel wire films for volumetric-energy-dense supercapacitors. *J Power Sources*. 2019;423:80-89.

27. Iqbal MZ, Faisal MM, Ali SR, Farid S, Afzal AM. Co-MOF/polyaniline-based electrode material for high performance supercapattery devices. *Electrochim Acta*. 2020;346:136039.

28. Tang HA, Zhang MM, Gong Y, Lin JH. Coordination polymer-based supercapacitors with matched energy levels: enhanced capacity under visible light illumination in the presence of methanol. *Dalton Trans*. 2018;47(32):11146-11157.

29. Chen Y, Wang N, Hu W, Komarneni S. In situ construction of porous Ni/Co-MOF@carbon cloth electrode with honeycomb-like structure for high-performance energy storage. *J Porous Mater*. 2019;26(3):921-929.

30. Jiao Y, Pei J, Yan C, Chen D, Hu Y, Chen G. Layered nickel metal–organic framework for high performance alkaline battery-supercapacitor hybrid devices. *J Mater Chem A*. 2016;4 (34):13344-13351.

31. Zhang X, Wang J, Ji X, et al. Nickel/cobalt bimetallic metal-organic frameworks ultrathin nanosheets with enhanced performance for supercapacitors. *J Alloys Compd*. 2020;825:154069.

32. Ran F, Xu X, Pan D, Liu Y, Bai Y, Shao L. Ultrathin 2D metal–organic framework nanosheets in situ interpenetrated by functional CNTs for hybrid energy storage device. *Nano-Micro Lett*. 2020;12(1):46.

33. Patel SS, Krishnamurthy G, Foro S. Chelated Zn–metal–organic frameworks: synthesis, crystal structure and electrochemical energy storage. *J Inorg Organomet Polym Mater*. 2020;30(7):2562-2571.

34. Zhang L, Zhang Y, Huang S, et al. Co_3O_4/Ni-based MOFs on carbon cloth for flexible alkaline battery-supercapacitor hybrid devices and near-infrared photocatalytic hydrogen evolution. *Electrochim Acta*. 2018;281:189-197.

35. Payami E, Ahadzadeh I, Mohammadi R, Teimuri-Mofrad R. Design and synthesis of novel binuclear ferrocenyl-intercalated graphene oxide and polyaniline nanocomposite for supercapacitor applications. *Electrochim Acta*. 2020;342:136078.

36. Chen Y, Ni D, Yang X, Liu C, Yin J, Cai K. Microwave-assisted synthesis of honeycomblike hierarchical spherical Zn-doped Ni-MOF as a high-performance battery-type supercapacitor electrode material. *Electrochim Acta*. 2018;278:114-123.

37. Jiao Y, Pei J, Chen D, et al. Mixed-metallic MOF based electrode materials for high performance hybrid supercapacitors. *J Mater Chem A*. 2017;5(3):1094-1102.

38. Wei T, Zhang M, Wu P, et al. POM-based metal-organic framework/reduced graphene oxide nanocomposites with hybrid behavior of battery-supercapacitor for superior lithium storage. *Nano Energy*. 2017;34:205-214.

39. Wang K, Lv B, Wang Z, Wu H, Xu J, Zhang Q. Two-fold inter-penetrated Mn-based metal–organic frameworks (MOFs) as battery-type electrode materials for charge storage. *Dalton Trans*. 2020;49(2):411-417.

40. Zhang Y, Zhen Z, Zhang Z, et al. In-situ synthesis of carbon nanotube/graphene composite sponge and its application as compressible supercapacitor electrode. *Electrochim Acta*. 2015;157:134-141.

41. Sahu V, Shekhar S, Sharma RK, Singh G. Ultrahigh performance supercapacitor from lacey reduced graphene oxide nanoribbons. *ACS Appl Mater Interfaces*. 2015;7(5):3110-3116.

42. Wang J-G, Kang F, Wei B. Engineering of MnO_2-based nanocomposites for high-performance supercapacitors. *Prog Mater Sci*. 2015;74:51-124.

43. Li L, Song H, Zhang Q, Yao J, Chen X. Effect of compounding process on the structure and electrochemical properties of ordered mesoporous carbon/polyaniline composites as electrodes for supercapacitors. *J Power Sources*. 2009;187(1): 268-274.

44. Liu M, Du Y, Miao Y-E, et al. Anisotropic conductive films based on highly aligned polyimide fibers containing hybrid materials of graphene nanoribbons and carbon nanotubes. *Nanoscale*. 2015;7(3):1037-1046.

45. Wang K, Zhang X, Sun X, Ma Y. Conducting polymer hydrogel materials for high-performance flexible solid-state supercapacitors. *Sci China Mater*. 2016;59(6):412-420.

46. Wulan Septiani NL, Kaneti YV, Fathoni KB, et al. Self-assembly of nickel phosphate-based nanotubes into two-dimensional crumpled sheet-like architectures for high-performance asymmetric supercapacitors. *Nano Energy*. 2020; 67:104270.

47. Azhar A, Li Y, Cai Z, et al. Nanoarchitectonics: a new materials horizon for Prussian blue and its analogues. *Bull Chem Soc Jpn*. 2019;92(4):875-904.

48. Li X, Yang X, Xue H, Pang H, Xu Q. Metal–organic frameworks as a platform for clean energy applications. *EnergyChem*. 2020;2(2):100027.

49. Zheng S, Li Q, Xue H, Pang H, Xu Q. A highly alkaline-stable metal oxide@metal–organic framework composite for high-performance electrochemical energy storage. *Natl Sci Rev*. 2020;7(2):305-314.

50. Zheng Y, Zheng S, Xu Y, Xue H, Liu C, Pang H. Ultrathin two-dimensional cobalt-organic frameworks nanosheets for electrochemical energy storage. *Chem Eng J*. 2019;373:1319-1328.

51. Belin T, Epron F. Characterization methods of carbon nanotubes: a review. *Mater Sci Eng: B*. 2005;119(2):105-118.

52. He S, Chen W. Application of biomass-derived flexible carbon cloth coated with MnO_2 nanosheets in supercapacitors. *J Power Sources*. 2015;294:150-158.

53. Dhawale DS, Kim S, Park D-H, et al. Hierarchically ordered porous CoOOH thin-film electrodes for high-performance supercapacitors. *ChemElectroChem*. 2015;2(4):497-502.

54. Wu Q, Xu Y, Yao Z, Liu A, Shi G. Supercapacitors based on flexible graphene/polyaniline nanofiber composite films. *ACS Nano*. 2010;4(4):1963-1970.

55. Li Z-F, Zhang H, Liu Q, Sun L, Stanciu L, Xie J. Fabrication of high-surface-area graphene/polyaniline nanocomposites and their application in supercapacitors. *ACS Appl Mater Interfaces*. 2013;5(7):2685-2691.

56. Chuang C-M, Huang C-W, Teng H, Ting J-M. Effects of carbon nanotube grafting on the performance of electric double layer capacitors. *Energy Fuel*. 2010;24(12):6476-6482.

57. Wang K-B, Bi R, Wang Z-K, Chu Y, Wu H. Metal–organic frameworks with different spatial dimensions for supercapacitors. *New J Chem*. 2020;44(8):3147-3167.

58. Wang K-B, Xun Q, Zhang Q. Recent progress in metal-organic frameworks as active materials for supercapacitors. *EnergyChem*. 2020;2(1):100025.

59. Salunkhe RR, Kaneti YV, Yamauchi Y. Metal–organic framework-derived nanoporous metal oxides toward

supercapacitor applications: Progress and prospects. *ACS Nano*. 2017;11(6):5293-5308.

60. Liu Y, Xu X, Shao Z, Jiang SP. Metal-organic frameworks derived porous carbon, metal oxides and metal sulfides-based compounds for supercapacitors application. *Energy Storage Mater*. 2020;26:1-22.

61. Salunkhe RR, Kaneti YV, Kim J, Kim JH, Yamauchi Y. Nanoarchitectures for metal–organic framework-derived nanoporous carbons toward supercapacitor applications. *Acc Chem Res*. 2016;49(12):2796-2806.

62. Wu S, Liu J, Wang H, Yan H. A review of performance optimization of MOF-derived metal oxide as electrode materials for supercapacitors. *Int J Energy Res*. 2019;43(2):697-716.

63. Tang J, Salunkhe RR, Zhang H, et al. Bimetallic metal-organic frameworks for controlled catalytic graphitization of Nanoporous carbons. *Sci Rep*. 2016;6(1):30295.

64. Li Y, Henzie J, Park T, et al. Fabrication of flexible micro-supercapacitors with binder-free ZIF-8 derived carbon films via electrophoretic deposition. *Bull Chem Soc Jpn*. 2019;93(1):176-181.

65. Liang Z, Zhao R, Qiu T, Zou R, Xu Q. Metal-organic framework-derived materials for electrochemical energy applications. *EnergyChem*. 2019;1(1):100001.

66. Díaz R, Orcajo MG, Botas JA, Calleja G, Palma J. Co8-MOF-5 as electrode for supercapacitors. *Mater Lett*. 2012;68:126-128.

67. Lee DY, Shinde DV, Kim E-K, et al. Supercapacitive property of metal–organic-frameworks with different pore dimensions and morphology. *Microporous Mesoporous Mater*. 2013;171:53-57.

68. Gao Y, Wu J, Zhang W, Tan Y, Zhao J, Tang B. The electrochemical performance of SnO_2 quantum dots@zeolitic imidazolate frameworks-8 (ZIF-8) composite material for supercapacitors. *Mater Lett*. 2014;128:208-211.

69. Gao Y, Wu J, Zhang W, et al. Synthesis of nickel carbonate hydroxide/zeolitic imidazolate framework-8 as a supercapacitors electrode. *RSC Adv*. 2014;4(68):36366-36371.

70. Campagnol N, Romero-Vara R, Deleu W, et al. A hybrid supercapacitor based on porous carbon and the metal-organic framework MIL-100(Fe). *ChemElectroChem*. 2014;1(7):1182-1188.

71. Zhang H, Zhang Y, Gu C, Ma Y. Electropolymerized conjugated microporous poly(zinc-porphyrin) films as potential electrode materials in supercapacitors. *Adv Energy Mater*. 2015;5(10):1402175.

72. Liu X, Shi C, Zhai C, Cheng M, Liu Q, Wang G. Cobalt-based layered metal–organic framework as an ultrahigh capacity supercapacitor electrode material. *ACS Appl Mater Interfaces*. 2016;8(7):4585-4591.

73. Liu X, Valentine HL, Pan W-P, Cao Y, Yan B. 2D metal–organic frameworks: syntheses, structures, and electrochemical properties. *Inorg Chim Acta*. 2016;447:162-167.

74. Qu C, Jiao Y, Zhao B, et al. Nickel-based pillared MOFs for high-performance supercapacitors: design, synthesis and stability study. *Nano Energy*. 2016;26:66-73.

75. Chen C, Zhu Z, Li X, Li J. Electropolymerization and energy storage of poly[Ni(salphen)]/MWCNT composite materials for supercapacitors. *J Appl Polym Sci*. 2017;134(7):44464. https://doi.org/10.1002/app.44464.

76. Rajak R, Saraf M, Mohammad A, Mobin SM. Design and construction of a ferrocene based inclined polycatenated Co-MOF for supercapacitor and dye adsorption applications. *J Mater Chem A*. 2017;5(34):17998-18011.

77. Wang G, Chen T, Li S, Pang H, Ma H. A coordination polymer based on dinuclear (pyrazinyl tetrazolate) copper(II) cations and Wells–Dawson anions for high-performance supercapacitor electrodes. *Dalton Trans*. 2017;46(40):13897-13902.

78. Feng D, Lei T, Lukatskaya MR, et al. Robust and conductive two-dimensional metal−organic frameworks with exceptionally high volumetric and areal capacitance. *Nat Energy*. 2018;3(1):30-36.

79. Teimuri-Mofrad R, Hadi R, Abbasi H. Synthesis and characterization of ferrocene-functionalized reduced graphene oxide nanocomposite as a supercapacitor electrode material. *J Organomet Chem*. 2019;880:355-362.

80. Liu J, Zhou Y, Xie Z, et al. Conjugated copper–catecholate framework electrodes for efficient energy storage. *Angew Chem Int Ed*. 2020;59(3):1081-1086.

81. Teimuri-Mofrad R, Abbasi H, Hadi R. Graphene oxide-grafted ferrocene moiety via ring opening polymerization (ROP) as a supercapacitor electrode material. *Polymer*. 2019;167:138-145.

82. Teimuri-Mofrad R, Hadi R, Abbasi H. Fadakar Bajeh Baj R. synthesis, characterization and electrochemical study of carbon nanotube/chitosan-ferrocene nanocomposite electrode as supercapacitor material. *J Electron Mater*. 2019;48(7):4573-4581.

83. Li W-H, Deng W-H, Wang G-E, Xu G. Conductive MOFs. *EnergyChem*. 2020;2(2):100029.

84. Zheng S, Xue H, Pang H. Supercapacitors based on metal coordination materials. *Coord Chem Rev*. 2018;373:2-21.

85. Zhao Y, Liu J, Horn M, Motta N, Hu M, Li Y. Recent advancements in metal organic framework based electrodes for supercapacitors. *Sci China Mater*. 2018;61(2):159-184.

86. Du W, Bai Y-L, Xu J, et al. Advanced metal-organic frameworks (MOFs) and their derived electrode materials for supercapacitors. *J Power Sources*. 2018;402:281-295.

87. Zhang Y, Lin B, Sun Y, Zhang X, Yang H, Wang J. Carbon nanotubes@metal–organic frameworks as Mn-based symmetrical supercapacitor electrodes for enhanced charge storage. *RSC Adv*. 2015;5(72):58100-58106.

88. Wang X, Liu X, Rong H, Song Y, Wen H, Liu Q. Layered manganese-based metal–organic framework as a high capacity electrode material for supercapacitors. *RSC Adv*. 2017;7(47):29611-29617.

89. Sundriyal S, Mishra S, Deep A. Study of manganese-1,4-benzenedicarboxylate metal organic framework electrodes based solid state symmetrical supercapacitor. *Energy Procedia*. 2019;158:5817-5824.

90. Liu J, Wang Z, Bi R, et al. A polythreaded Mn^{II}-MOF and its super-performances for dye adsorption and supercapacitors. *Inorg Chem Front*. 2020;7(3):718-730.

91. Yao S, Jiao Y, Sun S, Wang L, Li P, Chen G. Vertically co-oriented Mn-metal–organic framework grown on 2D cation-intercalated manganese oxide via a self-sacrificing template process for a high-performance asymmetric supercapacitor. *ACS Sustain Chem Eng*. 2020;8(8):3191-3199.

92. Cheng Z, Qiu Y, Tan G, Chang X, Luo Q, Cui L. Synthesis of a novel Mn(II)-porphyrins polycondensation polymer and its application as pseudo-capacitor electrode material. *J Organomet Chem*. 2019;900:120940.

93. Kannangara YY, Rathnayake UA, Song J-K. Hybrid supercapacitors based on metal organic frameworks using p-

phenylenediamine building block. *Chem Eng J.* 2019;361:1235-1244.

94. Wei W, Cui X, Chen W, Ivey DG. Manganese oxide-based materials as electrochemical supercapacitor electrodes. *Chem Soc Rev.* 2011;40(3):1697-1721.

95. Yang F, Zhao M, Sun Q, Qiao Y. A novel hydrothermal synthesis and characterisation of porous Mn_3O_4 for supercapacitors with high rate capability. *RSC Adv.* 2015;5(13):9843-9847.

96. Chang H-W, Lu Y-R, Chen J-L, et al. Electrochemical and in situ X-ray spectroscopic studies of MnO_2/reduced graphene oxide nanocomposites as a supercapacitor. *Phys Chem Chem Phys.* 2016;18(28):18705-18718.

97. Xiao G-B, Yao X-Q, Xie H, Ma H-C, Yan P-J, Qin D-D. Dinuclear cobalt-based pillar-layered-like MOF as an electrode material for supercapacitor and photocatalysis activity. *Polyhedron.* 2019;162:39-44.

98. Parnell CM, Chhetri BP, Mitchell TB, et al. Simultaneous electrochemical deposition of cobalt complex and poly(pyrrole) thin films for supercapacitor electrodes. *Sci Rep.* 2019;9(1):5650.

99. Lee DY, Yoon SJ, Shrestha NK, Lee S-H, Ahn H, Han S-H. Unusual energy storage and charge retention in Co-based metal-organic-frameworks. *Microporous Mesoporous Mater.* 2012;153:163-165.

100. Wang Z, Gao C, Liu Y, et al. Electrochemical performance and transformation of Co-MOF/reduced graphene oxide composite. *Mater Lett.* 2017;193:216-219.

101. Yang J, Ma Z, Gao W, Wei M. Layered structural Co-based mof with conductive network frames as a new supercapacitor electrode. *Chem - Eur J.* 2017;23(3):631-636.

102. Choi KM, Jeong HM, Park JH, Zhang Y-B, Kang JK, Yaghi OM. Supercapacitors of nanocrystalline metal–organic frameworks. *ACS Nano.* 2014;8(7):7451-7457.

103. Zhu G, Wen H, Ma M, et al. A self-supported hierarchical Co-MOF as a supercapacitor electrode with ultrahigh areal capacitance and excellent rate performance. *Chem Commun.* 2018;54(74):10499-10502.

104. Sanati S, Abazari R, Morsali A, Kirillov AM, Junk PC, Wang J. An asymmetric supercapacitor based on a non-calcined 3D pillared cobalt(II) metal–organic framework with long cyclic stability. *Inorg Chem.* 2019;58(23):16100-16111.

105. Dong J-L, Xie F, Du J-Q, Lan H-M, Yang R-X, Wang D-Z. Cobalt MOFs base on benzimidazol and varied carboxylate ligands with higher capacitance for supercapacitors and magnetic properties. *J Solid State Chem.* 2019;279:120917.

106. Abazari R, Sanati S, Morsali A, et al. Ultrafast post-synthetic modification of a pillared cobalt(II)-based metal–organic framework via sulfurization of its pores for high-performance supercapacitors. *J Mater Chem A.* 2019;7(19):11953-11966.

107. Abazari R, Sanati S, Morsali A, Slawin AL, Carpenter-Warren C. Dual-purpose 3D pillared metal–organic framework with excellent properties for catalysis of oxidative desulfurization and energy storage in asymmetric supercapacitor. *ACS Appl Mater Interfaces.* 2019;11(16):14759-14773.

108. Xue Y-Y, Li S-N, Jiang Y-C, Hu M-C, Zhai Q-G. Quest for 9-connected robust metal–organic framework platforms based on $[M_3(O/OH)(COO)_6(pyridine)_3]$ clusters as excellent gas separation and asymmetric supercapacitor materials. *J Mater Chem A.* 2019;7(9):4640-4650.

109. Punde NS, Rawool CR, Rajpurohit AS, Karna SP, Srivastava AK. Hybrid composite based on porous cobalt-benzenetricarboxylic acid metal organic framework and graphene nanosheets as high performance supercapacitor electrode. *ChemistrySelect.* 2018;3(41):11368-11380.

110. Ramachandran R, Zhao C, Luo D, Wang K, Wang F. Morphology-dependent electrochemical properties of cobalt-based metal organic frameworks for supercapacitor electrode materials. *Electrochim Acta.* 2018;267:170-180.

111. Xuan W, Ramachandran R, Zhao C, Wang F. Influence of synthesis temperature on cobalt metal-organic framework (Co-MOF) formation and its electrochemical performance towards supercapacitor electrodes. *J Solid State Electrochem.* 2018;22(12):3873-3881.

112. Wang L, Shao D, Guo J, Zhang S, Lu Y. Superstable porous Co-coordination polymer as the electrode material for supercapacitor. *J Solid State Chem.* 2019;277:630-635.

113. Ghosh S, Maity CK, Nayak GC, Nayek HP. A cobalt(II) metal-organic framework featuring supercapacitor application. *J Solid State Chem.* 2020;282:121093.

114. Wang K, Wang X, Zhang D, et al. Interpenetrated nano-MOFs for ultrahigh-performance supercapacitors and excellent dye adsorption performance. *CrstEngComm.* 2018;20(43):6940-6949.

115. Wang K, Cao X, Wang S, et al. Interpenetrated and polythreaded Co^{II}-organic frameworks as a supercapacitor electrode material with ultrahigh capacity and excellent energy delivery efficiency. *ACS Appl Mater Interfaces.* 2018;10(10):9104-9115.

116. Bai W, Li S, Ma J, Cao W, Zheng J. Ultrathin 2D metal-organic framework (nanosheets and nanofilms)-based xD-2D hybrid nanostructures as biomimetic enzymes and supercapacitors. *J Mater Chem A.* 2019;7(15):9086-9098.

117. Worrall SD, Mann H, Rogers A, Bissett MA, Attfield MP, Dryfe RAW. Electrochemical deposition of zeolitic imidazolate framework electrode coatings for supercapacitor electrodes. *Electrochim Acta.* 2016;197:228-240.

118. Gao Y, Wu J, Zhang W, et al. Synthesis of nickel oxalate/zeolitic imidazolate framework-67 (NiC_2O_4/ZIF-67) as a supercapacitor electrode. *New J Chem.* 2015;39(1):94-97.

119. Wang L, Feng X, Ren L, et al. Flexible solid-state supercapacitor based on a metal–organic framework interwoven by electrochemically-deposited PANI. *J Am Chem Soc.* 2015;137(15):4920-4923.

120. Hosseinian A, Amjad A, Hosseinzadeh-Khanmiri R, Ghorbani-Kalhor E, Babazadeh M, Vessally E. Nanocomposite of ZIF-67 metal–organic framework with reduced graphene oxide nanosheets for high-performance supercapacitor applications. *J Mater Sci Mater Electron.* 2017;28(23):18040-18048.

121. Wang L, Yang H, Pan G, Miao L, Chen S, Song Y. Polyaniline-carbon nanotubes@zeolite Imidazolate framework-67-carbon cloth hierarchical nanostructures for supercapacitor electrode. *Electrochim Acta.* 2017;240:16-23.

122. Xu X, Tang J, Qian H, et al. Three-dimensional networked metal–organic frameworks with conductive Polypyrrole tubes for flexible supercapacitors. *ACS Appl Mater Interfaces.* 2017;9(44):38737-38744.

123. Boorboor Ajdari F, Kowsari E, Ehsani A. P-type conductive polymer/zeolitic imidazolate framework-67 (ZIF-67) nanocomposite film: synthesis, characterization, and electrochemical performance as efficient electrode materials in pseudocapacitors. *J Colloid Interface Sci*. 2018;509:189-194.

124. Ajdari FB, Kowsari E, Ehsani A. Ternary nanocomposites of conductive polymer/functionalized GO/MOFs: synthesis, characterization and electrochemical performance as effective electrode materials in pseudocapacitors. *J Solid State Chem*. 2018;265:155-166.

125. Sundriyal S, Shrivastav V, Kaur H, Mishra S, Deep A. High-performance symmetrical supercapacitor with a combination of a ZIF-67/rGO composite electrode and a redox additive electrolyte. *ACS Omega*. 2018;3(12):17348-17358.

126. Liu Y, Xu N, Chen W, Wang X, Sun C, Su Z. Supercapacitor with high cycling stability through electrochemical deposition of metal–organic frameworks/polypyrrole positive electrode. *Dalton Trans*. 2018;47(38):13472-13478.

127. Cao W, Han M, Qin L, et al. Synthesis of zeolitic imidazolate framework-67 nanocube wrapped by graphene oxide and its application for supercapacitors. *J Solid State Electrochem*. 2019;23(1):325-334.

128. Zhou J, Yuan Y, Tang J, Tang W. Metal-organic frameworks governed well-aligned conducting polymer/bacterial cellulose membranes with high areal capacitance. *Energy Storage Mater*. 2019;23:594-601.

129. Shrivastav V, Sundriyal S, Kaur A, Tiwari UK, Mishra S, Deep A. Conductive and porous ZIF-67/PEDOT hybrid composite as superior electrode for all-solid-state symmetrical supercapacitors. *J Alloys Compd*. 2020;843:155992.

130. Tan L, Guo D, Liu J, et al. In-situ calcination of polyoxometallate-based metal organic framework/reduced graphene oxide composites towards supercapacitor electrode with enhanced performance. *J Electroanal Chem*. 2019;836:112-117.

131. Manjunatha N, Imadadulla M, Lokesh KS, Venugopala Reddy KR. Synthesis and electropolymerization of tetra-[β-(2-benzimidazole)] and tetra-[β-(2-(1-(4- aminophenyl)) benzimidazole)] embedded cobalt phthalocyanine and their supercapacitance behaviour. *Dyes Pigm*. 2018;153: 213-224.

132. Cheng J, Chen S, Chen D, et al. Editable asymmetric all-solid-state supercapacitors based on high-strength, flexible, and programmable 2D-metal–organic framework/reduced graphene oxide self-assembled papers. *J Mater Chem A*. 2018; 6(41):20254-20266.

133. Hua W, Xiu J, Xiu F, et al. Micro-supercapacitors based on oriented coordination polymer thin films for AC line-filtering. *RSC Adv*. 2018;8(53):30624-30628.

134. Yang C, Schellhammer KS, Ortmann F, et al. Coordination polymer framework based on-chip micro-supercapacitors with AC line-filtering performance. *Angew Chem Int Ed*. 2017;56 (14):3920-3924.

135. Yang J, Xiong P, Zheng C, Qiu H, Wei M. Metal–organic frameworks: a new promising class of materials for a high performance supercapacitor electrode. *J Mater Chem A*. 2014;2 (39):16640-16644.

136. Wen P, Gong P, Sun J, Wang J, Yang S. Design and synthesis of Ni-MOF/CNT composites and rGO/carbon nitride composites for an asymmetric supercapacitor with high energy and power density. *J Mater Chem A*. 2015;3(26): 13874-13883.

137. Yan Y, Gu P, Zheng S, Zheng M, Pang H, Xue H. Facile synthesis of an accordion-like Ni-MOF superstructure for high-performance flexible supercapacitors. *J Mater Chem A*. 2016;4 (48):19078-19085.

138. Zhou Y, Mao Z, Wang W, Yang Z, Liu X. In-situ fabrication of graphene oxide hybrid Ni-based metal–organic framework (Ni–MOFs@GO) with ultrahigh capacitance as electrochemical pseudocapacitor materials. *ACS Appl Mater Interfaces*. 2016;8(42):28904-28916.

139. Gao S, Sui Y, Wei F, Qi J, Meng Q, He Y. Facile synthesis of cuboid Ni-MOF for high-performance supercapacitors. *J Mater Sci*. 2018;53(9):6807-6818.

140. Yue L, Wang X, Sun T, et al. Ni-MOF coating MoS_2 structures by hydrothermal intercalation as high-performance electrodes for asymmetric supercapacitors. *Chem Eng J*. 2019;375:121959.

141. Kang L, Sun S-X, Kong L-B, Lang J-W, Luo Y-C. Investigating metal-organic framework as a new pseudo-capacitive material for supercapacitors. *Chin Chem Lett*. 2014;25(6):957-961.

142. Du P, Dong Y, Liu C, Wei W, Liu D, Liu P. Fabrication of hierarchical porous nickel based metal-organic framework (Ni-MOF) constructed with nanosheets as novel pseudo-capacitive material for asymmetric supercapacitor. *J Colloid Interface Sci*. 2018;518:57-68.

143. Yue L, Guo H, Wang X, et al. Non-metallic element modified metal-organic frameworks as high-performance electrodes for all-solid-state asymmetric supercapacitors. *J Colloid Interface Sci*. 2019;539:370-378.

144. Wang K, Wang Z, Wang X, Zhou X, Tao Y, Wu H. Flexible long-chain-linker constructed Ni-based metal-organic frameworks with 1D helical channel and their pseudo-capacitor behavior studies. *J Power Sources*. 2018;377:44-51.

145. Wu H, Zhang W, Kandambeth S, Shekhah O, Eddaoudi M, Alshareef HN. Conductive metal–organic frameworks selectively grown on laser-scribed graphene for electrochemical microsupercapacitors. *Adv Energy Mater*. 2019;9(21):1900482.

146. Li Y-L, Zhou J-J, Wu M-K, et al. Hierarchical two-dimensional conductive metal–organic framework/layered double hydroxide nanoarray for a high-performance supercapacitor. *Inorg Chem*. 2018;57(11):6202-6205.

147. Zhao S, Wu H, Li Y, et al. Core–shell assembly of carbon nanofibers and a 2D conductive metal–organic framework as a flexible free-standing membrane for high-performance supercapacitors. *Inorg Chem Front*. 2019;6(7):1824-1830.

148. Li Q, Teng W, Han L, Liu R. 2D Nanoflakes of metal-polyphenolic coordination assembly for high-performance supercapacitor. *Inorg Chem Commun*. 2018;90:51-56.

149. Zhou S, Kong X, Zheng B, Huo F, Strømme M, Xu C. Cellulose nanofiber @ conductive metal–organic frameworks for high-performance flexible supercapacitors. *ACS Nano*. 2019; 13(8):9578-9586.

150. Sheberla D, Bachman JC, Elias JS, Sun C-J, Shao-Horn Y, Dincă M. Conductive MOF electrodes for stable supercapacitors with high areal capacitance. *Nat Mater*. 2017;16(2):220-224.

151. Bi S, Banda H, Chen M, et al. Molecular understanding of charge storage and charging dynamics in supercapacitors with MOF electrodes and ionic liquid electrolytes. *Nat Mater*. 2020; 19(5):552-558.

152. Liao C, Zuo Y, Zhang W, et al. Electrochemical performance of metal-organic framework synthesized by a solvothermal method for supercapacitors. *Russ J Electrochem*. 2013;49(10):983-986.

153. Xu J, Yang C, Xue Y, Wang C, Cao J, Chen Z. Facile synthesis of novel metal-organic nickel hydroxide nanorods for high performance supercapacitor. *Electrochim Acta*. 2016;211:595-602.

154. Feng C, Lv C-P, Li Z-Q, Zhao H, Huang H-H. A porous 2D Ni-MOF material with a high supercapacitive performance. *J Solid State Chem*. 2018;265:244-247.

155. Xu F, Xu H, Chen X, et al. Radical covalent organic frameworks: a general strategy to immobilize open-accessible polyradicals for high-performance capacitive energy storage. *Angew Chem Int Ed*. 2015;54(23):6814-6818.

156. Yang J, Li P, Wang L, Guo X, Guo J, Liu S. In-situ synthesis of Ni-MOF@CNT on graphene/Ni foam substrate as a novel self-supporting hybrid structure for all-solid-state supercapacitors with a high energy density. *J Electroanal Chem*. 2019;848:113301.

157. Nguyen DK, Schepisi IM, Amir FZ. Extraordinary cycling stability of $Ni_3(HITP)_2$ supercapacitors fabricated by electrophoretic deposition: cycling at 100,000 cycles. *Chem Eng J*. 2019;378:122150.

158. Łępicka K, Pieta P, Gupta R, Dabrowski M, Kutner W. A redox conducting polymer of a meso-Ni(II)-SaldMe monomer and its application for a multi-composite supercapacitor. *Electrochim Acta*. 2018;268:111-120.

159. Srimuk P, Luanwuthi S, Krittayavathananon A, Sawangphruk M. Solid-type supercapacitor of reduced graphene oxide-metal organic framework composite coated on carbon fiber paper. *Electrochim Acta*. 2015;157:69-77.

160. Fu D, Li H, Zhang X-M, Han G, Zhou H, Chang Y. Flexible solid-state supercapacitor fabricated by metal-organic framework/graphene oxide hybrid interconnected with PEDOT. *Mater Chem Phys*. 2016;179:166-173.

161. Saraf M, Rajak R, Mobin SM. A fascinating multitasking Cu-MOF/rGO hybrid for high performance supercapacitors and highly sensitive and selective electrochemical nitrite sensors. *J Mater Chem A*. 2016;4(42):16432-16445.

162. Ehsani A, Khodayari J, Hadi M, Shiri HM, Mostaanzadeh H. Nanocomposite of p-type conductive polymer/Cu(II)-based metal-organic frameworks as a novel and hybrid electrode material for highly capacitive pseudocapacitors. *Ionics*. 2017;23(1):131-138.

163. Jafari EA, Moradi M, Borhani S, Bigdeli H, Hajati S. Fabrication of hybrid supercapacitor based on rod-like HKUST-1@polyaniline as cathode and reduced graphene oxide as anode. *Physica E*. 2018;99:16-23.

164. Ramachandran R, Zhao C, Luo D, Wang K, Wang F. Synthesis of copper benzene-1, 3, 5-tricarboxylate metal organic frameworks with mixed phases as the electrode material for supercapacitor applications. *Appl Surf Sci*. 2018;460:33-39.

165. Xu J, Wang Y, Cao S, et al. Ultrathin Cu-MOF@δ-MnO₂ nanosheets for aqueous electrolyte-based high-voltage electrochemical capacitors. *J Mater Chem A*. 2018;6(36):17329-17336.

166. Liu Q, Liu X, Shi C, et al. A copper-based layered coordination polymer: synthesis, magnetic properties and electrochemical performance in supercapacitors. *Dalton Trans*. 2015;44(44):19175-19184.

167. Yu L, Wang X, Cheng M, Rong H, Song Y, Liu Q. A three-dimensional copper coordination polymer constructed by 3-methyl-1*H*-pyrazole-4-carboxylic acid with higher capacitance for supercapacitors. *Cryst Growth des*. 2018;18(1):280-285.

168. Naseri M, Fotouhi L, Ehsani A, Dehghanpour S. Facile electrosynthesis of nano flower like metal-organic framework and its nanocomposite with conjugated polymer as a novel and hybrid electrode material for highly capacitive pseudocapacitors. *J Colloid Interface Sci*. 2016;484:314-319.

169. Chai D, Hou Y, O'Halloran KP, et al. Enhancing energy storage via tea-dependent controlled syntheses: two series of polyoxometalate-based inorganic-organic hybrids and their supercapacitor properties. *ChemElectroChem*. 2018;5(22):3443-3450.

170. Wang H-N, Zhang M, Zhang AM, et al. Polyoxometalate-based metal–organic frameworks with conductive polypyrrole for supercapacitors. *ACS Appl Mater Interfaces*. 2018;10(38):32265-32270.

171. Chai D, Gómez-García CJ, Li B, et al. Polyoxometalate-based metal-organic frameworks for boosting electrochemical capacitor performance. *Chem Eng J*. 2019;373:587-597.

172. Chai D, Xin J, Li B, et al. Mo-based crystal POMOFs with a high electrochemical capacitor performance. *Dalton Trans*. 2019;48(34):13026-13033.

173. Liu Y-Z, Yao W, Gan H-M, Sun C-Y, Su Z-M, Wang X-L. Polyoxometalates-based metal–organic frameworks made by electrodeposition and carbonization methods as cathodes and anodes for asymmetric supercapacitors. *Chem - Eur J*. 2019;25(72):16617-16624.

174. Wang K, Wang Z, Wang S, et al. Layered CuI-MOFs containing $[Mo_8O_{26}]^{4-}$ clusters as supercapacitor electrode materials. *Chem Eng J*. 2019;367:239-248.

175. Li W-H, Ding K, Tian H-R, et al. Conductive metal–organic framework nanowire array electrodes for high-performance solid-state supercapacitors. *Adv Funct Mater*. 2017;27(27):1702067.

176. Du X, Zhang J, Wang H, et al. Solid–solid interface growth of conductive metal–organic framework nanowire arrays and their supercapacitor application. *Mater Chem Front*. 2020;4(1):243-251.

177. Hou R, Miao M, Wang Q, et al. Integrated conductive hybrid architecture of metal–organic framework nanowire array on polypyrrole membrane for all-solid-state flexible supercapacitors. *Adv Energy Mater*. 2020;10(1):1901892.

178. Wang Y-F, Yang S-Y, Yue Y, Bian S-W. Conductive copper-based metal-organic framework nanowire arrays grown on graphene fibers for flexible all-solid-state supercapacitors. *J Alloys Compd*. 2020;835:155238.

179. Yao H, Zhang F, Zhang G, et al. A novel two-dimensional coordination polymer-polypyrrole hybrid material as a high-performance electrode for flexible supercapacitor. *Chem Eng J*. 2018;334:2547-2557.

180. Zhao W, Peng J, Wang W, et al. Interlayer hydrogen-bonded metal porphyrin frameworks/mxene hybrid film with high capacitance for flexible all-solid-state supercapacitors. *Small*. 2019;15(18):1901351.

181. Zhao W, Wang W, Peng J, et al. Wrinkled two-dimensional ultrathin Cu(II)-porphyrin framework nanosheets hybridized with polypyrrole for flexible all-solid-state supercapacitors. *Dalton Trans*. 2019;48(26):9631-9638.

182. Prakash S, Raj JA, Muthuraja P, Kalaignan GP, Manisankar P. Copper based metal-organic coordination polymer for high-performance supercapacitors. *Mater Lett*. 2019;247:48-51.

183. Gao P, Chen Z, Zhao-Karger Z, et al. A porphyrin complex as a self-conditioned electrode material for high-performance energy storage. *Angew Chem Int Ed*. 2017;56(35):10341-10346.

184. Wang L, Han Y, Feng X, Zhou J, Qi P, Wang B. Metal–organic frameworks for energy storage: batteries and supercapacitors. *Coord Chem Rev*. 2016;307:361-381.

185. Wu Z-S, Winter A, Chen L, et al. Three-dimensional nitrogen and boron co-doped graphene for high-performance all-solid-state supercapacitors. *Adv Mater*. 2012;24(37):5130-5135.

186. Lee JH, Park N, Kim BG, et al. Restacking-inhibited 3D reduced graphene oxide for high performance supercapacitor electrodes. *ACS Nano*. 2013;7(10):9366-9374.

187. Chang T-H, Young C, Lee M-H, et al. Synthesis of MOF-525 derived nanoporous carbons with different particle sizes for supercapacitor application. *Chem - Asian J*. 2017;12(21):2857-2862.

188. Zhang X, Hou L, Richard F, Samori P. Modular preparation of graphene-based functional architectures through two-step organic reactions: towards high-performance energy storage. *Chem - Eur J*. 2018;24(69):18518-18528.

189. Lim AC, Jadhav HS, Seo JG. Electron transport shuttle mechanism via an Fe-N-C bond derived from a conjugated microporous polymer for a supercapacitor. *Dalton Trans*. 2018;47(3):852-858.

190. Lim AC, Kwon HJ, Jadhav HS, Seo JG. Porphyrin-stabilized CNT in nanofiber via non-covalent interaction for enhanced electrochemical performance. *Electrochim Acta*. 2018;274:112-120.

191. Jin S, Hill JP, Ji Q, Shrestha LK, Ariga K. Supercapacitive hybrid materials from the thermolysis of porous coordination nanorods based on a catechol porphyrin. *J Mater Chem A*. 2016;4(15):5737-5744.

192. Cao F, Zhao M, Yu Y, et al. Synthesis of two-dimensional $CoS_{1.097}$/nitrogen-doped carbon nanocomposites using metal–organic framework nanosheets as precursors for supercapacitor application. *J Am Chem Soc*. 2016;138(22):6924-6927.

193. Song Y, Wang H, Yan L. Cobalt-porphyrin modified three-dimensional graphene hydrogel electrode for high performance asymmetric supercapacitors. *Nano*. 2019;14(5):1950062.

194. Taşaltın N, Zirek Y, Şan M, Taşaltın C, Karakuş S, Kilislioğlu A. Flexible GO-CoPc and GO-NiPc nanocomposite electrodes for hybrid supercapacitors. *Physica E*. 2020;116:113766.

195. Liao M-S, Scheiner S. Electronic structure and bonding in metal porphyrins, metal=Fe, Co, Ni, Cu, Nn. *J Chem Phys*. 2002;117(1):205-219.

196. Liu Y-N, Jin L-N, Wang H-T, Kang X-H, Bian S-W. Fabrication of three-dimensional composite textile electrodes by metal-organic framework, zinc oxide, graphene and polyaniline for all-solid-state supercapacitors. *J Colloid Interface Sci*. 2018;530:29-36.

197. Cao X-M, Han Z-B. Hollow core–shell ZnO@ZIF-8 on carbon cloth for flexible supercapacitors with ultrahigh areal capacitance. *Chem Commun*. 2019;55(12):1746-1749.

198. Kannangara YY, Rathnayake UA, Song J-K. Redox active multi-layered Zn-pPDA MOFs as high-performance supercapacitor electrode material. *Electrochim Acta*. 2019;297:145-154.

199. Yan Y, Luo Y, Ma J, Li B, Xue H, Pang H. Facile synthesis of vanadium metal-organic frameworks for high-performance supercapacitors. *Small*. 2018;14(33):1801815.

200. Wang Q, Shao L, Ma Z, Xu J, Li Y, Wang C. Hierarchical porous PANI/MIL-101 nanocomposites based solid-state flexible supercapacitor. *Electrochim Acta*. 2018;281:582-593.

201. Liu L, Yan Y, Cai Z, Lin S, Hu X. Growth-oriented Fe-based mofs synergized with graphene aerogels for high-performance supercapacitors. *Adv Mater Interfaces*. 2018;5(8):1701548.

202. Borenstein A, Strauss V, Kowal MD, et al. Laser-reduced graphene-oxide/ferrocene: a 3-D redox-active composite for supercapacitor electrodes. *J Mater Chem A*. 2018;6(41):20463-20472.

203. Rajak R, Saraf M, Mobin SM. Mixed-ligand architected unique topological heterometallic sodium/cobalt-based metal–organic framework for high-performance supercapacitors. *Inorg Chem*. 2020;59(3):1642-1652.

204. Kazemi SH, Hosseinzadeh B, Kazemi H, Kiani MA, Hajati S. Facile synthesis of mixed metal–organic frameworks: electrode materials for supercapacitors with excellent areal capacitance and operational stability. *ACS Appl Mater Interfaces*. 2018;10(27):23063-23073.

205. Yang J, Zheng C, Xiong P, Li Y, Wei M. Zn-doped Ni-MOF material with a high supercapacitive performance. *J Mater Chem A*. 2014;2(44):19005-19010.

206. Banerjee PC, Lobo DE, Middag R, Ng WK, Shaibani ME, Majumder M. Electrochemical capacitance of Ni-doped metal organic framework and reduced graphene oxide composites: more than the sum of its parts. *ACS Appl Mater Interfaces*. 2015;7(6):3655-3664.

207. Gao S, Sui Y, Wei F, et al. Dandelion-like nickel/cobalt metal-organic framework based electrode materials for high performance supercapacitors. *J Colloid Interface Sci*. 2018;531:83-90.

208. Zhao S, Zeng L, Cheng G, Yu L, Zeng H. Ni/Co-based metal-organic frameworks as electrode material for high performance supercapacitors. *Chin Chem Lett*. 2019;30(3):605-609.

209. Wang J, Zhong Q, Xiong Y, Cheng D, Zeng Y, Bu Y. Fabrication of 3D Co-doped Ni-based MOF hierarchical micro-flowers as a high-performance electrode material for supercapacitors. *Appl Surf Sci*. 2019;483:1158-1165.

210. Wang J, Zhong Q, Zeng Y, Cheng D, Xiong Y, Bu Y. Rational construction of triangle-like nickel-cobalt bimetallic metal-organic framework nanosheets arrays as battery-type electrodes for hybrid supercapacitors. *J Colloid Interface Sci*. 2019;555:42-52.

211. Xu C, Feng Y, Mao Z, et al. Binary nickel–cobalt metal–organic frameworks as electrode for high performance

pseudocapacitor. *J Mater Sci Mater Electron*. 2019;30(21): 19477-19486.

212. Liu Y, Wang Y, Chen Y, Wang C, Guo L. NiCo-MOF nanosheets wrapping polypyrrole nanotubes for high-performance supercapacitors. *Appl Surf Sci*. 2020;507:145089.

213. Rahmanifar MS, Hesari H, Noori A, Masoomi MY, Morsali A, Mousavi MF. A dual Ni/Co-MOF-reduced graphene oxide nanocomposite as a high performance supercapacitor electrode material. *Electrochim Acta*. 2018;275:76-86.

214. Wang X, Li Q, Yang N, et al. Hydrothermal synthesis of NiCo-based bimetal-organic frameworks as electrode materials for supercapacitors. *J Solid State Chem*. 2019;270:370-378.

215. Wang X, Yang N, Li Q, et al. Solvothermal synthesis of flower-string-like NiCo-MOF/MWCNT composites as a high-performance supercapacitor electrode material. *J Solid State Chem*. 2019;277:575-586.

216. Wang Y, Nie S, Liu Y, et al. Room-temperature fabrication of a nickel-functionalized copper metal–organic framework (Ni@Cu-MOF) as a new pseudocapacitive material for asymmetric supercapacitors. *Polymers*. 2019;11(5):821.

217. Xia H, Zhang J, Yang Z, Guo S, Guo S, Xu Q. 2D MOF nanoflake-assembled spherical microstructures for enhanced supercapacitor and electrocatalysis performances. *Nano-Micro Lett*. 2017;9(4):43.

218. Hong J, Park S-J, Kim S. Synthesis and electrochemical characterization of nanostructured Ni-Co-MOF/graphene oxide composites as capacitor electrodes. *Electrochim Acta*. 2019;311:62-71.

219. Beka LG, Bu X, Li X, Wang X, Han C, Liu W. A 2D metal–organic framework/reduced graphene oxide heterostructure for supercapacitor application. *RSC Adv*. 2019;9(62):36123-36135.

220. Zhu C, He Y, Liu Y, Kazantseva N, Saha P, Cheng Q. ZnO@MOF@PANI core-shell nanoarrays on carbon cloth for high-performance supercapacitor electrodes. *J Energy Chem*. 2019;35:124-131.

221. Khrizanforov M, Shekurov R, Miluykov V, et al. Excellent supercapacitor and sensor performance of robust cobalt phosphinate ferrocenyl organic framework materials achieved by intrinsic redox and structure properties. *Dalton Trans*. 2019;48 (45):16986-16992.

222. Chen L, Ou D, Zhang G, et al. Ni–Co coordination hollow spheres for high performance flexible all-solid-state supercapacitor. *Electrochim Acta*. 2020;337:135828.

223. Matsubara K, Huang S, Iwamoto M, Pan W. Enhanced conductivity and gating effect of p-type Li-doped NiO nanowires. *Nanoscale*. 2014;6(2):688-692.

224. Xu H, Zeng M, Li J, Tong X. Facile hydrothermal synthesis of flower-like Co-doped NiO hierarchical nanosheets as anode materials for lithium-ion batteries. *RSC Adv*. 2015;5(111): 91493-91499.

225. Zheng JP. The limitations of energy density of battery/double-layer capacitor asymmetric cells. *J Electrochem Soc*. 2003;150 (4):A484.

226. Yuan C, Zhang X, Su L, Gao B, Shen L. Facile synthesis and self-assembly of hierarchical porous NiO nano/micro spherical superstructures for high performance supercapacitors. *J Mater Chem*. 2009;19(32):5772-5777.

227. Yuan Z, Wang Y, Qian Y. A facile room-temperature route to flower-like CuO microspheres with greatly enhanced lithium storage capability. *RSC Adv*. 2012;2(23): 8602-8605.

AUTHOR BIOGRAPHIES

Bulin Chen is currently a PhD student at The Hong Kong Polytechnic University under the supervision of Prof. Wai-Yeung Wong. He received both his BS and MS degrees from Hubei University. His research interests focus on the supercapacitor electrode materials based on electropolymerized metal-organic polymers.

Linli Xu is a Research Assistant Professor at The Hong Kong Polytechnic University working with Prof. Wai-Yeung Wong. She obtained her PhD degree in 2010 from Guangzhou Institute of Chemistry, Chinese Academy of Sciences (CAS), in Polymer Chemistry and Physics. She did her postdoctoral research at Technical Institute of Physics and Chemistry, CAS, from 2010 to 2012. Then she is an assistant researcher at Technical Institute of Physics and Chemistry, CAS, from 2012 to 2017.

Zhiyuan Xie received his PhD degree in Solid-State Electronics and Microelectronics in 1999 from Jilin University. From 2000 to 2003, he worked at City University of Hong Kong as a Senior Research Associate. Since 2004, he joined the State Key Laboratory of Polymer Physics and Chemistry of the Changchun Institute of Applied Chemistry, Chinese Academy of Sciences as a Full Professor. He received the support from the National Science Fund for Distinguished Young Scholars in 2013. His research interests include organic/polymer electroluminescent materials & devices, organic/polymer solar cells, organic semiconductor interface engineering & photophysics and organic-perovskite hybrid materials & devices.

Wai-Yeung Wong received his PhD degree from The University of Hong Kong. After postdoctoral works at Texas A&M University and the University of Cambridge, he joined Hong Kong Baptist University from 1998 to 2016 and he is currently the Interim

Dean of the Faculty of Applied Science and Textiles and Chair Professor of Chemical Technology at The Hong Kong Polytechnic University. His research focuses on metallo-polymers and metallo-organic molecules with energy functions and photofunctional properties. He was named for seven consecutive years in the list of Highly Cited Researchers from 2014 to 2020 published by Thomson Reuters/Clarivate Analytics. He is currently the Editor-in-chief of Topics in Current Chemistry, Editor of Journal of Organometallic Chemistry, and Associate Editor of Journal of Materials Chemistry C and Materials Advances. He is also the President of the Hong Kong Chemical Society. He was awarded the RSC Chemistry of the Transition Metals Award, FACS Distinguished Young Chemist Award, State Natural Science Award from China and RGC Senior Research Fellow Award, among others.